2013

Experimental and modeling study of foam flow in pipes with two foam-flow regimes

Ali Reza Edrisi
Louisiana State University and Agricultural and Mechanical College

EXPERIMENTAL AND MODELING STUDY OF FOAM FLOW IN PIPES WITH TWO FOAM-FLOW REGIMES

A Dissertation

Submitted to the Graduate Faculty of the
Louisiana State University and
Agricultural and Mechanical College
in partial fulfillment of the
requirements for the degree of
Doctor of Philosophy

in

The Craft & Hawkins Department of Petroleum Engineering

by
Ali Reza Edrisi
B.S., Petroleum University of Technology, 2003
M.S., University of Tehran, 2007
December 2013

This dissertation is lovingly dedicated to my beloved mother, Zahra Kordi. Her support, encouragement, and constant love have sustained me throughout my life.

ACKNOWLEDGMENTS

First of all, I would like to thank the Craft and Hawkins Department of Petroleum Engineering at Louisiana State University for their support of this study. I would like to express my appreciation to Chevron Inc., Rural Research Institute, Donald and Gayle Keller Professorship for the financial support. Additional gratitude goes out to our industry partners, especially Stepan and Drilling Specialties Company, who provided us with surfactant and polymer samples tested in this study.

I would like to express my sincere gratitude to my advisor Dr. Seung Ihl Kam for his inspiration, motivation and directions throughout this process. Without his patience and continues guidance this dissertation would not have been possible.

I am grateful to my committee members Dr. Dandina Rao, Dr. Mayank Tyagi and Dr. Paulo Waltrich for their encouragement, insightful comments, and hard questions. They have been so kind to provide me with their immense support and intellectual stimulation in regards to my research. I also would like to thank Dr. Rahul Gajbhiye, Ms. Sneha Panchadhara and the staff at LSU petroleum engineering department, especially Fenelon Nunes for their assistance in laboratory foam flow experiments.

I take this opportunity to express my gratitude to my wonderful family and friends for their unconditional love and support throughout my life. The people who make my life so happy in so many ways. Especially, I would like to express my deepest appreciation to my mom for her immeasurable patience, limitless care and infinite faith in me. The mother who sacrificed her life selflessly, the one who taught me everything, and the one who prayed for me every day. Without you I wouldn't be where I am today. You are my hero. Thank you.

TABLE OF CONTENTS

ACKNOWLEDGMENTS iii

LIST OF TABLES vi

LIST OF FIGURES vii

ABSTRACT xii

CHAPTER 1: SUMMARY 1
1.1 Summary of Three Major Tasks 1
1.1.1 Two Foam-Flow Regimes in Presence of Oil and Polymer (Part 1) 1
1.1.2 Modeling Foam Flow in Pipes Using Two Foam-Flow Regimes Concept (Part 2) 2
1.1.3 Use of New Foam Modeling Technique in Drilling Hydraulics (Part 3) 2
1.2 Chapter Contents 3

CHAPTER 2: LITERATURE REVIEW 4
2.1 Definition and General Use 4
2.2 Foam Underbalanced or Near-balanced Drilling 4
2.3 Foam Fracturing 7
2.4 Foam Rheology 10
2.5 Recent Developments 11

CHAPTER 3: TWO FOAM-FLOW REGIMES IN PRESENCE OF OIL AND POLYMER 15
3.1 Methods 15
3.2 Results and Discussions 18
3.2.1 Polymer Preparation 19
3.2.2 Flow Experiments with Surfactant Foams (without Oil and Polymer) 21
3.2.3 Flow Experiments with Surfactant Foams and Oil 25
3.2.4 Flow Experiments with Polymer-added Surfactant Foams 27

CHAPTER 4: MODELING FOAM FLOW IN PIPES USING TWO FOAM-FLOW REGIMES CONCEPT 41
4.1 Methods 41
4.2 Results and Discussions 44
4.2.1 Data Interpretation 44
4.2.2 Modeling Techniques 47
4.2.3 Rebuilding Two Flow Regime Map and its Implications 52

CHAPTER 5: USE OF NEW FOAM MODELING TECHNIQUE IN DRILLING HYDRAULICS 60
5.1 Methods 60
5.2 Results and Discussions 63

CHAPTER 6: ADDITIONAL DISCUSSIONS 72
6.1 Surface tension measurement of surfactant polymer solutions 72
6.2 Use of dimensionless numbers for two flow regime map 74
6.3 Extension of two foam-flow regimes model into other cases 78
6.3.1 Surfactant foams with oil 78
6.3.2 Surfactant foams with polymer 79

6.3.3 Surfactant foams for a larger pipe diameter 80

CHAPTER 7: CONCLUSIONS AND RECOMMENDATIONS 81
7.1 Conclusions 81
7.1.1 Two Foam-Flow Regimes in Presence of Oil and Polymer (Part 1) 81
7.1.2 Modeling Foam Flow in Pipes Using Two Foam-Flow Regimes Concept (Part 2) 82
7.1.3 Use of New Foam Modeling Technique in Drilling Hydraulics (Part 3) 83
7.2 Recommendations and Future Directions 84

REFERENCES 87

APPENDIX 1: FOAM DRILLING HYDRAULICS CALCULATIONS 93

APPENDIX 2: LETTERS OF PERMISSION 99

VITA 106

LIST OF TABLES

Table 5.1: Input data for foam hydraulics calculation 62

Table 6.1: Surface tension and density measurements of Stepanform 1050 surfactant solutions..... 73

LIST OF FIGURES

Figure 2.1: U.S. rig count by type from 2000 to 2012 showing the trend of increasing horizontal drilling activities (Aleklett (2013) with original data from Baker-Hughes (2012)). 6

Figure 2.2: U.S. dry gas production history and projection (EIA Annual Energy Outlook 2011). 8

Figure 2.3: A schematic plot of apparent foam viscosity as a function of foam quality (Gajbhiye and Kam, 2011). 11

Figure 2.4: Two foam-flow regimes conjectured by Bogdanovic et al. (2009): the pressure contours and the boundary (f_g*) are hand-drawn and approximated by linear lines. (1 wt% of Cedepal FA-406 surfactant in distilled water as a liquid phase; nitrogen as gas phase; ΔP measured over 8.5 ft length 0.36 inch ID horizontal stainless steel pipe) 13

Figure 2.5: A schematic of different flow regimes of foam flow in pipes based on foam texture and flow pattern (Gajbhiye and Kam, 2011). 14

Figure 3.1: Experimental set-up for foam flow in horizontal pipes in this study. 16

Figure 3.2: Preparation of polymer solutions: (a) addition of Liquid Guar CM before mixing; (b) a homogeneous polymer solution after mixing; and (c) a heterogeneous polymer solution after incomplete mixing. 19

Figure 3.3: Viscosity of polymer solution at two different rates, 300 and 600 RPM, as a function of time: (a) mixing with Hamilton Beach Mixer (first 60 minutes) followed by magnetic stirring bar; (b) mixing with a magnetic bar only. 20

Figure 3.4: Pressure profile of polymer solution (0.5 wt% Liquid Guar CM, Q_w = 20 cm^3/min) measured at 8 pressure taps along the pipe: (a) without foam generator; and (b) with foam generator (90 micron filter). The system fails to generate fine-textured foams at low shear rate (i.e., without foam generator) as expected. 21

Figure 3.5: Pressure profile of surfactant foams (Stepanform 0.5 wt%, Q_w=60 cm^3/min): gas injection rate was increased from 200 to 5000 cm^3/min, and then was reduced back to 200 cm^3/min. 22

Figure 3.6: Pressure profile of surfactant foams (Stepanform 0.5 wt%): (a) Q_w=20 cm^3/min, (b) Q_w=40 cm^3/min, (c) Q_w=60 cm^3/min, and (d) Q_w=80 cm^3/min at various Q_g from 200 to 5000 sccm. 23

Figure 3.7: Pressure drop between ports B and G (ΔP_{BG}) as a function of various gas and liquid rates during surfactant foam injection (Stepanform 0.5 wt%). 24

Figure 3.8: Contour plot of pressure drop between ports B and G (ΔP_{BG}) in psi for surfactant foams (Stepanform 0.5 wt%) as a function of gas and liquid velocities. Note that the pressures in boxes are experimentally measured values, and f_g* is the boundary line separating the high-quality and low-quality regimes based on the pressure contours. (1 psi = 6900 Pa) 24

Figure 3.9: Pressure profile of surfactant foams (Stepanform 0.5 wt%) with oil (0.5 cm^3/min): (a) Q_w=20 cm^3/min, (b) Q_w=40 cm^3/min, (c) Q_w=60 cm^3/min, and (d) Q_w=80 cm^3/min at various Q_g from 200 to 5000 sccm. 26

Figure 3.10: Pressure drop between ports B and G (ΔP_{BG}) as a function of various gas and liquid rates during surfactant foam injection (Stepanform 0.5 wt%) with oil (Q_o= 0.5 cm^3/min). 26

Figure 3.11: Contour plot of pressure drop between ports B and G (ΔP_{BG}) in psi for surfactant foams (Stepanform 0.5 wt%) in presence of oil (Q_o= 0.5 cm^3/min) as a function of gas and liquid velocities. Note that the pressures in boxes are experimentally measured values, and f_g* is the boundary line separating the high-quality and low-quality regimes based on the pressure contours. (1 psi = 6900 Pa)... 27

Figure 3.12: Pressure profile of polymer-added surfactant foams (Stepanform 0.5 wt%, Liquid Guar CM 0.5 wt%) at Q_w= 10 cm^3/min. 28

Figure 3.13: Pressure profile of polymer-added surfactant foams (Stepanform 0.5 wt%, Liquid Guar CM 0.5 wt%) at Q_w= 20 cm^3/min. 28

Figure 3.14: Pressure profile of polymer-added surfactant foams (Stepanform 0.5 wt%, Liquid Guar CM 0.5 wt%) at Q_w= 40 cm^3/min. 29

Figure 3.15: Pressure profile of polymer-added surfactant foams (Stepanform 0.5 wt%, Liquid Guar CM 0.5 wt%) at Q_w= 10 cm^3/min: repeated to compare with Fig. 3.12. 30

Figure 3.16: Contour plot of pressure drop between ports B and G (ΔP_{BG}) in psi for polymer-added surfactant foams (Stepanform 0.5 wt%, Liquid Guar CM 0.5 wt%) as a function of gas and liquid velocities. (1 psi = 6900 Pa) 32

Figure 3.17: Pressure profile of polymer-added surfactant foams (Stepanform 0.5 wt%, Liquid Guar CM 0.1 wt%) at Q_w= 20 cm^3/min. 32

Figure 3.18: Pressure drop between ports B and G (ΔP_{BG}) during surfactant foam injection during polymer-added surfactant foam injection (Stepanform 0.5 wt%, Liquid Guar CM 0.1 wt%) at Q_w= 20 cm^3/min. 33

Figure 3.19: Comparison of foam flow characteristics between (a) polymer-free and (b) polymer-added surfactant foams in terms of pressure profile plot. 35

Figure 3.20: Actual photos of different flow characteristics shown in Fig. 3.19. 36

Figure 3.21: Comparison of foam flow characteristics between (a) polymer-free and (b) polymer-added surfactant foams in terms of contour plot. 38

Figure 3.22: Snapshots of foam flow in pipe with 2 second time intervals for foams in chaotic region (Q_g = 300 cm^3/min as shown in Fig. 3.15). 40

Figure 4.1: Two flow patterns of interest in this modeling study – slug-flow pattern to represent the high-quality regime and plug-flow pattern to represent the low-quality regime (see Figure 4.2 for more). 45

Figure 4.2: Photos from lab experiments showing foam flow mechanisms in the low-quality and high-quality regimes in response to the changes in gas and liquid velocities (Although it is not shown clearly on this scale, water film thickness at the wall in (1) (i.e., wetter condition) is greater than that in (2) (i.e., drier condition)). 46

Figure 4.3: Pressure contour plot (Edrisi et al. (2012) using surfactant foams (0.5 wt% Stepanform and nitrogen)) analyzed by a sketch of a series of straight pressure contour lines for model fit. (See Figure 3.8 for original data) 48

Figure 4.4: Construction of the best-fit straight lines for each set of pressure contours. (See Figure 3.8 for original data) 49

Figure 4.5: Unified pressure contours by using representative slopes from both regimes. (See Figure 3.8 for original data) 49

Figure 4.6: Construction of f_g* line from the model fit to pressure contours (Fig 4.5). (See Figure 3.8 for original data) 50

Figure 4.7: Foam rheology along the f_g* line by using (a) power-law model and (b) Bingham-plastic model. 51

Figure 4.8: Model reconstruction of data points along the f_g* line and corresponding pressure contours. (See Figure 3.8 for original data) 52

Figure 4.9: Reconstruction of two-flow-regime pressure-drop contours by using the model at a small (a) and a large (b) number of sample data points. (See Figure 3.8 for original data) 54

Figure 4.10: A schematic of the change in foam flow mechanisms along the same contour line penetrating both regimes. 55

Figure 4.11: Calculated wall slip effect along the same pressure contour lines for foams in the low-quality regime: (a) slip velocity (u_s) and (b) slip coefficient (β_c) 57

Figure 4.12: Calculated relative size of free-gas segment (L_g/L_t) along the same pressure contour lines for foams in the high-quality regime. 58

Figure 5.1: A schematic of the well configuration used in this study. 63

Figure 5.2: Base Case pressure contours in a wide range of gas and liquid velocities by using empirical equations from Chen et al. (2009) showing only low-quality regime: (a) foam inside drill pipe and (b) foam in the annulus. 64

Figure 5.3: Comparison between (a) Chen et al. (2009) and (b) Base case of this study; the aqueous foam case in (a) is reproduced successfully by the hydraulics model developed in this study. 65

Figure 5.4: Case 1 pressure contours by using Chen et al. (2009) and Edrisi et al. (2013) at f_g^*= 85%; (a) inside drill pipe and (b) inside annulus. 66

Figure 5.5: Case 1 constructed rheograms (shear stress τ_w vs. shear rate γw) for foams along f_g^* line; (a) inside drill pipe and (b) inside annulus. 67

Figure 5.6: Case 2 (a) pressure contour and (b) rheogram in the annulus where f_g^* = 75% (foam rheology within drill pipe is identical to Case 1 as shown in Fig 5.4 (a) and Fig 5.5 (a)) 67

Figure 5.7: Comparison of Base Case, Case 1 and Case 2 in term of pressure along the well. (see Fig. 5.1 and Table 5.1 for more details) 68

Figure 5.8: Comparison of Base Case, Case 1 and Case 2 in term of foam quality along the well. (see Fig. 5.1 and Table 5.1 for more details) 69

Figure 5.9: Comparison of Base Case, Case 1 and Case 2 in term of density of foam mixture along the well. (see Fig. 5.1 and Table 5.1 for more details)..... 70

Figure 5.10: Comparison of Base Case, Case 1 and Case 2 in term of foam total velocity along the well. (see Fig. 5.1 and Table 5.1 for more details) 71

Figure 5.11: Comparison of Base Case, Case 1 and Case 2 in term of total pressure gradient along the well. (see Fig. 5.1 and Table 5.1 for more details)..... 71

Figure 6.1: Pictures taken from surface tension measurements: (A) deionized water; (B) 0.5 wt% Stepanform surfactant solution; and (C) 0.5 wt% liquid guar CM in 0.5 wt% Stepanform solution. 72

Figure 6.2: Surface tension measurement as a function of surfactant concentration wt% of Stepanform 1050 in deionized water) with no polymer. 73

Figure 6.3: Surface tension measurement as a function of polymer concentration (0.5 wt% Stepanform 1050 solution). 74

Figure 6.4: Surface tension measurement as a function of surfactant concentration (0.5 wt% Liquid Guar CM solution). 74

Figure 6.5: Translation of (a) pressure contours (psi) into (b) apparent foam viscosity (centipoise) contours..... 75

Figure 6.6: Translation into dimensionless capillary number contours. 76

Figure 6.7: Translation of pressure contours into (a) Reynolds number and (b) Froude Number. 76

Figure 6.8: Comparison of Base Case, Case 1 and Case 2 in terms of dimensionless numbers along the well. (see Fig. 5.1 and Table 5.1 for more details)..... 77

Figure 6.7: Pressure-drop contours for surfactant foams and oil. 78

Figure 6.8: Reconstruction of two-flow-regime pressure contours for surfactant foams and oil. 79

Figure 6.9: Original (a) and reconstructed (b) pressure contours for polymer-added surfactant foams. 79

Figure 6.10: Original (a) and reconstructed (b) pressure contours (1 wt% Cedepal FA-406 surfactant solution in 12 ft length 1 inch NPS stainless steel horizental pipe). 80

Figure A.1. The algorithm used in this study for foam drilling hydraulics calculation (details on parameters and variables in Appendix 1)..... 98

ABSTRACT

The use of foams can be found abundantly in many applications in a wide range of industries, including oil and gas industry. Although understanding foam flow behavior is crucial for the optimization of such applications, the complex flow behavior of foams has been a major challenge. Recent experimental studies with surfactant foams presented a new way to characterize foam flow characteristics by using two flow regimes: the low-quality regime showing either plug-flow or segregated-flow pattern, and the high-quality regime showing slug-flow pattern.

This study consists of three main components: (1) experimental investigation of foam rheology in pipes; (2) building up of a new foam model consistent with lab-measured experimental data; and (3) use of the model in petroleum drilling hydraulics modeling and simulation.

The major outcome of this study can be summarized as follows.

First (Part 1), by conducting foam flow experiments in pipes, this study shows the concept of two foam-flow regimes is still valid and effective not only with surfactant foams but also with foams in the presence of additives such as polymers and oils. This finding is important because many field applications of foam flow involve some levels of additives.

Second (Part 2), this study for the first time presents how to build a foam model which is consistent with two foam-flow regimes evidenced by experimental data. The model requires four model parameters – two parameters to capture rheological properties (e.g. consistency index and flow behavior index, if power-law rheology is applied) and two parameters to define the dependence of foam rheology to gas and liquid flow rates in both foam flow regimes.

Third and last (Part 3), the significance of this model is verified by implementing it into existing foam drilling hydraulics calculations in a 10,000 ft vertical well in which foams are injected down into the drill pipe, through the drill bit and circulated up to the surface along the annulus. The results show that this new foam model equipped with two flow regimes is advantageous over the conventional foam model especially when foams become dry and unstable in the well, improving the accuracy.

CHAPTER 1: SUMMARY

1.1 Summary of Three Major Tasks

The background, results, and objectives of the three major components can be summarized as follows.

1.1.1 Two Foam-Flow Regimes in Presence of Oil and Polymer (Part 1)

Earlier studies with surfactant foams "without" oils and polymers show that foam flow in pipe can be represented by two different flow regimes: the low-quality regime showing either plug-flow or segregated-flow pattern, and the high-quality regime showing slug-flow pattern. These behaviors have not been tested in the presence of oils and polymers, which are common additives in numerous petroleum engineering applications. Therefore, the objective of Part 1 is to experimentally investigate foam flow characteristics in horizontal pipes at different injection conditions – surfactant foams with or without oils, and surfactant foams with or without polymers. The results of this study were presented in two different ways: (i) steady-state pressure drops (or, apparent foam viscosity, equivalently) measured by multiple pressure taps and (ii) visualization of bubble size, size distribution and flow patterns in transparent pipes. The results with surfactant foams and oil showed that (i) oil reduced the stability of foams in pipes, hence, decreasing the steady-state pressure drops and foam viscosities, and (ii) the presence of oil tended to lower the transition between the high-quality and the low-quality regimes (i.e., lower foam quality at the boundary, or lower f_g^* equivalently). In addition, the results with surfactant foams with polymer showed that (i) polymer thickened the liquid phase and, if enough agitation was supplied, could make foams long-lived and increase foam viscosities, and (ii) the system sometimes did not reach the steady state readily, showing systematic oscillations. In both cases, though, the experiments carried out in this study showed the presence of two distinct high-quality and low-quality flow regimes.

1.1.2 Modeling Foam Flow in Pipes Using Two Foam-Flow Regimes Concept (Part 2)

As a follow-up study of Part 1, Part 2 presents how to develop a comprehensive foam model that can handle a variety of bubble-size distributions and both stable and unstable flow patterns by using two-flow-regime concept. Building an improved foam model based on such a new concept can potentially help better design and optimize many foam-associated processes including tight-gas and shale-gas foam fracturing, foam underbalanced drilling, and cutting transports.

Analyzing experimental data of surfactant foams and polymer-added foams shows that (i) in the low-quality regime, foam rheology is governed by bubble slippage at the wall with no significant change in its fine foam texture and (ii) in the high-quality regime, foam rheology is governed by the relative size of free-gas segment to fine-textured foam-slug segment. By using these governing mechanisms, this improved foam model successfully reproduces foam flow characteristics as observed in the experiments, including almost horizontal pressure contours in the low-quality regime and inclined pressure contours in the high-quality regimes. Although the model is built with a power-law fluid model, the same procedure can be taken for Bingham-plastic or yield-power-law fluids.

1.1.3 Use of New Foam Modeling Technique in Drilling Hydraulics (Part 3)

Foam underbalanced drilling has unique advantages such as reduced formation damage, improved rate of penetration, higher cutting-transport capacity, and lower circulation losses. The objective of Part 3 is to construct foam drilling hydraulics model consistent with two foam-flow regimes concept, and investigate how it improves current foam drilling hydraulics modeling.

The results demonstrated the significance of this new approach, capturing both stable/steady flow at low foam quality and unstable/unsteady flow at high foam quality. The results from three different cases indicated significant differences in drilling hydraulics calculations when a conventional foam model is replaced by a two foam-flow regimes map. An example drilling scenario simulated for a 10,000 ft deep

vertical well was shown to have as much as 19 %, 25 %, and 16 % difference in calculated foam density, total velocity, and pressure gradient, respectively, at the bottom hole.

1.2 Chapter Contents

The contents of each individual chapter can be summarized as follows:

Chapter 1 describes the summary of this study and introduces the contents of each chapter.

Chapter 2 reviews previous studies related to this research area, including fundamentals of foam flow in pipes and its applications such as foam drilling, foam fracturing, etc.

Chapter 3 investigates foam flow characteristics by conducting laboratory foam flow experiments in horizontal pipes (Part 1). The results are analyzed by the theory of two foam-flow regimes in pipes. The effects of oils and polymers on foam rheology are examined and discussed.

Chapter 4 focuses on how to establish a foam model to match experimental data exhibiting two foam-flow regimes (Part 2). The detailed procedure is described in a step-by-step manner and the implication of the model is discussed in terms of foam flow characteristics (i.e., bubble size and bubble size distribution).

Chapter 5 demonstrates how such a new foam modeling technique presented in Chapter 4 can be incorporated into existing foam UBD (underbalanced drilling) hydraulics calculations (Part 3). By comparing with the results of conventional foam drilling hydraulics calculations in a published paper, the strength of this new foam model is demonstrated.

Finally, Chapter 6 includes conclusions from this study and recommendations for the future directions.

CHAPTER 2: LITERATURE REVIEW

2.1 Definition and General Use

Foam is defined as an agglomeration of discontinuous gas bubbles dispersed within a continuous external liquid phase. The gas phase is, typically, made up of air, nitrogen, carbon dioxide, hydrocarbon gas, and so on, while the liquid phase consists of water and surface active agents, commonly called surfactants. The presence of surfactants reduces interfacial tension between water and gas, and endows a better stability to liquid films for pre-existing foams (Bikerman, 1973; Kraynik, 1988). Other additives such as polymers and gels are commonly added to the aqueous phase for improved foam properties.

Foam has been used for many different purposes in a huge range of applications including chemical and mechanical engineering, food industry, fire-fighting, pharmaceutical industry, and so on (Kim and Dlugogorski, 1997; Gardiner et al., 1999; Schramm, 2005). When it comes to petroleum industry, foam application can be easily found in drilling, workover, cementing, fracturing, and improved and enhanced oil recovery processes (Aubert et al., 1986; Kam et al., 2007; Kam, 2008; Aadnoy et al., 2009). When foam is applied to drilling processes, their low-density and high-viscosity characteristics provide a great advantage. These characteristics, more specifically, include high lifting capacity, hole cleaning, minimizing lost circulation, and low formation damage (Hall and Roberts, 1984; Falk and McDonald, 1995; Capo et al., 2006). Foam is also regarded as an attractive option in the applications where the use of small amount of water is highly desirable due to environmental impacts, for example, as shown in shale-gas hydraulic fracturing treatments (Abbott and Vaughn, 1976; Penny et al, 1993; Aadnoy et al., 2009; Edrisi and Kam, 2012).

2.2 Foam Underbalanced or Near-balanced Drilling

Underbalanced drilling (UBD) is defined as a drilling practice when bottomhole circulating pressure inside the well is kept below the formation pore pressure intentionally (Lyons et al, 2009),

allowing formation fluid to flow into the wellbore and essentially keeping the well in the kick condition. Since the first use of compressible fluids in drilling operations was patented in 1866 (Shale, 1994), UBD has evolved to a common practice worldwide especially for low pressure reservoirs, fractured formations, and water-sensitive environments (Shadravan et al., 2009; Lage et al., 1996; Muqeem et al., 2008; Paknejad et al., 2007; Yao et al., 2011). In spite of concerns associated with wellbore stability, high risk operations, and safety issues (Bennion et al., 1996), UBD processes have the following major advantages: i) improving the rate of penetration (ROP) and hence making drilling faster and more economical; ii) reducing or removing the concerns about damaging formations near the productive target layers; iii) minimizing the lost circulation; iv) eliminating the risk of differential sticking; and v) extending bit life.

Among many different types of drilling fluids for UBD such as air, gases, gasified fluids, mist and etc., foam has been particularly of interest because of its low-density and high-viscosity properties (Guo et al., 2003). Foam offers additional benefits, including yield stress and high carrying capacity, which help control fluid influx into the drilling hole and keep the bottomhole clean (Hall and Roberts, 1984; Falk and McDonald, 1995; Capo et al., 2006).

Foam drilling operation experiences reduced formation damage, improved rate of penetration, and lower circulation losses compared to conventional over-balanced drilling technique. Maintaining foam stability in foam drilling applications can be a challenge, especially when the formation oil is allowed to flow into the drilling hole due to underbalanced condition. By using the magnitudes of entering coefficient and spreading coefficient, typical reservoir oils are shown to deteriorate foam stability, even though some variations are observed depending on the composition of the oils (Nikolov et al., 1985; Novosad et al., 1989; Manlowe and Rake, 1990; Mannhardt et al., 2000; Rojas et al., 2001). The use of polymer together with surfactant foams is a common and popular technique if improved foam stability is required. Polymer not only increases foam viscosity due to enhanced film stability to mechanical disturbance, but it also allows foam films meta-stable due to very viscous foam films prohibiting a rapid transport of liquid phase (Reidenbach et.al., 1986; Harris and Heath, 1996; Sani and

Shah, 2001; Khade and Shah, 2004; Hutchins and Miller, 2005). Different kinds of polymers are available in the market, such as Hydroxyethyl cellulose (HEC), Xanthan Gum, Guar, and Hydroxypropyl guar (HPG), and the major selection criteria are cost, hydration, and biodegradability in addition to improved foam stability.

It should be pointed out that in underbalanced drilling operations, fine-textured and continuous foams are preferred (and sometimes even crucial), no matter what the inclination angle is, in order to control bottomhole pressure accurately and clean the hole efficiently. Failure to obtain such characteristics required for foam drilling may jeopardize the entire drilling process.

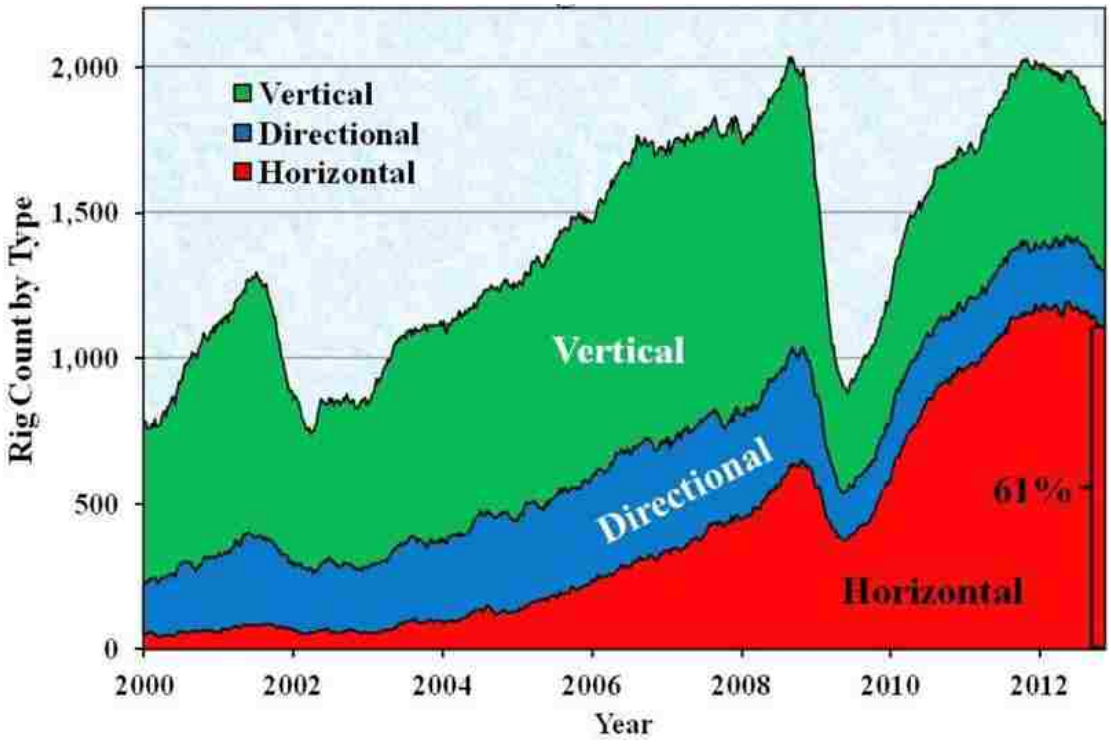

Figure 2.1: U.S. rig count by type from 2000 to 2012 showing the trend of increasing horizontal drilling activities (Aleklett (2013) with original data from Baker-Hughes (2012)).

Recent increase in drilling activities in the U.S., evidenced by rig count as shown in Fig. 2.1 - not only horizontal drilling has become popular reaching nearly 61 % in late 2012, but vertical and directional

drilling also has become more challenging due to ever increasing well depth and water depth – requires that more and more wells be drilled using underbalanced drilling (UBD) or near-balanced drilling technique (Bietz et al, 1993; Shah et al, 2010) rather than conventional overbalanced drilling techniques (OBD). Foam drilling seems to be a promising means to fit the technological challenges associated with deepwater and deep well environments.

2.3 Foam Fracturing

Natural gas production in the U.S. has been increasing rapidly during the past decade. The U.S. Energy Information Administration (EIA) reported 22.6 trillion cubic feet (Tcf) of annual total natural gas production in 2010 which is the highest since 1973 (U.S. EIA, 2011). Unconventional gas resources like tight gas and shale gas have an important role in this dramatic gas production growth. It is reported in 2011 that more than 40 percent of total natural gas production in the U.S. is coming from tight gas and shale gas resources (Newell, 2011). Just shale gas production alone has increased about 12 times in the last decade in the U.S. gas production, and the U.S. shale gas proved reserves have also tripled from 23 at 2007 to 60 trillion cubic feet at 2009 (U.S. EIA, 2011). The U.S. EIA's 2011 Annual Energy Outlook, as shown in Fig. 2.2, predicts that shale gas production would occupy 46 percent of the U.S. dry gas production by 2035, which is a significant increase from 14 percent in 2009. Most of the shale gas production in the U.S. currently originates from five major shale gas fields such as Barnett (TX), Haynesville (LA and TX), Fayetteville (AR), Woodford (OK) and Marcellus (PA and other eastern states).

The developments of shale gas reservoirs are different from conventional gas fields in many aspects. First, the average absolute permeability of the shale gas formations is very low typically less than 0.001 Darcy (Curtis, 2002). This makes shale gas formations suffering from extremely low productivity, often below the commercially feasible production rate. Second, due to such a low productivity, the development of shale gas formations requires horizontal drilling and multi-stage hydraulic fracturing techniques in order to boost up the conductivity of the media (Hill and Nelson, 2000; Sumi, 2008;

Cardott, 2008). Third and last, because shale gas formations, usually containing high organic contents, are composed of fine grained clay rocks, any drilling and production activities with high water contents should be carried out carefully (Curtis, 2002; Zelenev et al, 2010). The use of massive amount of surface water associated with the conventional hydraulic fracturing has also caused environmental concerns.

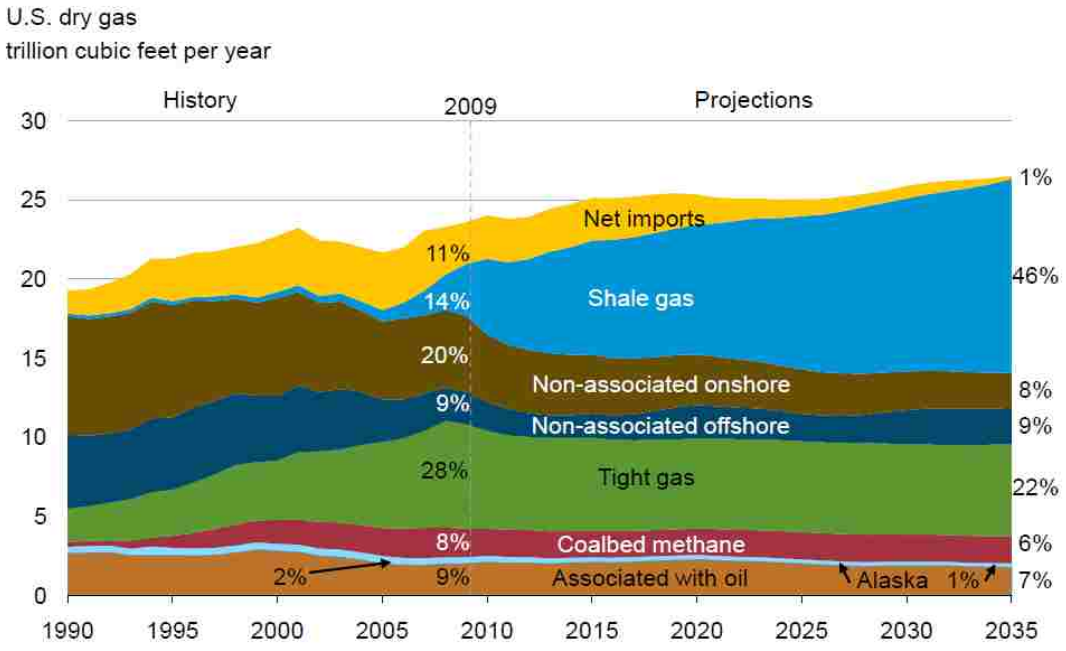

Figure 2.2: U.S. dry gas production history and projection (EIA Annual Energy Outlook 2011).

Hydraulic fracturing (often called “fracking” in the media) is a technique to induce fractures into geological formations by injecting a pressurized fluid (often, water-based) in order to improve the conductivity or the transport capability. Newly created facture faces and channels are connected to small pores in a low permeability rock, and provide highly conductive paths for hydrocarbon to reach the well resulting in enhanced production rate and ultimate recovery. Among many design parameters, the selection of proper fracturing fluids plays a key role in the success of fracturing process. The fracturing fluids should be able to open up new fractures during initial pressurization stage, effectively flow deep into the reservoir propagating the fractures without difficulties, transport and carry solid proppants to every corner of the facture faces, and flow back and be recovered easily not to cause damage to the

formation prior to major production. To achieve these various goals, fracturing fluids are expected to have proper characteristics including viscosity, surface tension, leak-off, and water chemistry (Gupta, 2009; Martin and Rylance, 2010).

For water-sensitive formations and water-deficient environments, foam has long been considered as one of the fracturing fluids (Neill et al, 1964; Blauer and Kohlhaas, 1974; Komar et al., 1979; Gupta, 2009). Consisting of a high fraction of dispersed and discontinuous gas phase within a low fraction of continuous liquid phase with surfactants in it, foams are believed to be an appropriate means for fracturing shale gas reservoirs as shown by previous studies (Komar, 1978; Matthews et al., 2007; Rowan, 2009). The lower water content is obviously an attractive aspect because it requires less water consumption, less formation damage in water sensitive area, and less liquid to recover after fracturing job (Ballard, 1977; Harris and Heath, 1996; Gupta et al., 2005). Expansion of the gas phase after the treatment also helps recover the liquid phase introduced into the formation with foams (Gaydos and Harris, 1980; Chen et al., 2005). For shale gas development in environmentally sensitive regions, foam fracturing is advantageous over the conventional water-based hydraulic fracturing because less amount of water usage can be translated into fewer amounts of health-hazardous chemical additives in fracturing liquid.

Foams also have a growing demand for unconventional gas reservoir developments. It is because unconventional gas resources like tight gas and shale gas, which are reported to be more than 40 percent of total natural gas production in the U.S. in 2011 (Newell, 2011), cannot be produced efficiently because of low permeability leading to low productivity (Curtis, 2002). Although such an extremely low productivity requires the use of horizontal drilling and multi-stage hydraulic fracturing techniques, the use of high water contents in hydraulic fracturing causes concerns about serious wellbore damage (Curtis, 2002; Hill and Nelson, 2000; Zelenev et al., 2010). The use of massive amount of surface water associated with the conventional hydraulic fracturing has also caused environmental concerns.

For water-sensitive formations and water-deficient environments, foam has long been considered as one of the fracturing fluids (Neill et al, 1964). The lower water content is obviously an attractive aspect

because it requires less water consumption, less formation damage in water sensitive layers, and less liquid to recover after fracturing job (Harris and Heath, 1996; Gupta et al., 2005). Expansion of the gas phase after the treatment also helps recover the liquid phase introduced into the formation with foams (Chen et al., 2005).

2.4 Foam Rheology

For processes associated with foams, understanding foam rheology is critical. An important parameter to quantify foam behavior is foam quality, which is, simply the volume fraction of gas in the whole foam mixture. Foams with high quality, therefore, are dry foams while foams with low quality are wet foams. Foams with a very low foam-quality value, let's say lower than 65%, behaves similarly to the external liquid phase because internal bubbles are dispersed and not interacting each other significantly during the flow. On the other hand, foams with a very high foam-quality value, higher than 98% in general, tend to convert to a mist flow which has liquid as the internal phase and gas as the external phase. Therefore it is foam with 65 - 98% qualities that is of major importance in many applications. Other foam characteristics such as stability, drainage, yield stress, Newtonian/non-Newtonian behavior, wall slip, average bubble size, bubble-size distribution, and many more are related to foam quality directly and/or indirectly. Although there have been numerous studies accumulated in this area, the complex nature of foam flow behavior is yet to be understood clearly primarily due to countless factors that affect foam rheology – for example, temperature, pressure, foam quality, foam texture, foam density, liquid phase properties, pipe materials, interaction between foams and surroundings (liquid and pipe wall) and so forth (Bonilla and Shah, 2000; Ozbayoglu et al., 2000; Briceno and Joseph, 2003). The addition of polymers into aqueous foams in foam drilling obviously adds more complexity.

One of the key parameters to describe foam rheology for modeling and simulation purpose is its viscosity. Foam viscosity is typically much higher than the viscosity of external liquid phase - as much as several orders of magnitude difference - and is sensitive to the change in foam quality and injection velocity (Patton et al., 1983). As shown in Fig. 2.3 in which the flow experiments are conducted in a wide

range of foam quality at fixed total flow rate, foam viscosity increases gradually with foam quality at low foam quality ($f_g < f_{gth1}$); increases sharply at intermediate foam quality ($f_{gth1}<f_g < f_{gth2}$); and decreases dramatically at high foam quality ($f_{gth2}<f_g$). Previous studies show that foams can be modeled by power-law model (Raza and Marsden, 1967; David and Marsden, 1969; Sanghani and Ikoku, 1983; Martins et al., 2001), Bingham plastic model (Blauer et al., 1974; Calvert and Nezhati, 1987), or yield-power-law or Harshel-Bulkley model (Reidenbach et al., 1986; Saintpere et. al., 1999). It is worth mentioning that the interaction between bubbles under shear flow plays a central role in determining the yield stress and viscosity of foam mixture (Princen, 1983; Kraynik, 1988; Kam et al., 2002).

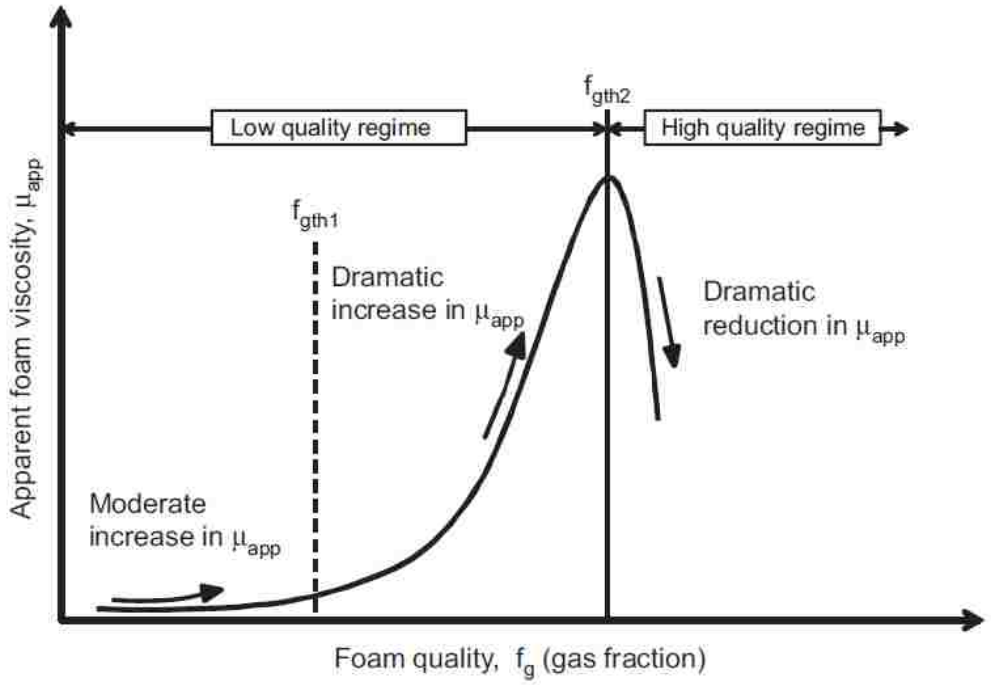

Figure 2.3: A schematic plot of apparent foam viscosity as a function of foam quality (Gajbhiye and Kam, 2011).

2.5 Recent Developments

Originated from foam flow in porous media (Gauglitz et al., 2002; Kam and Rossen, 2003), recent studies show that foam rheology in pipes exhibits two very distinct behaviors (Bogdanovic et al.,

2009) as shown by the pressure contour plot in Fig. 2.4. The low-quality regime, characterized by almost horizontal pressure contours, is governed by either segregated flow (i.e., upper foam layer and lower liquid layer) or plug flow (i.e., foams with fine and homogeneous texture). On the other hand, the high-quality regime, characterized by pressure contours with finite slopes, is governed by slug flow (i.e., repetitions of fine/homogeneous textured foams and free gas section). These two regimes are shown to be separated by a critical foam quality called f_g*. These aspects are well summarized by the visualization study of Gajbhiye and Kam (2011) as shown in Fig. 2.5. The same behaviors are also found consistently at various inclination angles (Gajbhiye and Kam, 2012). When Gajbhiye (2011) compared the range of flow rates in these studies with flow regime maps such as Taitel and Dukler's, Baker's, and Beggs and Brill's, most injection conditions fell within the stratified flow region.

Recent experimental studies (Bogdanovic et al., 2009; Gajbhiye and Kam, 2011; Gajbhiye and Kam, 2012; Edrisi et al., 2012) show that foam rheology can be represented by two distinct flow regimes if pressure contours are plotted as a function of gas and liquid velocities as shown in Figs. 2.4 and 2.5. The low-quality regime (i.e., lower right-hand side portion) has pressure contours almost horizontal, meaning that the pressure drop is very sensitive to gas velocity (u_g) but less sensitive to liquid velocity (u_w). On the other hand, the high-quality regime (i.e., upper left-hand side portion) has pressure contours inclined with finite slopes, meaning that the pressure drop is sensitive to both gas and liquid velocities. The boundary between these regimes are shown by a straight line from the origin, called "f_g*" (Fig. 2.4). A visualization study (Gajbhiye and Kam, 2011) as summarized in Fig. 2.5 shows that the f_g* is a threshold value of foam quality (f_g) below which foams are stable exhibiting either fine-textured homogeneous "plug-flow pattern" or "segregated-flow pattern", and above which the flow consists of a repetition of fine-textured foam slugs and free-gas segments forming "slug-flow pattern". One may notice that a plot similar to Fig. 2.3 is no other than the change in effective foam viscosity along the vertical scanning line in Fig. 2.4 or 2.5, (i.e., increasing u_g at a fixed value of u_w). Then the low-quality regime and high-quality regime are described by the regions with $f_g<f_{gth2}$ and $f_g>f_{gth2}$, respectively, implying that

f_{gth2} is in fact identical to f_g*. No modeling attempts have been made to implement these trends observed by experiments, however.

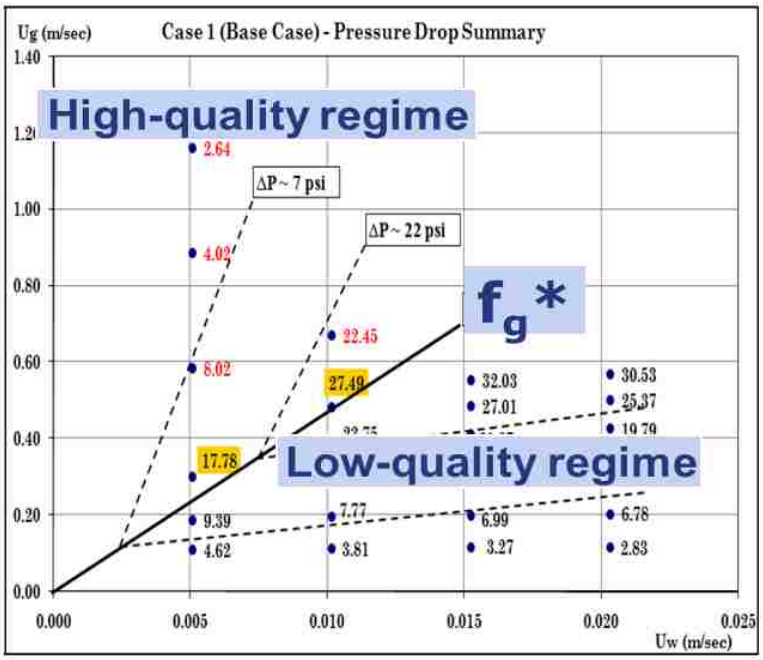

Figure 2.4: Two foam-flow regimes conjectured by Bogdanovic et al. (2009): the pressure contours and the boundary (f_g*) are hand-drawn and approximated by linear lines. (1 wt% of Cedepal FA-406 surfactant in distilled water as a liquid phase; nitrogen as gas phase; ΔP measured over 8.5 ft length 0.36 inch ID horizontal stainless steel pipe) .

Gajbhiye and Kam (2012) investigated the effect of inclination angles on two foam-flow regimes concept through an experimental study. They found out that in plug flow or slug flow pattern, where fine-textured foam is achieved, the direction of flow (or, inclination angle) has no significant effects on foam rheology because the viscous force is dominant in these flow regimes. However in segregated flow pattern, where there is a liquid layer is flowing with foam, foam rheology depends on flow direction because the gravitational force becomes more dominant over the viscous force.

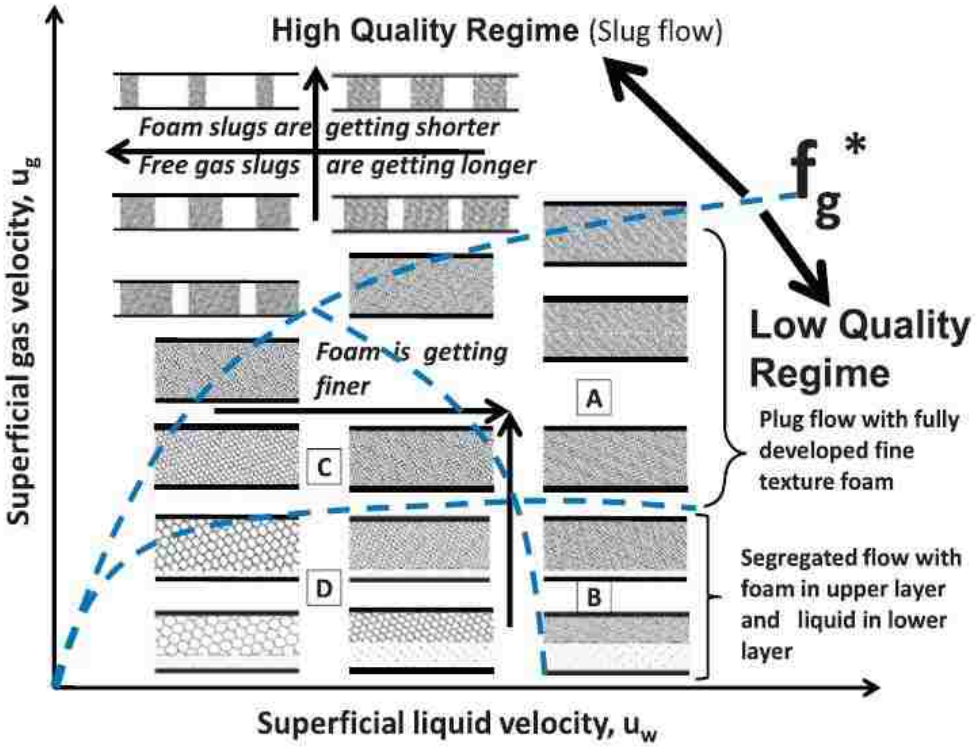

Figure 2.5: A schematic of different flow regimes of foam flow in pipes based on foam texture and flow pattern (Gajbhiye and Kam, 2011).

CHAPTER 3: TWO FOAM-FLOW REGIMES IN PRESENCE OF OIL AND POLYMER[1]

The objective of this chapter is to investigate foam flow characteristics using the concept of high-quality and low-quality regimes in horizontal pipes at different injection conditions with a special emphasis on the effects of oil and polymer, which is more relevant to the actual foam field applications. The specific goals from this chapter include (i) how the presence of oil shifts surfactant foam rheology by affecting foam rheology; (ii) how the behavior of polymer-added foams is different from that of polymer-free surfactant foams; and (iii) how to capture foam flow characteristics by using bubble size, bubble-size distribution, and flow patterns in a wide range of injection conditions to show the effects of oil and polymer comprehensively.

3.1 Methods

All experiments were conducted using experimental facilities shown in Fig. 3.1. The experimental set-up consisted of a transparent nylon pipe (12.6 ft long (3.84 m), 0.38/0.5 inch (0.97/1.27 cm) inner/outer diameters) with eight equally-spaced Omega pressure transducers (Omegadyne Inc., OH) named A through H from the inlet. The measured pressure data from transducers were transmitted into the data acquisition system. Surfactant solution and oil were injected into the pipe by using two Optos 3HM pumps (Eldex, CA) with the flow rate range of 0.04–80 cm^3/min and 0.04–10 cm^3/min, respectively. A 5850E Brooks mass flow controller (Brooks Instruments, PA) was used to regulate gas phase flow from a high-pressure nitrogen gas cylinder. Gas and liquid phases were introduced into the main pipe through 1/8-inch (0.32 cm) inner-diameter stainless steel tubing. For experiments with polymer-added surfactant foams, a 90 micron filter was placed upstream of the pipe in order to create high shear rate, which helps

[1] This chapter previously appeared as Edrisi, A.R., Gajbhiye, R.N., and Kam, S.I., Experimental Study of Polymer-free and Polymer-added Foams for Underbalanced Drilling: Are Two Foam-Flow Regimes Still There? Paper SPE162712 presented at the SPE Canadian Unconventional Resources Conference, Calgary, Canada, 30 October – 1 November, 2012. It is reprinted by permission of Society of Petroleum Engineers. Copyright 2012, Society of Petroleum Engineers. Further reproduction prohibited without permission. See appendix 2 for more details.

polymer solution create fine-textured polymerized foams. All the experiments have been carried out in a room temperature. A digital camera was used to videotape the flow of foam mixture inside the pipe for future analysis. Foam exiting from the pipe was accumulated in a bucket to be disposed of appropriately later. In all experiments, Stepanform-1050 (Stepan, IL) was used to prepare surfactant solutions; N-decane and nitrogen were used as oil and gas phase respectively; and Liquid Guar CM (Drilling Specialties Company, TX) was used as polymer chemical.

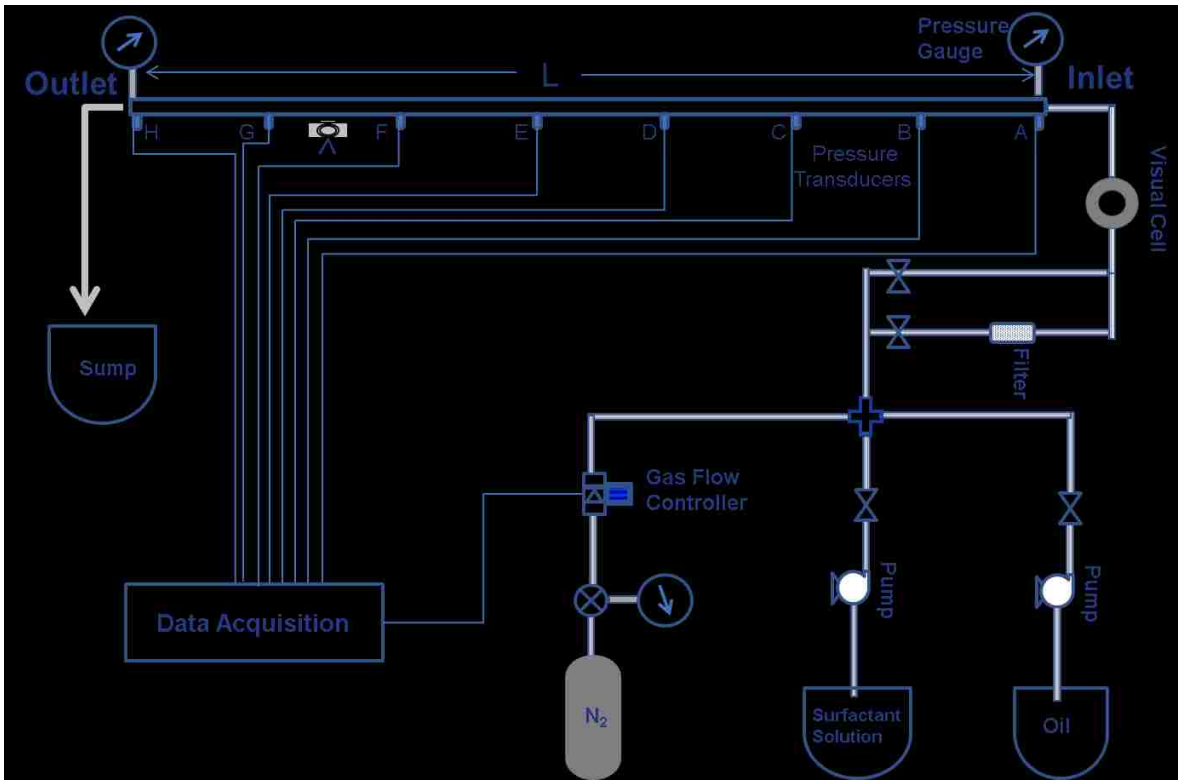

Figure 3.1: Experimental set-up for foam flow in horizontal pipes in this study.

Care should be taken during the preparation of polymer and surfactant solutions in order to produce samples with identical properties. Especially polymer hydrolysis should be conducted by repeating the same procedures due to the sensitivity of polymer solution to the magnitude and history of

shear rates. The steps described below were employed to produce 600 gram of 0.5 weight percent (wt%) surfactant solution with 0.5 wt% concentration of polymer used in this study.

Step 1: Pour 594 grams of deionized water into a blender cup.

Step 2: Add 3 grams of Liquid Guar CM.

Step 3: Stir the solution continuously with 14,000 rpm Single Spindle Hamilton Beach Mixer (Hamilton Beach, TX) for 10 minutes.

Step 4: Measure the viscosity of solution by using Fann V-G rotational viscometer (Fann Instrument Company, Houston, TX) at 300 RPM and 600 RPM.

Step 5: Add 3 grams of Stepanform surfactant into the polymer solution prepared.

Step 6: Pour the entire solution in a beaker and keep stirring with a magnetic bar. The solution is ready to be used for flow experiments.

The Hamilton Beach Mixer (part # 152-00 static upright stand mixer from OFITE Catalogue) offers rotational speeds ranging from 14,000 rpm to 24,000 rpm. Preliminary experiments showed that the duration of 10 minutes, a typical industry practice, was long enough to reproduce the same polymer solutions even at the lowest 14,000 rpm, which was then employed in all experiments in this study. Failure to create polymer solutions with the same properties affects the level of generating fine-textured foams at high shear rate in flow experiments.

For given gas and liquid flow rates, expressed by Q_g and Q_w respectively, the superficial velocities are defined as follows:

$$u_g = \frac{Q_g}{A} \quad \text{and} \tag{3-1}$$

$$u_w = \frac{Q_w}{A} \quad , \tag{3-2}$$

where A is the internal cross-sectional area of the pipe.

Apparent foam viscosity (μ_{app}) can be calculated based on the wall shear stress (τ_w) and wall shear rate ($\dot{\gamma}_w$) from fluid mechanics, i.e.,

$$\mu_{app} = \frac{\tau_w}{\dot{\gamma}_w} \quad , \tag{3-3}$$

$$\tau_w = \frac{\Delta P}{L}\frac{D}{4} \quad , \text{and} \tag{3-4}$$

$$\dot{\gamma}_w = \frac{8\, u_t}{D} \tag{3-5}$$

where, u_t is the total superficial velocity (i.e., $u_t = Q_t/A = (Q_g + Q_w)/A = u_g + u_w$), Δp is the pressure drop over the distance of L, and D is the pipe inner diameter.

3.2 Results and Discussions

Different types of foam flow experiments carried out in this study can be summarized as follows: (i) surfactant foam flow tests without oil and polymer; (ii) surfactant foam flow tests with oil but without polymer; and (iii) surfactant foam flow tests with polymer but without oil. In all experiments, 0.5 wt % Stepanform 1050 is used as surfactant solution, N-decane as oil phase, and Liquid Guar CM as polymer. In addition, the pressure drop between pressure ports B and G (i.e., the second and the second-last transducers from the inlet; cf. Fig. 3.1) is used to evaluate foam viscosity in order to eliminate possible inlet and outlet effects that influence pressure readings at ports A and H. Such a step is shown to be necessary as shown by Bogdanovic et al. (2009) in similar experimental designs. This section covers details about polymer preparation followed by experimental results of the three types of flow tests mentioned above.

3.2.1 Polymer Preparation

Because the properties of polymer-added foams are sensitive to the way how polymer solutions are prepared, caution should be taken to make homogeneous and reproducible polymer solutions. As shown in Fig. 3.2, the addition of Liquid Guar CM polymer into water (i.e., heterogeneous solution in Fig. 3.2(a) before hydrolysis) should be followed by agitation of the fluid with high rpm resulting in a homogeneous solution after hydrolysis (cf. Fig. 3.2(b)). If the agitation is not vigorous enough (or the applied rpm is not high enough), the polymer is not fully dispersed in the solution leaving crumbs on the water surface (Fig. 3.2(c)). The testing with the Single Spindle Hamilton Beach Mixer at three values of rpm available (14,000, 21,000, and 23,900 rpm) shows that 14,000 rpm is high enough to achieve a homogeneous solution. Additional experiments with different agitation times (5, 15, 30, and 60 minutes) show that the apparent viscosity values at 300 rpm and 600 rpm measured by Fan VG rotational viscometer are almost identical and stable irrespective of agitation time when 14,000 rpm is tried.

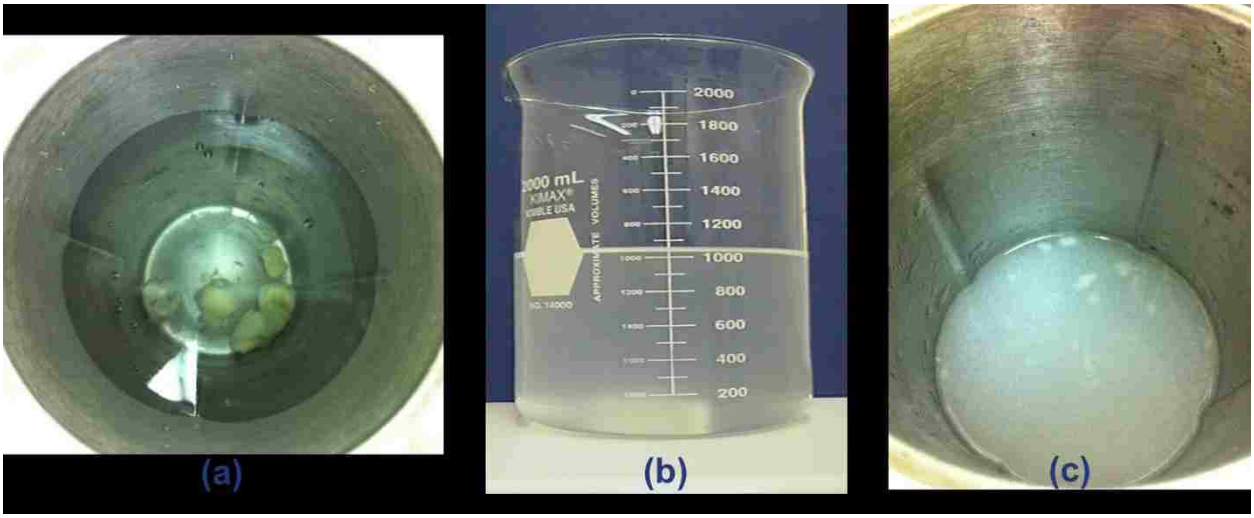

Figure 3.2: Preparation of polymer solutions: (a) addition of Liquid Guar CM before mixing; (b) a homogeneous polymer solution after mixing; and (c) a heterogeneous polymer solution after incomplete mixing.

Next testing is carried out to figure out the role of Single Spindle Hamilton Beach Mixer. Two different experiments are compared: (i) the use of a magnetic stirring bar at its highest rotation speed without Single Spindle Hamilton Beach Mixer involved and (ii) the use of Single Spindle Hamilton Beach Mixer (14,000 rpm for 60 minutes) followed by continuous agitation with a stirring bar at its highest rotation speed. Notice that the use of a stirring bar at its highest rotation speed also gives a homogeneous solution after 60 minutes of agitation (cf. Fig. 3.2(b)). The apparent viscosity results measured at 300 rpm and 600 rpm in Fig. 3.3 show that the Liquid Guar CM polymer solution prepared by the mixer not only provides higher values during initial mixing period, but it also produces a solution which can maintain the initial viscosity values for a longer period – there is a significant decay in viscosity values once the solution is prepared by stirring bar only. This outcome is important because the polymer solution prepared by the mixer (Fig. 3.3(a)) guarantees the long-term stability of the polymer solution, which then hints how often fresh polymer solutions should be made during lab experiments.

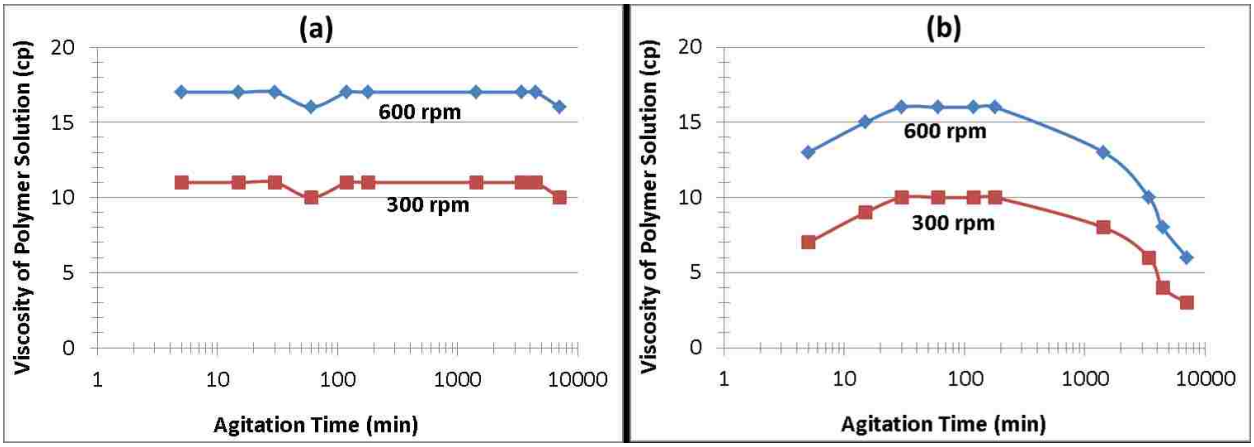

Figure 3.3: Viscosity of polymer solution at two different rates, 300 and 600 RPM, as a function of time: (a) mixing with Hamilton Beach Mixer (first 60 minutes) followed by magnetic stirring bar; (b) mixing with a magnetic bar only.

Another testing is conducted after mixing the polymer solution, prepared as described above, with Stepanform surfactant chemicals in order to evaluate foaming capability in the presence and absence of

foam generator. Note that the foam generator in this study is a filter with 90 micron opening size. When this polymer-added surfactant solution (0.5 wt% Stepanform and 0.5 wt% Liquid Guar CM) is injected into the pipe through stainless steel tubing (1/16 inch (0.16 cm) inner diameter) at Q_w = 20 cc/min together with nitrogen at various Q_g values as shown in Fig. 3.4, the measured pressure drops at eight pressure transducers are remarkably different between the case without foam generator (maximum pressure near up to 1.2 psi in Fig. 3.4(a)) and the case with foam generator (maximum pressure up to 9 psi in Fig. 3.4(b)). This proves that the common technique of using high shear rate to create fine-textured polymer-added foam is consistent with the observation in this study.

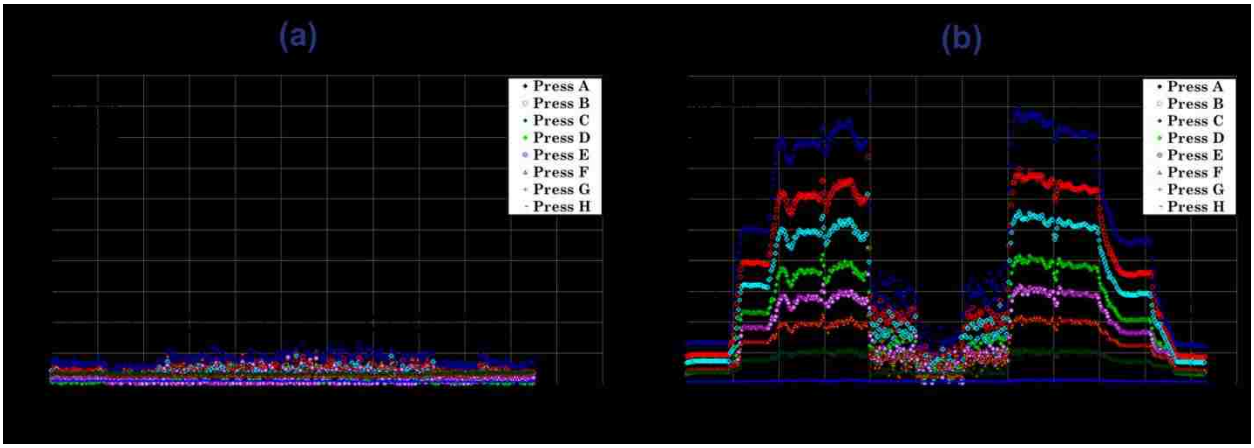

Figure 3.4: Pressure profile of polymer solution (0.5 wt% Liquid Guar CM, Q_w = 20 cm^3/min) measured at 8 pressure taps along the pipe: (a) without foam generator; and (b) with foam generator (90 micron filter). The system fails to generate fine-textured foams at low shear rate (i.e., without foam generator) as expected.

3.2.2 Flow Experiments with Surfactant Foams (without Oil and Polymer)

Fig. 3.5 shows pressure responses from all eight pressure ports (A through H) during coinjection of gas and surfactant solution in the absence of oil and polymer. The liquid injection rate (Q_w) is fixed at 60 cm^3/min while the gas injection rate (Q_g) varies from 200 to 5000 cm^3/min, and then back to 200 cm^3/min. As previous studies reported (Bogdanovic et al., 2009; Gajbhiye and Kam, 2011), the pressure

drop increases with increasing gas rate at low Q_g range (which is a typical symptom of low-quality regime), while the pressure drop decreases with increasing gas rate at high Q_g range (which is a symptom of high-quality regime).

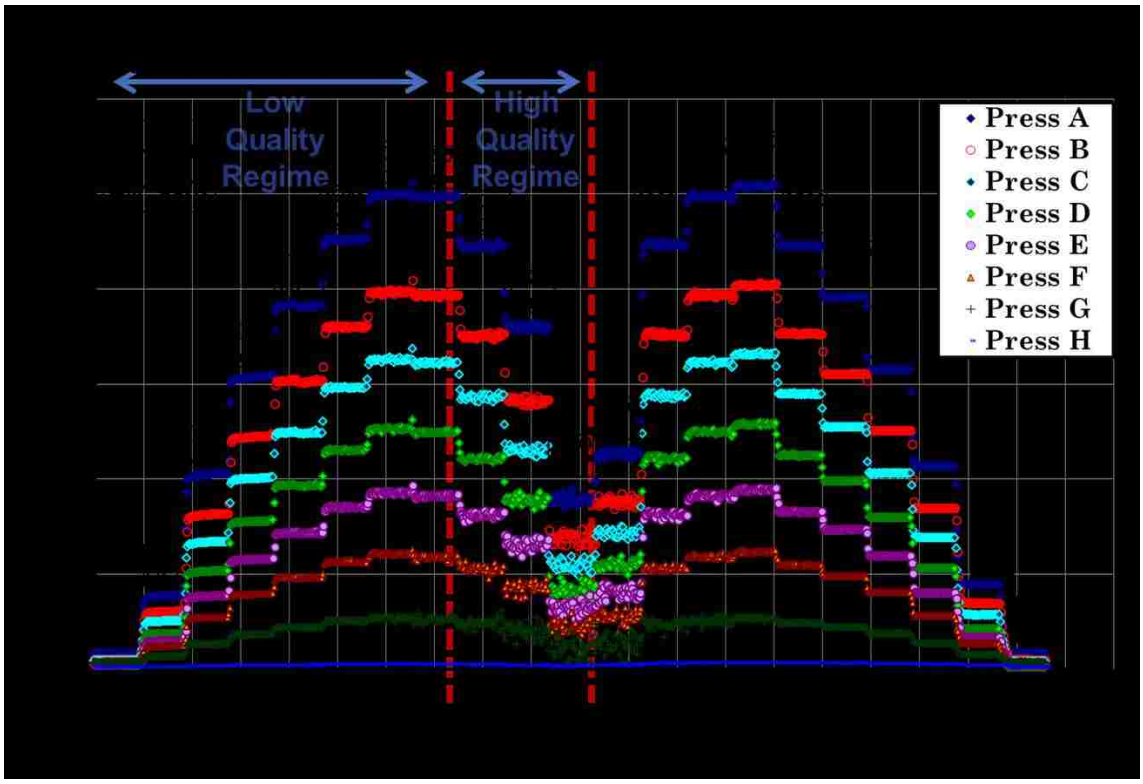

Figure 3.5: Pressure profile of surfactant foams (Stepanform 0.5 wt%, Q_w=60 cm^3/min): gas injection rate was increased from 200 to 5000 cm^3/min, and then was reduced back to 200 cm^3/min.

Fig. 3.6 shows the pressure responses at four liquid injection rates (20, 40, 60 and 80 cm^3/min) in experiments similar to Fig. 3.5 (Note that Fig. 3.6(c) is identical to Fig. 3.5). The stabilized pressure drop measured between pressure ports B and G (ΔP_{BG}) at each combination of gas and liquid rates in Figs. 3.6(a) through 3.6(d) can be plotted as shown in Fig. 3.7. Note that the actual gas rate (Q_g^{actual}) on the x axis is calculated at the average system pressure (P_{avg}), which is, $P_{avg} = P_{back} + (P_B + P_G)/2$ where P_{back} is kept at 1 atm in all experiments. Foam quality (f_g) values reported in this study are also based on the actual gas rate (Q_g^{actual}) and injection liquid rate (Q_w), accordingly. There are two sets of data available

from each of the plots in Fig. 3.6 – one by increasing and the other by decreasing gas flow rate – which are expressed by filled and open symbols, respectively, in Fig. 3.7. A pressure contour plot can be constructed as shown in Fig. 3.8, by using the data points with filled symbols in Fig. 3.7. It is worth mentioning that the maximum ΔP_{BG} at each curve in Fig. 3.7 is translated into the value of f_g* in Fig. 3.8 such that the 2-dimensional contour plot is separated by a locus of f_g*. Bogdanovic et al. (2009) named the region above f_g* "high quality regime" and below f_g* "low quality regime". Overall responses in Figs. 3.5 through 3.8 are consistent with their findings.

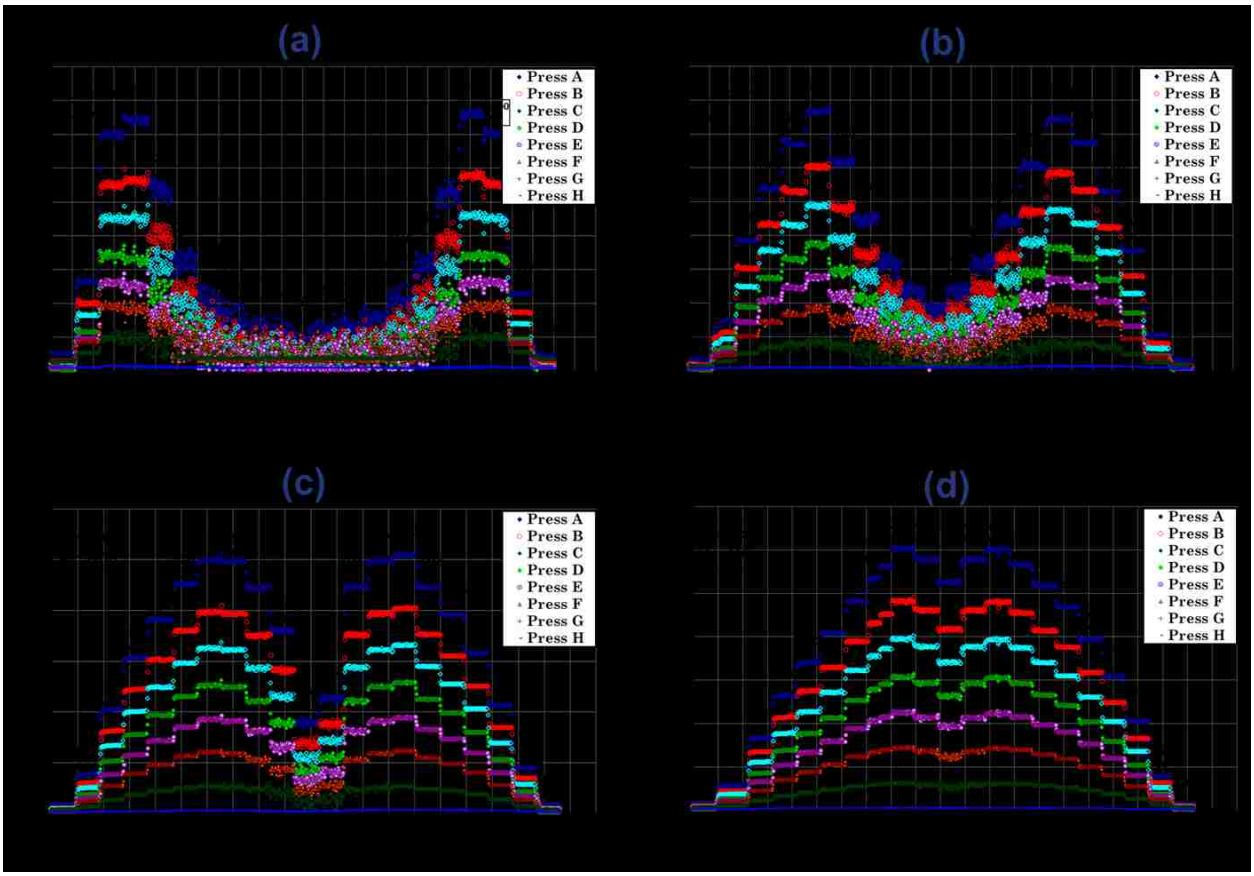

Figure 3.6: Pressure profile of surfactant foams (Stepanform 0.5 wt%): (a) Q_w=20 cm^3/min, (b) Q_w=40 cm^3/min, (c) Q_w=60 cm^3/min, and (d) Q_w=80 cm^3/min at various Q_g from 200 to 5000 sccm.

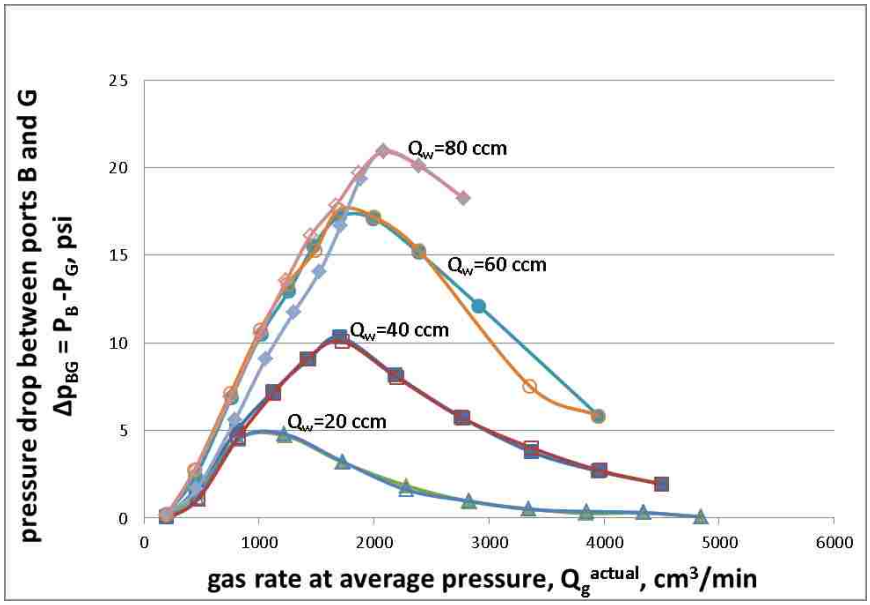

Figure 3.7: Pressure drop between ports B and G (ΔP_{BG}) as a function of various gas and liquid rates during surfactant foam injection (Stepanform 0.5 wt%).

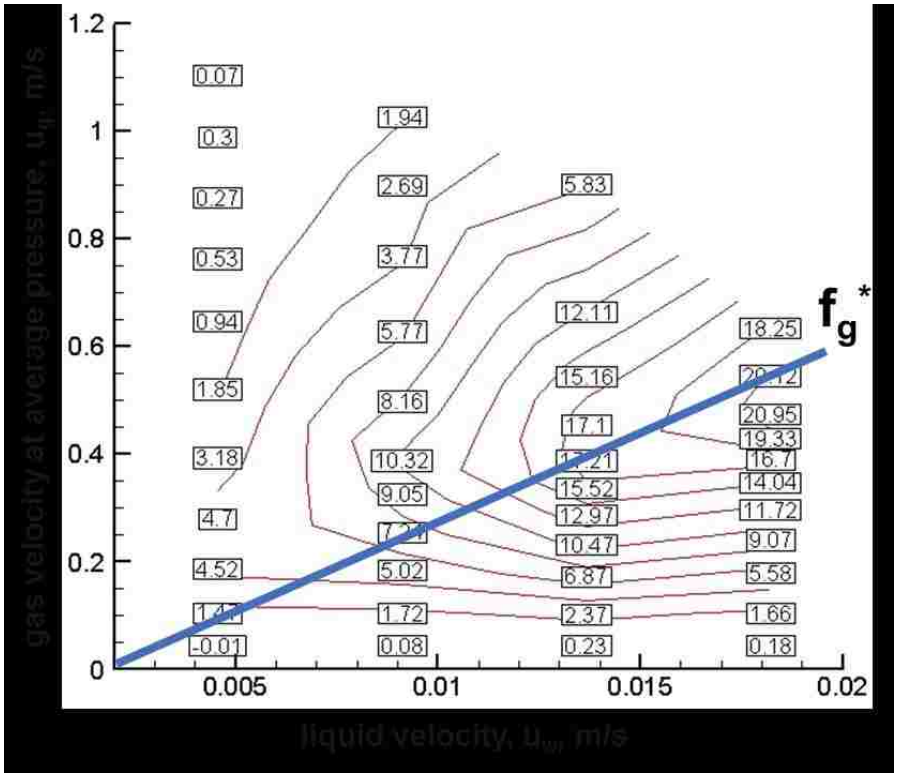

Figure 3.8: Contour plot of pressure drop between ports B and G (ΔP_{BG}) in psi for surfactant foams (Stepanform 0.5 wt%) as a function of gas and liquid velocities. Note that the pressures in boxes are experimentally measured values, and f_g^* is the boundary line separating the high-quality and low-quality regimes based on the pressure contours. (1 psi = 6900 Pa)

3.2.3 Flow Experiments with Surfactant Foams and Oil

Fig. 3.9 shows foam experiments at the same four surfactant injection rates (Q_w = 20, 40, 60 and 80 cm^3/min) but with oil injected together at Q_o = 0.5 cm^3/min. Note that Q_o is significantly smaller than Q_w because the situation of interest is a trace amount of oil entering the bottom hole during foam underbalanced drilling. Compared with Fig. 3.6 with no oil, the responses with oil in Fig. 3.9 are similar: (i) at given surfactant injection rates (Q_w), the pressure drop increases with Q_g until foam quality (f_g) reaches f_g* (i.e., low-quality regime), then decreases with Q_g as f_g goes beyond f_g* (i.e., high-quality regime); (ii) all plots are mirror-imaged meaning that there is no hysteresis involved; and (iii) the pressure data are stable in the low-quality regime but are fluctuating significantly in the high-quality regime, which is caused by different foam flow patterns (stable plug flow or segregated flow in the low-quality regime, while unstable slug flow pattern in the high quality regime) as illustrated in Fig. 2.3. The first two aspects are also well demonstrated in Fig. 3.10.

In addition, when compared with Fig. 3.7, the measured ΔP_{BG} in Fig. 3.10 shows two typical symptoms in the presence of oil: (i) the peak value of ΔP_{BG} is lower with oil (for example, ΔP_{BG} = 4, 8, 13, and 19 psi in Fig. 3.10 while ΔP_{BG} = 5, 10, 18, and 22 psi in Fig. 3.7 at Q_w = 20, 40, 60, and 80 cm^3/min, respectively) and (ii) the magnitude of Q_g at which the ΔP_{BG} peak takes place is also reduced with oil (for example, Q_g at the ΔP_{BG} peak = 849 and 1476 cm^3/min in Fig. 3.10 while Q_g at the ΔP_{BG} peak = 1220 and 1724 cm^3/min in Fig. 3.7 at Q_w = 20 and 40 cm^3/min, respectively). These two aspects are also shown in pressure contours in Fig. 3.11 – a slight reduction in pressure drop and f_g* value. Although not shown in this study, the additional experiments at different oil rates (Q_o = 0.1 and 0.5 cm^3/min) and different surfactants also show similar responses. This implies that the intrusion of oil during foam drilling, although in small quantity, influences foam stability, and therefore should be accounted for in foam drilling hydraulics calculations.

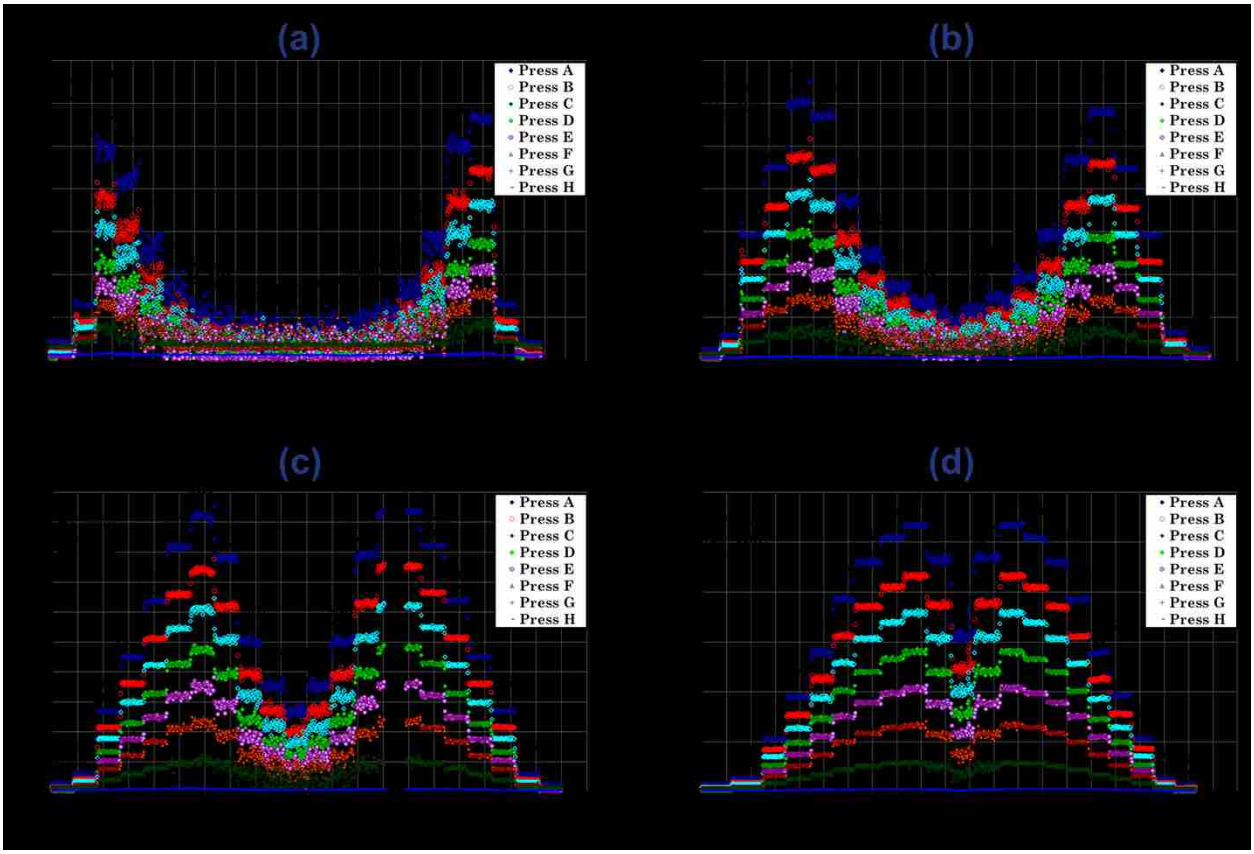

Figure 3.9: Pressure profile of surfactant foams (Stepanform 0.5 wt%) with oil (0.5 cm^3/min): (a) Q_w=20 cm^3/min, (b) Q_w=40 cm^3/min, (c) Q_w=60 cm^3/min, and (d) Q_w=80 cm^3/min at various Q_g from 200 to 5000 sccm.

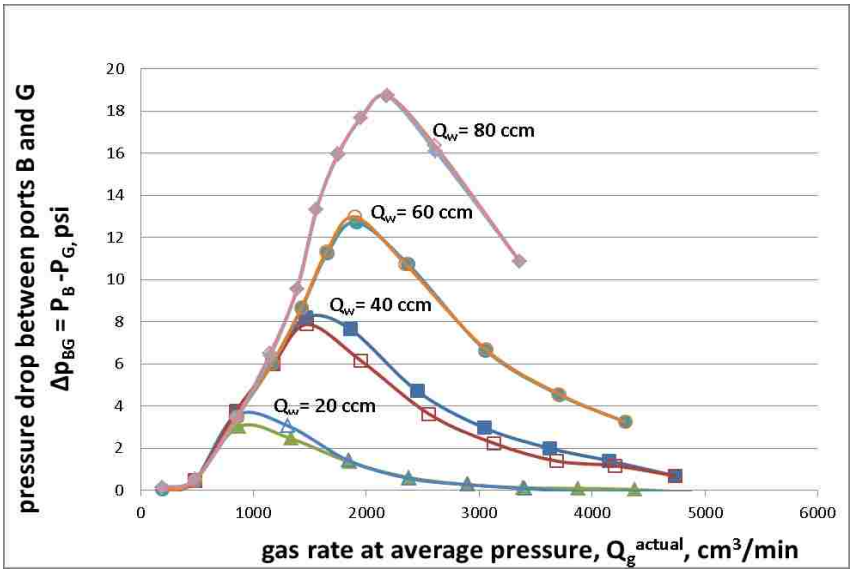

Figure 3.10: Pressure drop between ports B and G (ΔP_{BG}) as a function of various gas and liquid rates during surfactant foam injection (Stepanform 0.5 wt%) with oil (Q_o= 0.5 cm^3/min).

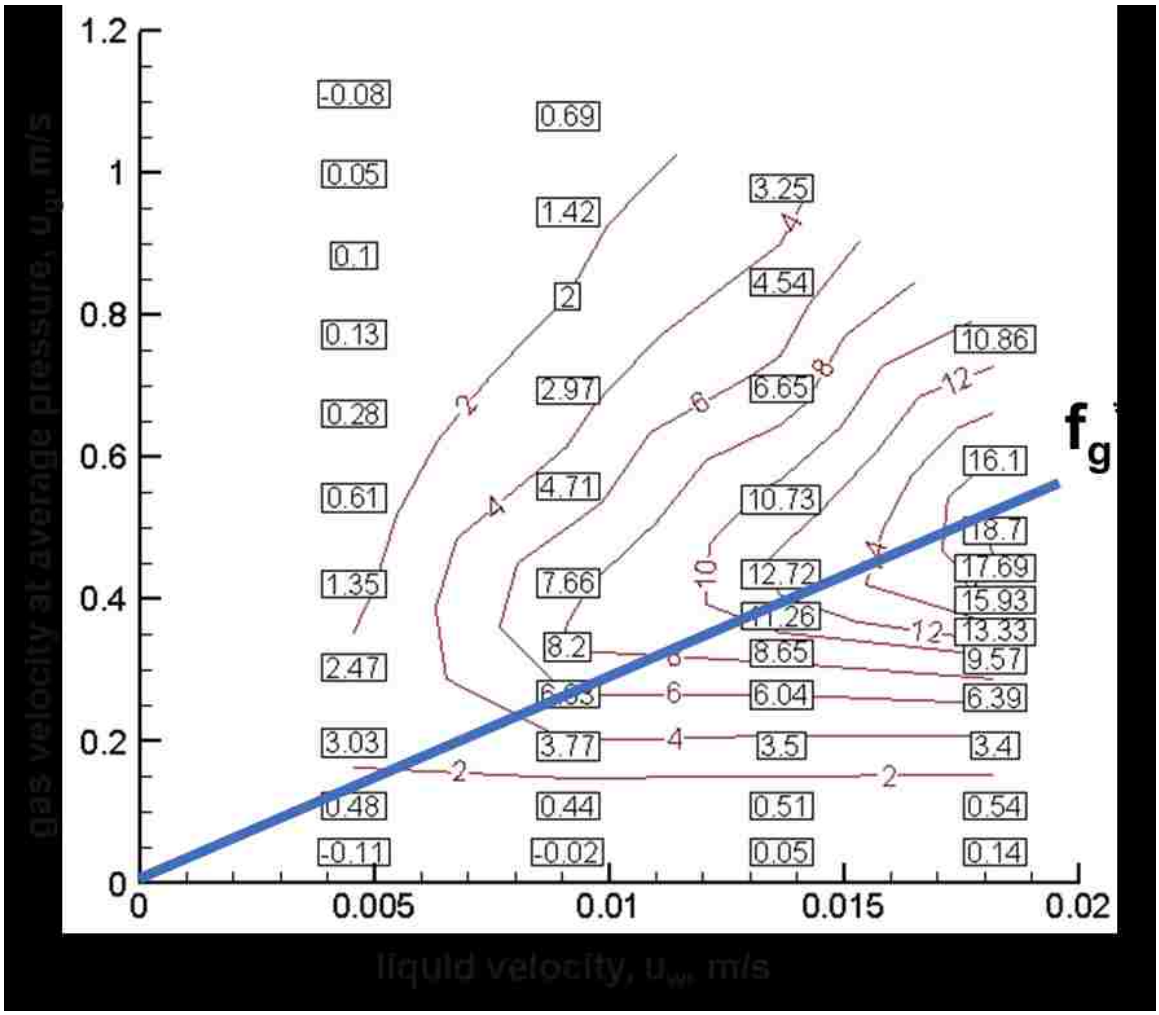

Figure 3.11: Contour plot of pressure drop between ports B and G (ΔP_{BG}) in psi for surfactant foams (Stepanform 0.5 wt%) in presence of oil (Q_o= 0.5 cm^3/min) as a function of gas and liquid velocities. Note that the pressures in boxes are experimentally measured values, and f_g* is the boundary line separating the high-quality and low-quality regimes based on the pressure contours. (1 psi = 6900 Pa)

3.2.4 Flow Experiments with Polymer-added Surfactant Foams

The experiments with polymer are conducted with surfactant solution with 0.5 wt% Stepanform and 0.5 wt% Liquid Guar CM. Because of the time required for preparing polymer solution, liquid injection rates of 10, 20, and 40 cm^3/min are attempted as shown in Figs. 3.12, 3.13, and 3.14, respectively.

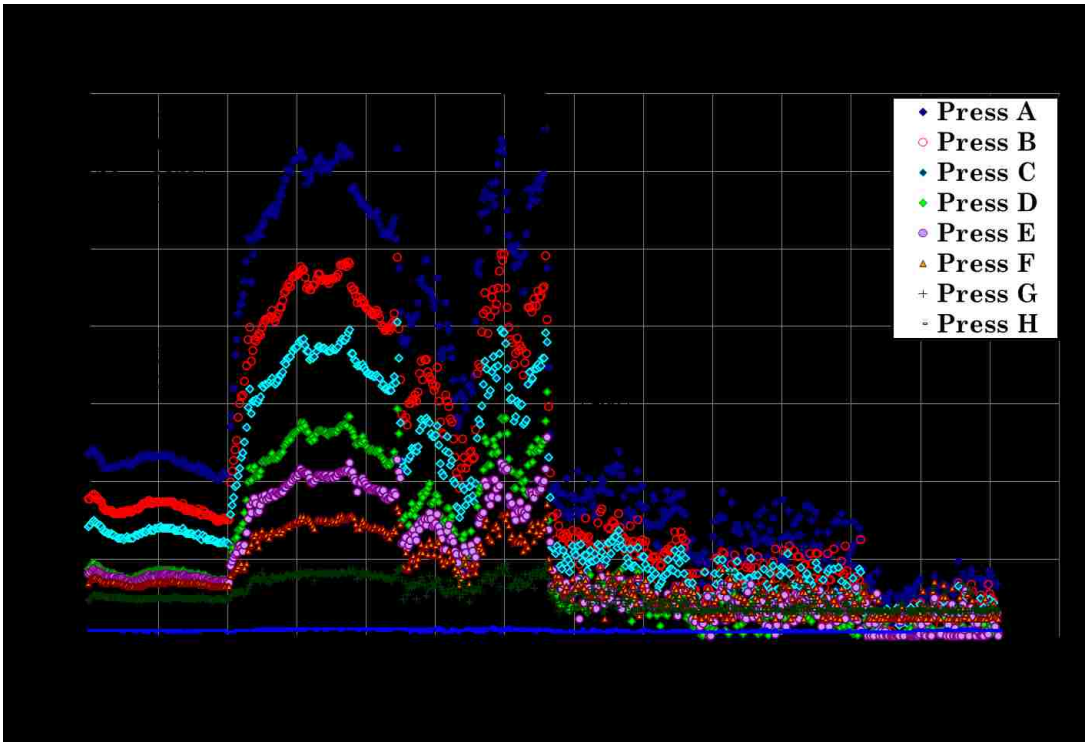

Figure 3.12: Pressure profile of polymer-added surfactant foams (Stepanform 0.5 wt%, Liquid Guar CM 0.5 wt%) at Q_w= 10 cm^3/min.

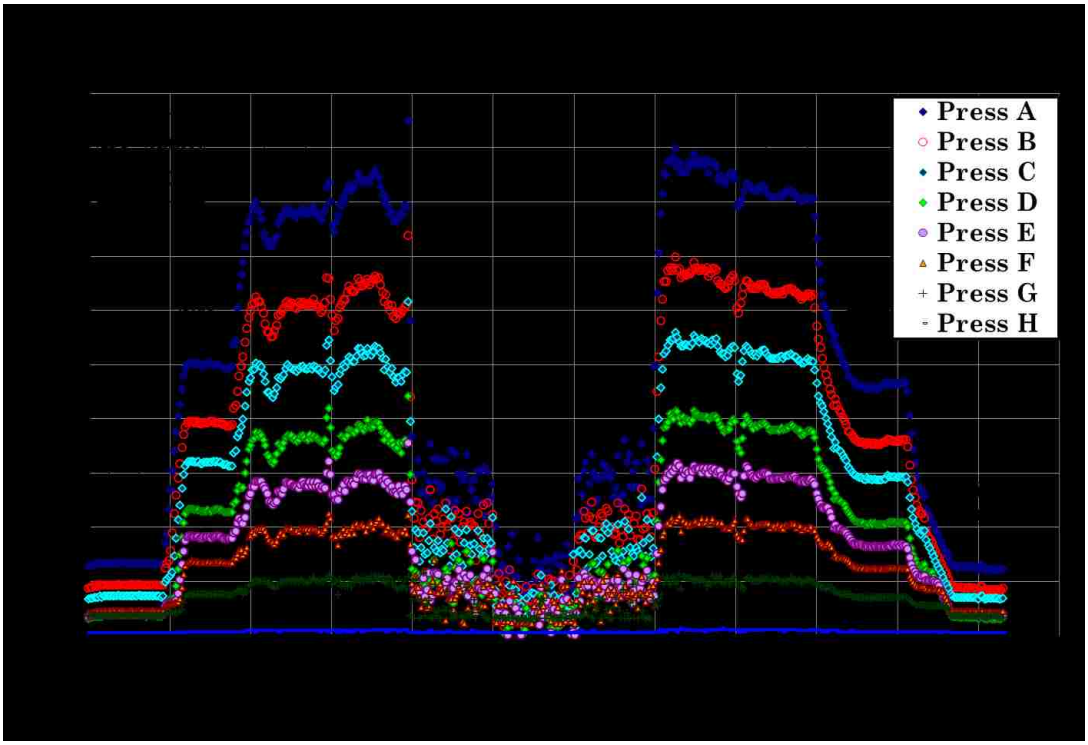

Figure 3.13: Pressure profile of polymer-added surfactant foams (Stepanform 0.5 wt%, Liquid Guar CM 0.5 wt%) at Q_w= 20 cm^3/min.

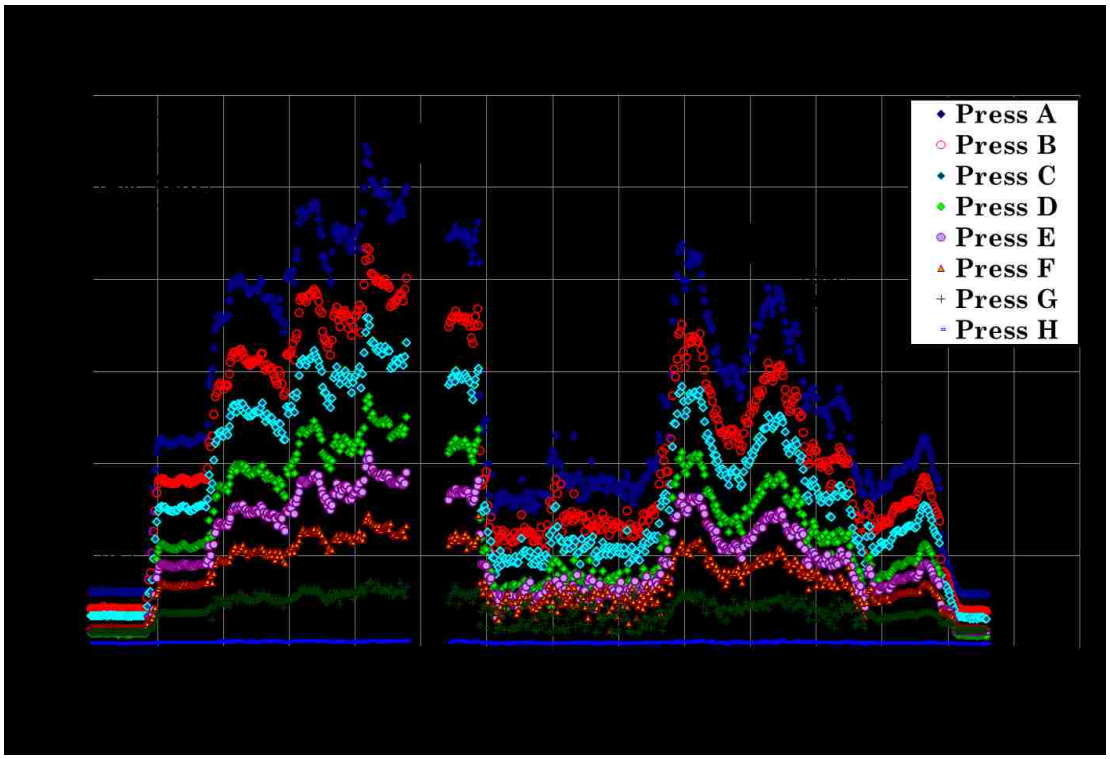

Figure 3.14: Pressure profile of polymer-added surfactant foams (Stepanform 0.5 wt%, Liquid Guar CM 0.5 wt%) at Q_w= 40 cm^3/min.

Fig. 3.12 shows a series of experiments by varying Q_g from 200 to 2,000 cm^3/min at fixed Q_w of 10 cm^3/min. The overall system response may seem similar to those responses in Figs. 3.6 and 3.9: the flow pattern at low Q_g (i.e., Q_g=200 cm^3/min) is plug flow with fine-textured foams, leading to stable pressure responses (note that this is a typical symptom of low-quality regime at $f_g<f_g^*$); and the flow pattern at high Q_g (i.e., Q_g=500, 1,000, and 2,000 cm^3/min) is slug flow with intermittency between free gas and fine-textured foam, leading to unstable pressure responses (note that this is a typical symptom of high-quality regime at $f_g>f_g^*$). A dramatic difference, however, is observed in between (i.e., Q_g=300 and 400 cm^3/min) where the pressure response becomes hardly converging into a stabilized value. For example, when Q_g is set to 300 cm^3/min, the pressure rises rapidly at first (1,000 sec < t < 1,500 sec on

the x axis) but drops fast immediately after that (1,800 sec < t < 2,700 sec). The same response is also observed when Q_g is set to 400 cm^3/min – the pressure response seems changing chaotically.

The same experiments are shown in Figs. 3.13 and 3.14 where the injection Q_w is 20 and 40 cm^3/min, respectively, by changing Q_g (200 – 2,000 cm^3/min in Fig. 13 or 200 – 3,000 cm^3/min in Fig. 3.14). Although the behavior at low Q_g with stable pressure responses backed by plug flow and the behavior at high Q_g with unstable pressure responses backed by slug flow are the same, the unusual responses – the system not converging - are still there. For example, Q_g = 500 cm^3/min in Fig. 13 and Q_g = 600, 800, and 1,000 cm^3/min in Fig. 3.14 do not show converging responses. In addition, this chaotic behavior occurring in mid-range Q_g values often makes the plot not mirror-imaged any longer (cf. Q_g = 600, 800, and 1,000 cm^3/min in Fig. 3.14).

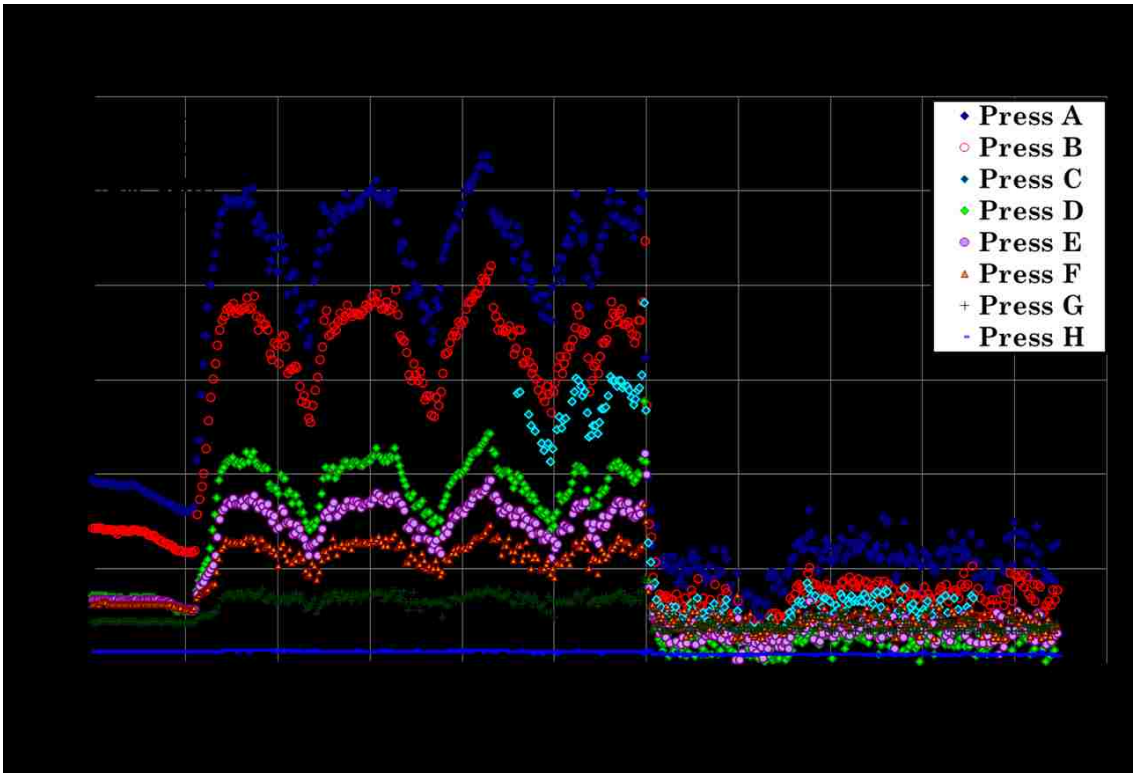

Figure 3.15: Pressure profile of polymer-added surfactant foams (Stepanform 0.5 wt%, Liquid Guar CM 0.5 wt%) at Q_w= 10 cm^3/min: repeated to compare with Fig. 3.12.

In order to understand this chaotic behavior better, more experiments are carried out. One example is shown in Fig. 3.15 in which Q_w is fixed at 10 cm^3/min but Q_g is varied from 200 to 400 cm^3/min, to be compared with Fig. 3.12 (1,000 sec < t < 3,300 sec). This result shows two interesting findings: (i) the chaotic behavior shown with Q_g = 300 cm^3/min in Fig. 3.12 is still observed in Fig. 3.15 and, furthermore, the behavior repeats between the upper and lower ends of pressure; and (ii) the pressure response with Q_g = 400 cm^3/min in Fig. 3.12 is not shown in Fig. 3.15, implying that the chaotic behavior may not be easily reproducible in some cases.

Fig. 3.16 shows pressure contours with the average pressure values measured during the experiments. The range of gas and liquid rates which ends up with chaotic behavior (never reaching a steady state as shown in Figs. 3.12 through 3.15) is shown by the envelope expressed by dashed line. It is interesting to find that (i) the overall pressure contours still exhibit both high-quality and low-quality regimes, and (ii) the region, which is affected by the chaotic behavior, is located near the boundary between the two regimes. The implication of this outcome is that polymer-added surfactant foams can still be modeled by two flow regime concepts with some uncertainty near the f_g* value.

The experimental responses shown in Figs. 3.13 to 3.16 with 0.5 wt% Liquid Guar CM seem typical in polymer-added surfactant foams. Fig. 3.17 shows an example with 0.1 wt% Liquid Guar CM at Q_w = 20 cm^3/min to be compared with Fig. 3.13. At this lower polymer concentration, the pressure values do not converge easily in the Q_g range of 300 - 600 cm^3/min, showing a dramatic change in pressure values especially at Q_w = 600 cm^3/min. The plot of pressure drop shown in Fig. 3.18, once again, demonstrates the same behavior as described in Fig. 3.15, which is, the high-quality regime at high f_g, the low-quality regime at low f_g, and the chaotic transition region in between.

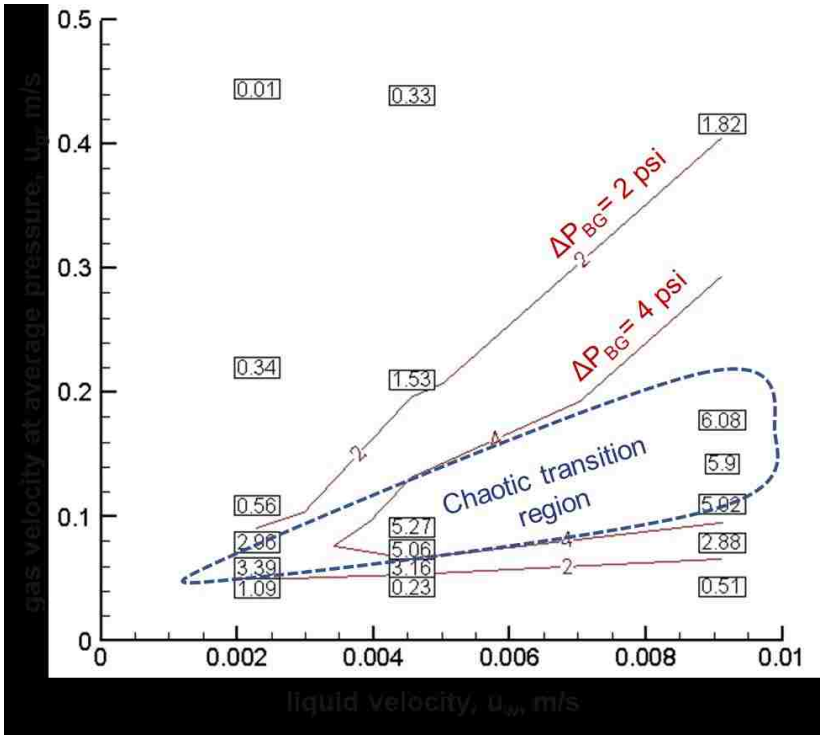

Figure 3.16: Contour plot of pressure drop between ports B and G (ΔP_{BG}) in psi for polymer-added surfactant foams (Stepanform 0.5 wt%, Liquid Guar CM 0.5 wt%) as a function of gas and liquid velocities. (1 psi = 6900 Pa)

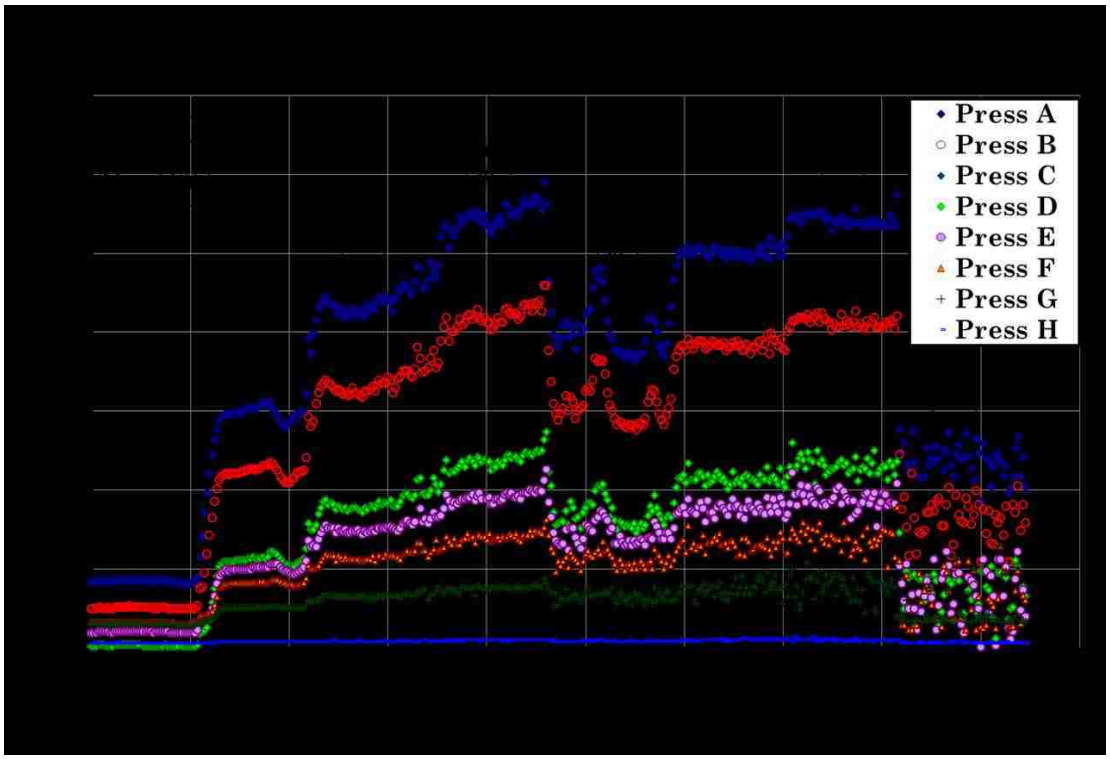

Figure 3.17: Pressure profile of polymer-added surfactant foams (Stepanform 0.5 wt%, Liquid Guar CM 0.1 wt%) at Q_w= 20 cm^3/min.

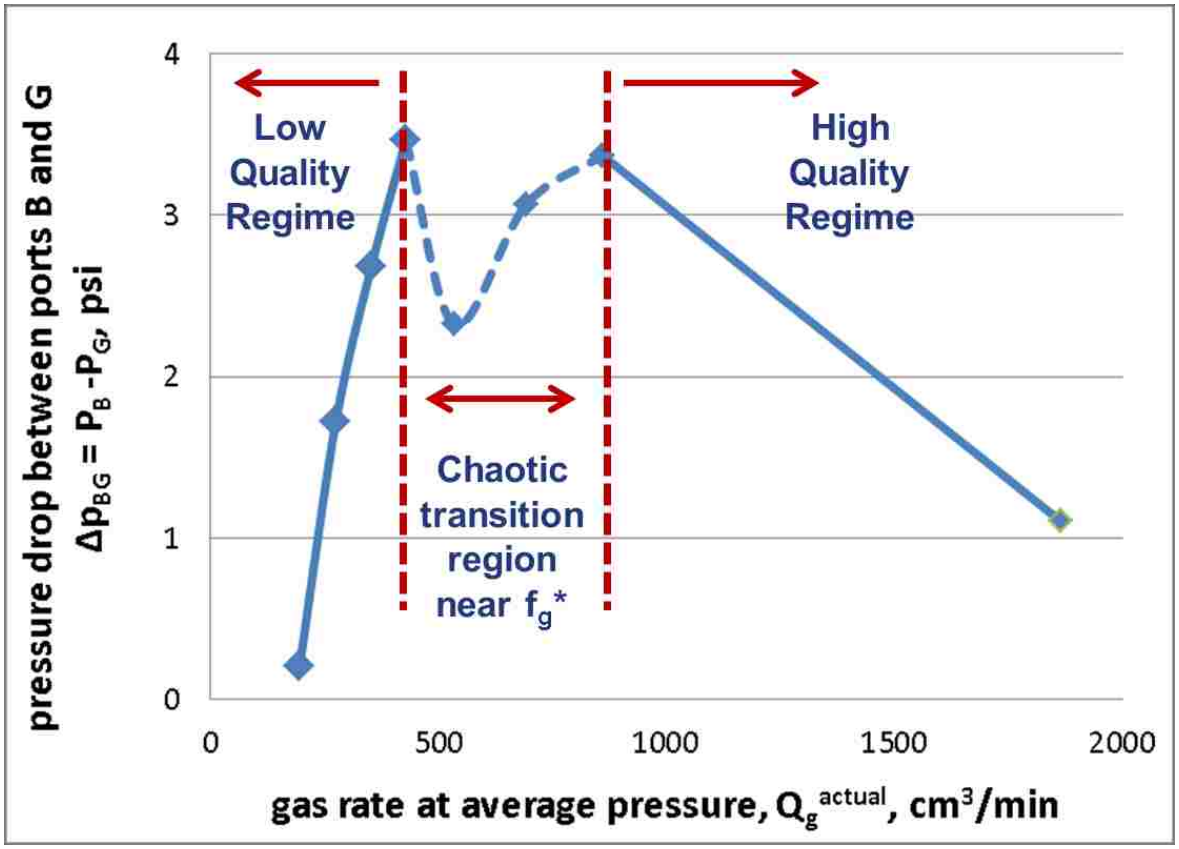

Figure 3.18: Pressure drop between ports B and G (ΔP_{BG}) during surfactant foam injection during polymer-added surfactant foam injection (Stepanform 0.5 wt%, Liquid Guar CM 0.1 wt%) at Q_w= 20 cm^3/min.

In order to investigate what makes this difference near f_g*, a careful visual analysis is followed as shown in Fig. 3.19, comparing polymer-free (Fig. 3.19(a)) and polymer-added (Fig. 3.19(b)) surfactant foams. In the absence of polymers (Fig. 3.19(a)), there are four flow patterns observed based on the pressure response and flow pattern – segregated and plug flow patterns in the low-quality regime and slug and mist flow patterns in the high-quality regime. Note that a schematic drawing for each flow pattern is also provided: (1) for segregated flow pattern with bubbles flowing at the top and liquid flowing on the bottom at different velocities; (2) for plug flow pattern with homogeneous fine-textured foam flow; (3) for slug flow pattern near f_g* showing foams and free gas, intermittently and repeatedly, with relatively

short free-gas sections, and (4) for slug flow pattern away from f_g* (i.e., closer to mist flow pattern) showing foams and free gas intermittently and repeatedly with relatively short foam sections. Beyond that, mist flow pattern is observed with liquid droplets as internal phase within external gas phase (with some foam residue occasionally flow on the bottom).

When the same experiments are conducted in the presence of polymers (Fig. 3.19(b)), the overall response is similar to two flow regimes and four flow patterns explained in Fig. 3.19(a), but with the chaotic transition region as described in Figs. 3.13 through 3.16. Close visual observation shows that the bubble size distribution and flow pattern in the chaotic region do not reach an equilibrium state – the system tends to continuously shift from one to another among three states depicted by (5), (6) and (7) in which the foam mixture consists of different bubble size distributions. That is why the pressure response tends to change dramatically even at fixed gas and liquid rates – when foams are made of relatively narrower bubble size distribution as shown in (5), the pressure drop is higher; while when foams are made of relatively broader bubble size distribution as shown in (7), the pressure drop is lower. It appears that there is a strong competition between bubble-generation and bubble-coalescence mechanisms within the chaotic transition region, but the system simply fails to be governed by any one state. This implies that, at fixed liquid rate, a slight decrease in gas rate is likely to push the mixture to fine-textured plug-flow pattern (i.e., bubble generation dominant induced by wetter foams), and a slight increase in gas rate is likely to push to the mixture to slug flow pattern (i.e., bubble coalescence dominant induced by drier foams), which is in fact consistent with Fig. 3.19(b). Fig. 3.20 shows actual photos taken from experiments showing different foam flow patterns depicted from (1) through (7).

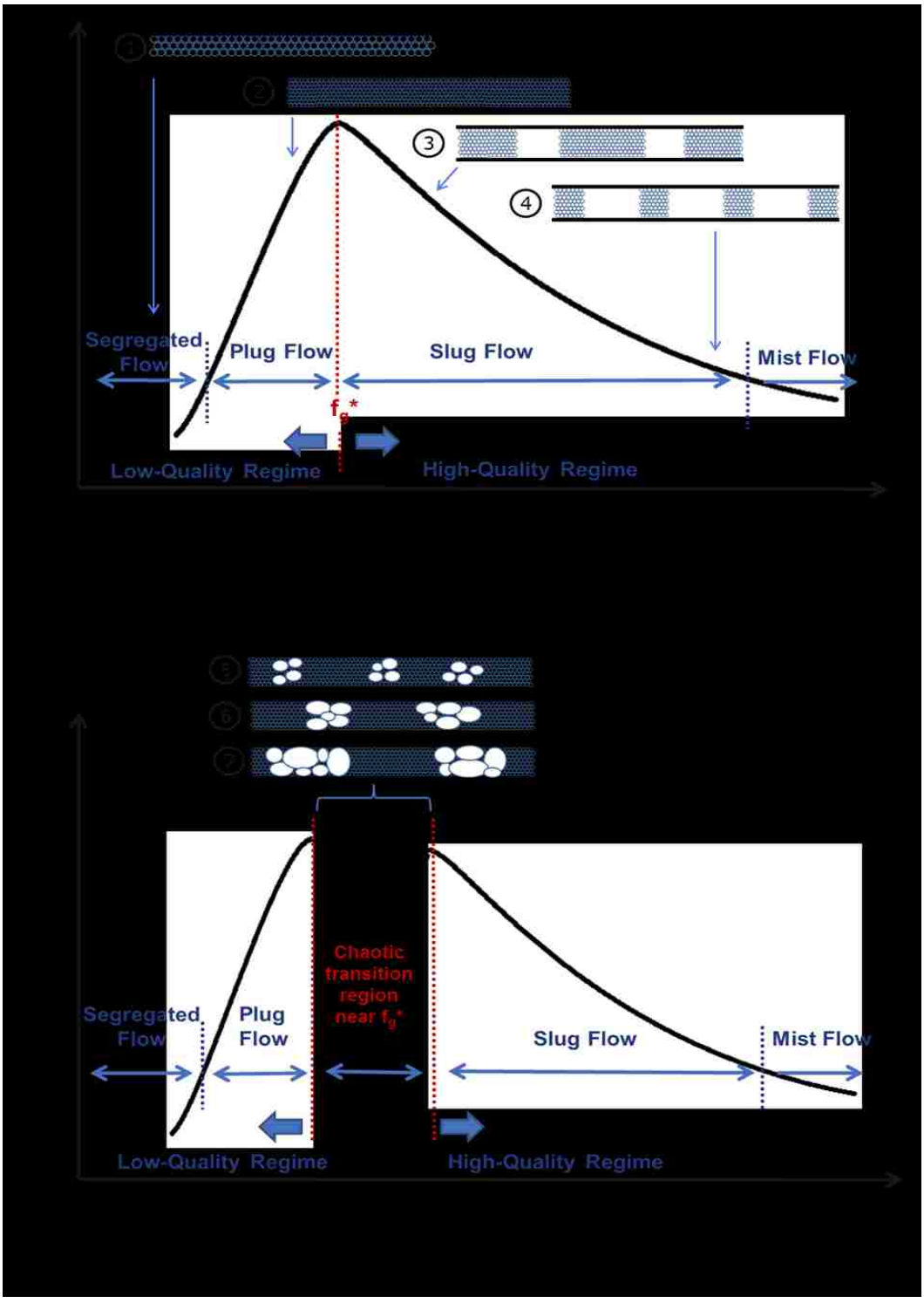

Figure 3.19: Comparison of foam flow characteristics between (a) polymer-free and (b) polymer-added surfactant foams in terms of pressure profile plot.

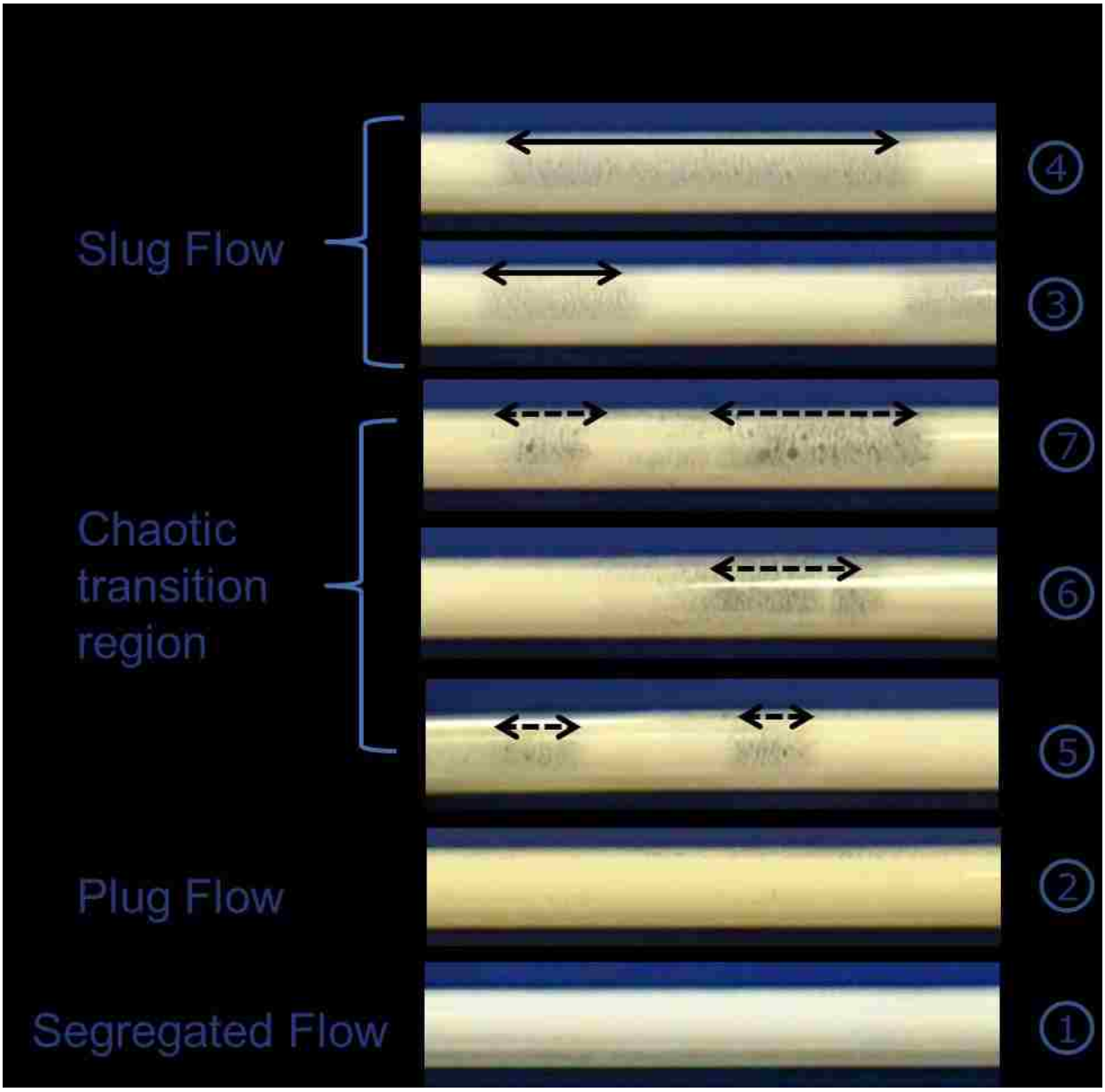

Figure 3.20: Actual photos of different flow characteristics shown in Fig. 3.19.

This chaotic behavior represented by (5) to (7) in Fig. 3.19(b) is believed to happen due to the increase in water viscosity by adding polymers. Without polymers, the mixture reaches equilibrium rapidly because large bubbles easily break up into smaller bubbles by high shear rate, and small bubbles readily coalesce into large bubbles due to mechanical disturbance and film drainage of water into the

Plateau boarders (Kraynik, 1988). With polymers present, however, the water with higher viscosity reduces bubble creation even at high shear stress because it is more difficult to agitate high-viscosity fluid, and slows down water transport through foam films and thus resists to bubble coalescence. It is unclear at this stage if the mixture converges into equilibrium essentially, if the experiments are conducted for an extended period.

Fig. 3.21 shows the effect of chaotic transition region in terms of pressure contours. In the absence of polymers, the pressure contours exhibit two flow regimes and four flow patterns ((1) through (4) consistent with drawings in Fig. 3.19(a)). On the other hand, once polymers are present, the chaotic transition region appears between slug and plug flow patterns ((1) through (7) consistent with drawings in Figs. 3.19(a) and 3.19(b)). Remarkably, the two flow regimes can be identified by two distinct pressure contours – almost horizontal slope in the low-quality regime and finite slope in the high-quality regime – irrespective of polymers. This implies that, for modeling purpose, a single foam model can be used consistently for surfactant foams with and without polymers.

It is worthwhile to think about what the chaotic behavior observed with polymer-added foams means in actual foam field drilling applications where the process continues for a much longer duration and in a much longer system. The oscillating chaotic transition region (i.e., earlier part of Fig. 3.15 as marked in Fig. 3.16) may only exist within a short distance, and thus such a behavior may cancel or averaged out when the entire system is considered. Or once such a chaotic behavior takes place, the system may prefer to moving from one flow pattern to another (i.e., plug flow to slug flow, or slug flow to plug flow, and so on) with time. These issues are beyond the scope of this study and deserve further research efforts in larger facilities. In addition, it should also be pointed out that exactly how these flow patterns (such as plug flow, slug flow, and chaotic behavior) should be translated at different conditions, especially different pipe materials/roughness and diameters, is largely unknown at this stage, even though the theoretical descriptions provided in this study by using bubble size, bubble-size distributions, film stability during shear flow and so on are believed to be still applicable.

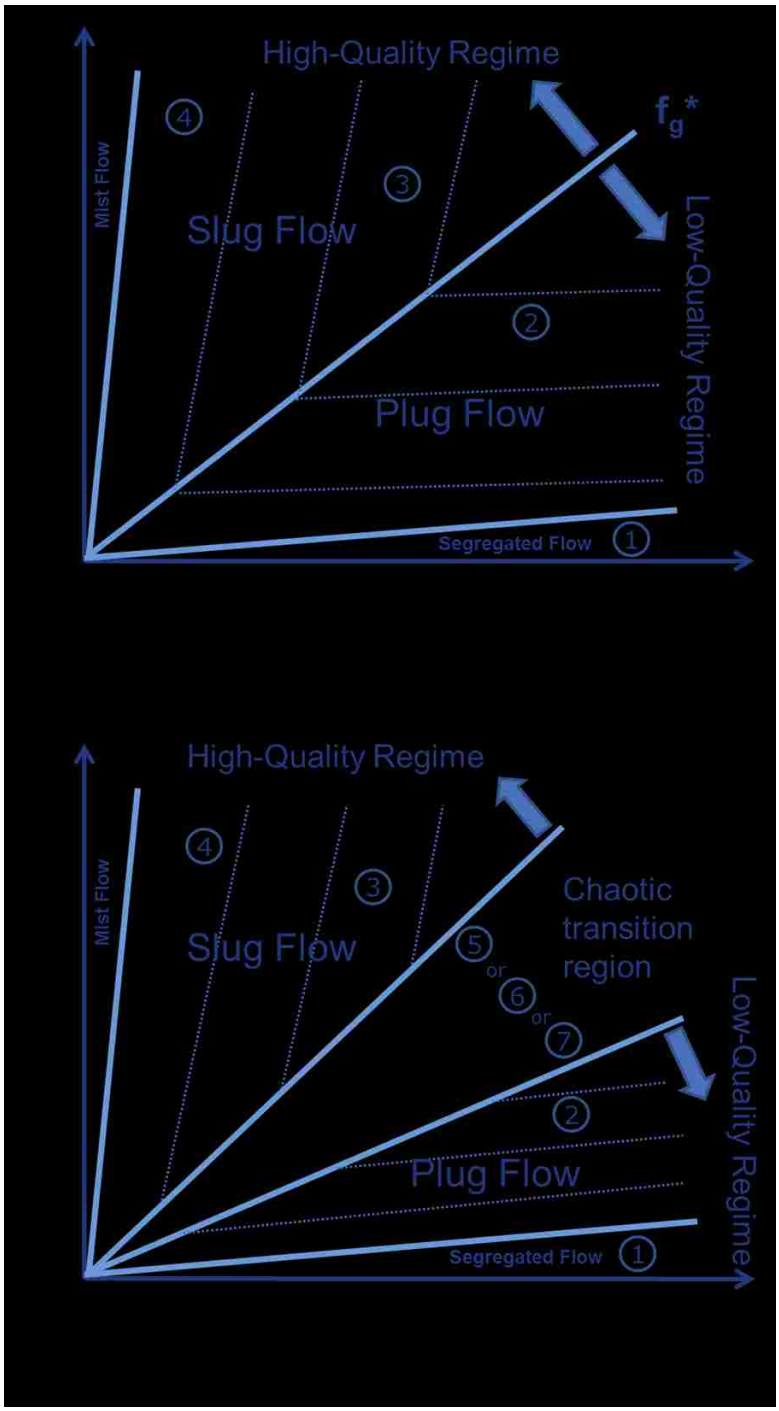

Figure 3.21: Comparison of foam flow characteristics between (a) polymer-free and (b) polymer-added surfactant foams in terms of contour plot.

In general, all experiments shown in this study are repeatable. For example, the experiments with increasing gas flow rate are similar to those with decreasing gas flow rates evidenced by mirror imaged

plots (eg. Figs. 3.5, 3.6, 3.9, 3.13 and 3.14), exhibiting nearly the same steady-state (or time-averaged) pressure and magnitude of data scattering. The only exception applies to the chaotic transition region with polymer-added foams, where the individual pressure responses are unpredictable and thus not repeatable necessarily. Even so, the range of total flow rates and foam qualities showing the chaotic regions is highly repeatable, which allows characterization as shown in Fig. 3.21 (b).

Although this study investigated the effect of oil and polymer separately, the combined effect of oil and polymer together is yet to be covered. It is primarily because the outcome is expected to be very oil-specific and polymer-specific, varying significantly with the types and concentrations of those chemicals. A comprehensive study for polymer-added foams in presence of oils remains as a future research topic. It is worth noting based on experimental results in this study, however, that what matters for understanding foam rheology is not the presence of those foreign chemicals itself, but how they interact with foams affecting film stability and bubble generation/coalescence mechanisms.

To recapitulate, the term "chaotic" or "chaotic transition" zone in this study is selected to describe unstable pressure responses near f_g* for polymer-added surfactant foams. The term is used to represent the system not really reaching the state of homogeneous flow of fine-textured in the low-quality regime, or the state of periodic alternation of free gas and fine-textured foams in the high-quality regime. Therefore, not only the steady-state pressure response but also the steady-state foam texture is unpredictable. The main reason behind such a behavior is caused by two different mechanisms competing each other: higher water viscosity with polymer gives a better stability to foam films which inhibits getting into the high-quality regime even at higher gas fraction; and thicker fluid mixture gives a harder time to agitate which inhibits getting into the low-quality regime even at lower gas fraction. How this response should be translated in a field-scale application (i.e., for a longer system where a larger time is to elapse) is not clear. Figure 3.22 shows a series of snapshots of foam flow in pipe with 2 second time intervals for foams in chaotic region (Q_g = 300 cm^3/min as shown in Fig. 3.15).

Figure 3.22: Snapshots of foam flow in pipe with 2 second time intervals for foams in chaotic region (Q_g = 300 cm^3/min as shown in Fig. 3.15).

CHAPTER 4: MODELING FOAM FLOW IN PIPES USING TWO FOAM-FLOW REGIMES CONCEPT[1]

The main objective of this chapter is to develop a comprehensive foam model which can accommodate the recent findings of foam rheology represented by high-quality and low-quality regimes. By using the term "comprehensive", this new modeling approach is expected to be distinguished from empirical foam equations in the literature because it covers a broad range of foam characteristics dealing with stable and unstable flows, slug-flow and plug-flow patterns, and low and high foam qualities.

4.1 Methods

Typical laboratory foam flow experiments are involved in pressure measurements at fixed gas and liquid injection flow rates or velocities (cf. Figs. 2.4 and 2.5). Superficial gas velocity (u_g) and superficial liquid velocity (u_w) are calculated from gas flow rate (Q_g) and liquid flow rate (Q_w), respectively, i.e.,

$$u_g = \frac{Q_g}{A};\ u_w = \frac{Q_w}{A} \tag{4-1}$$

and the total velocity (u_t) and total flow rate (Q_t) are then related as follows:

$$u_t = u_w + u_g = \frac{Q_w}{A} + \frac{Q_g}{A} = \frac{Q_t}{A} \tag{4-2}$$

where A is the internal cross-sectional area of the pipe.

Once foam forms plug-flow pattern represented by a flow of homogeneous fine-textured foams (cf. low-quality regime in Figs. 2.3, 2.4 and 2.5), the slip effect at the wall becomes important to

[1] This chapter previously appeared as Edrisi, A.R., and Kam, S.I., A New Foam Rheology Model for Shale-Gas Foam Fracturing Applications, Paper SPE162709 presented at the SPE Canadian Unconventional Resources Conference, Calgary, Canada, 30 October – 1 November, 2012. It is reprinted by permission of Society of Petroleum Engineers. Copyright 2012, Society of Petroleum Engineers. Further reproduction prohibited without permission. See appendix 2 for more details.

understand foam rheology. This concept is well described by previous studies on lubricating and drainage effects (Enzendorfer et al., 1995; Bekkour, 1999; Gardiner et al., 1999; Rojas et al., 2001; Briceno and Joseph, 2003). Among many, this study borrows an equation from Beyer et al. (1972) for the modeling purpose, which is,

$$u_t = \frac{Q_t}{A} = u_f + u_s \tag{4-3}$$

where, the total volumetric flux (u_t) is the addition of fine-textured homogeneous bulk foam velocity (u_f) and wall slip velocity (u_s). Gardiner et al. (1999) relate wall slip velocity (u_s) with slip coefficient (β_c) and the thickness of liquid slip layer on the wall (δ) as follows:

$$u_s = \frac{\beta_c \tau_w}{D} \qquad \text{and} \tag{4-4}$$

$$\tau_w = \frac{\mu u_s}{\delta} \tag{4-5}$$

where τ_w, μ, and D are the wall shear stress, fluid viscosity, and pipe diameter, respectively. Note that if the slip velocity (u_s) is measured at given experimental conditions (i.e., total velocity, foam quality, pipe roughness and diameter, and so on), Eqs. 4-4 and 4-5 allow the estimation of wall slip coefficient (β_c) and slip layer thickness (δ) which are essential to foam-related fluid mechanics calculations.

For foams forming slug-flow pattern, the system in some sense never reaches a steady state. Rather it consists of free-gas and foam-slug segments alternating each other periodically (cf. Figs. 2.3, 2.4 and 2.5). For the slug flow pattern with repetitions of two stable states (let's say, state 1 and state 2), the injected foam quality (f_g) is no other than the volume-averaged (or length averaged if the cross-sectional area is kept constant) foam quality of the two states, i.e.,

$$f_g = \frac{L_1}{L_t} f_{g1} + \frac{L_2}{L_t} f_{g2} \tag{4-6}$$

where L_t is the total length of the repeating unit consisting of segment 1 and segment 2, L_1 and L_2 are the lengths of segment 1 and segment 2 respectively; and f_{g1} and f_{g2} represent foam qualities of the segment 1 and 2, respectively. If the slug-flow pattern is viewed as a combination of free-gas segment and fine-textured foam-slug segment at f_g* (cf. Figs. 2.3, 2.4 and 2.5), then Eq. (4-6) becomes

$$f_g = \frac{L_g}{L_t} + \frac{L_t - L_g}{L_t} f_g^* \tag{4-7}$$

Note that L_1 and f_{g1} are replaced by the length of free gas segment (L_g) and gas fraction of free-gas segment ($f_g = 1$), and L_2 and f_{g2} are replaced by the length of foam-slug segment (L_t - L_g) and gas fraction of foam at f_g* ($f_g = f_g$*). More details about this approximation are given in the results section.

The wall shear stress (τ_w) and wall shear rate ($\dot{\gamma}_w$) for a laminar flow of a Newtonian fluid in a circular tube with length of L and diameter of D can be calculated from fluid mechanics (Darby, 2001) using

$$\tau_w = \frac{\Delta P}{L}\frac{D}{4} \qquad \text{and} \tag{4-8}$$

$$\dot{\gamma}_w = \frac{8\, u_t}{D} \tag{4-9}$$

where, Δp is the pressure drop over the distance of L. For power-law fluid and Bingham-plastic fluid, the wall shear stress (τ_w) and wall shear rate ($\dot{\gamma}_w$) are expressed as follows, respectively:

$$\tau_w = K\, \dot{\gamma}_w^n \qquad \text{and} \tag{4-10}$$

$$\tau_w = \tau_y + \mu_p\, \dot{\gamma}_w \tag{4-11}$$

where K is the flow consistency index and n is the flow behavior index for power-law rheology, and τ_y is the yield point and μ_p is the plastic viscosity for Bingham plastic rheology.

The improved foam model proposed in this study first uses the rheology of fine-textured foams (either Bingham-plastic or power-law) as shown in previous studies (Eqs. 4-10 and 4-11) for plug-flow pattern in the low-quality regime. Then, for foams with slug-flow pattern in the high-quality regime, foam rheology is expressed by putting fine-textured foams and free gas phase together as observed by the visualization study of Gajbhiye and Kam (2011). Therefore the rheology of foams in the high-quality regime is similar to time- and space-averaged property as shown in Eq. 4-6.

4.2 Results and Discussions

4.2.1 Data Interpretation

The presence of two flow regimes and corresponding changes in foam texture and flow patterns are observed consistently in a wide range of gas and liquid velocities not only with conventional surfactant foams but also with polymer-added foams and foams flowing together with oils (Edrisi et al., 2012). The basic concept is demonstrated in Fig. 4.1(a) for this modeling study. Strictly speaking, there exist many possible foam flow patterns, not only slug-flow and plug-flow patterns, but also (i) mist-flow pattern at very dry flow conditions where the phase inversion takes place such that the external continuous gas phase entrains the internal discontinuous liquid droplets, (ii) segregated-flow pattern in horizontal flow at relatively wet flow conditions where foams flow on the top of lower liquid layer; and (iii) bubbly-flow pattern at wet flow condition with low total flow rate where bubbles do not interact significantly during shear flow. Because most foam field applications in petroleum industry deal with relatively high flow rate and moderate foam quality (i.e., not too dry or not too wet), this study assumes that there are only two flow patterns of interest, slug-flow pattern to represent the high-quality regime and plug-flow pattern to represent the low-quality regime. More complexities, of course, can be added to this modeling technique later on if such an assumption over-simplifies the situation.

The previous visualization study (Gajbhiye and Kam, 2011) describes how bubble size and bubble-size distribution change within the contour plot, which can be summarized as follow for this study

(Fig. 4.1(b)): suppose there are two scanning lines (shown by the vertical line A-A' and the horizontal line B-B' in Fig. 4.1(a)) and the total injection velocity is relatively high so that foam texture in the plug-flow pattern is fully developed. Then it is observed that (i) along the vertical line from the bottom to the top (or, A to A'), the flow pattern changes from segregated-flow to slug-flow pattern (note that the segregated-flow pattern is ignored because it only happens near the x-axis). It means that there are almost

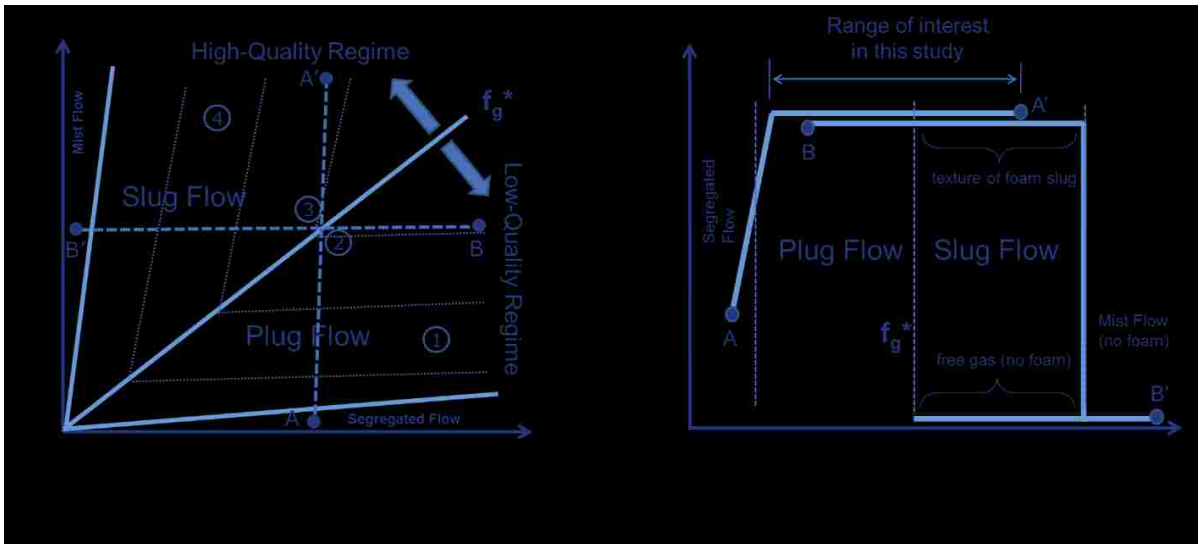

Figure 4.1: Two flow patterns of interest in this modeling study – slug-flow pattern to represent the high-quality regime and plug-flow pattern to represent the low-quality regime (see Figure 4.2 for more).

no noticeable changes in the steady-state foam texture until f_g reaches f_g*. Once f_g goes beyond f_g*, free-gas segments appear and alternate with fine-textured foams. This free-gas segment tends to grow and the foam-slug segment tends to shrink as f_g further increases. Foam texture in these foam slugs are not meaningfully different from that in foams in the plug-flow pattern; and (ii) along the horizontal line from the right to the left (or, B to B'), only homogeneous fine-textured foams are present until f_g reaches f_g*. Once f_g goes beyond f_g* (moving to the left towards B'), fine-textured foams alternate with free-gas segments before moving into mist-flow pattern near B' (again, note that the mist-flow pattern is ignored in this study because it only happens near the y axis).

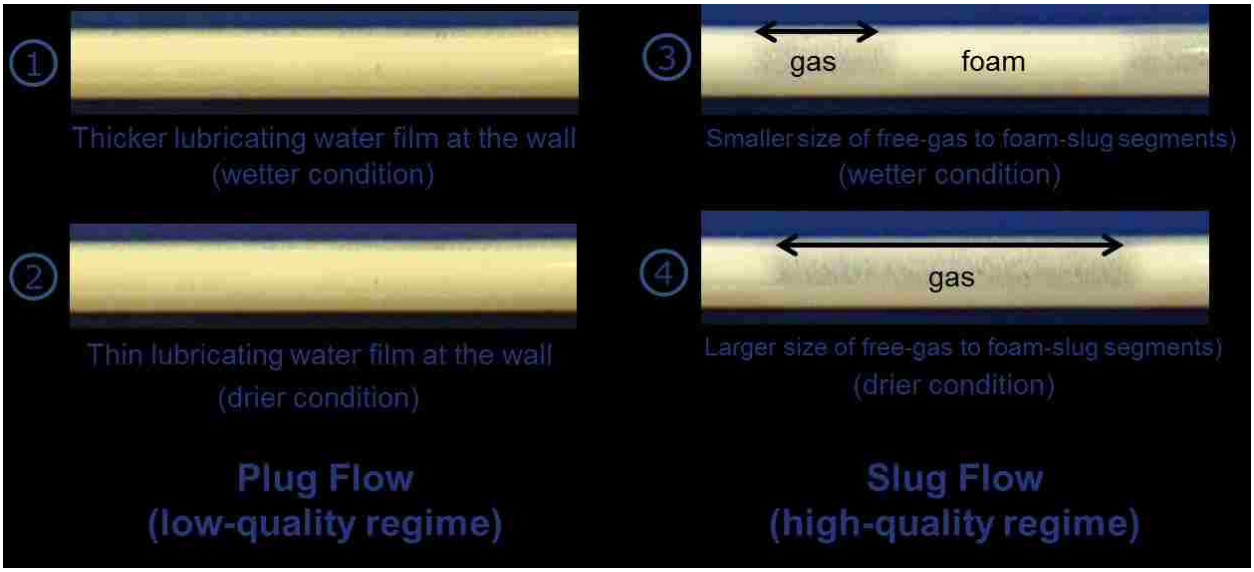

Figure 4.2: Photos from lab experiments showing foam flow mechanisms in the low-quality and high-quality regimes in response to the changes in gas and liquid velocities (Although it is not shown clearly on this scale, water film thickness at the wall in (1) (i.e., wetter condition) is greater than that in (2) (i.e., drier condition)).

Brief foam flow experiments in a 0.5-inch diameter nylon pipe are conducted by using nitrogen gas and Stepanform surfactant solutions to visually ensure the concept of lubricating and drainage effects and changes in foam texture described in Fig. 4.1(b) (see Edrisi et al. (2012) for more details on experiments). The results indeed revealed that if foam flow becomes wetter (eg. decrease in gas velocity or increase in water velocity), water tends to accumulate more at the wall making water film thicker; if the flow becomes drier, the opposite occurs (see (1) and (2) in Fig. 4.2). In addition, foams exhibiting slug-flow pattern show the change in the lengths of free-gas segment and foam-slug segment (or, the relative size of free-gas segment to foam-slug segment, equivalently; see (3) and (4) in Fig. 4.2) as follows: if foam flow becomes drier, the length of free-gas segment increases but the length of foam-slug segment decreases, still keeping the same foam texture in the foam slugs. (The free gas segments expressed by thick arrows in Fig. 4.2 were entirely filled by free gas with no foams, if not very coarse-textured foams, even though the pipe surface seemed to be somewhat white-colored in the photos because of bubble residues staying *on the pipe wall surface* not inside the pipe.)

4.2.2 Modeling Techniques

As a first step of modeling approach, Fig. 4.3 shows how to draw a series of pressure contour lines in both regimes in order to fit the experimental data (see the original plot in Fig. 3.8). First, those sections, believed to be with segregated-flow pattern (i.e., lower part of the plot near the x axis in Fig. 4.3) and mist-flow pattern (upper left part of the plot near the y axis in Fig. 4.3), are ignored because they are not of interest in this study. Second, roughly draw a straight line from the origin (i.e., f_g* line) to split the two distinct pressure contours representing slug-flow pattern in the high-quality regime and plug-flow in the low-quality regime. Third, draw a series of straight lines for each regime from the location reasonably away from the intersection between the f_g* line and pressure contours – this automatically removes the transition behavior between the two flow regimes near f_g* (i.e., the smooth and round parts of the contour lines near f_g*) in the modeling.

Fig. 4.4 shows several data points for each pressure contour value extracted from the straight pressure contour lines drawn in Fig. 4.3 ("not" from actual data points from experiments) for the steady-state pressure drops from 4 to 14 psi. For each set of data, a best-fit straight line equation can be determined. Since the slope is shown to be pretty comparable, an average value is calculated to represent the slope in each regime: 7.14 for the low-quality regime (i.e., (4.85 + 6.17 + 6.76 + 8.06 + 8.17 + 8.75)/6) and 91.08 for the high-quality regime (i.e., 96.35 + 90.01 + 90.60 + 92.74 + 87.04 + 89.77)/6). It should be pointed out that the selection of pressure contours of interest may not be unique for the analysis. For example, although the lower and upper bounds of the pressure drops (4 psi and 14 psi, respectively) and the interval in between (2 psi) as shown in Fig. 4.4 seem reasonable in this particular case, one may of course choose different pressure ranges and intervals depending on the number of data points and accuracy of pressure measurements. The reconstructed pressure contours, however, should not be very different based on the experience gained, as long as the trends of pressure contours are read and interpreted consistently.

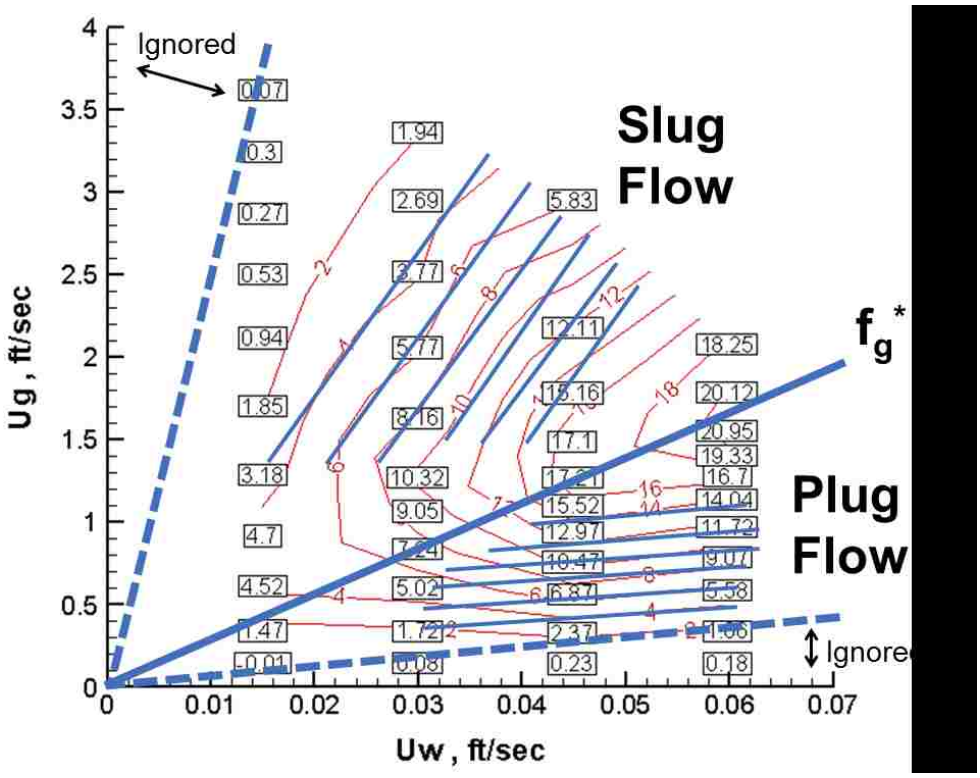

Figure 4.3: Pressure contour plot (Edrisi et al. (2012) using surfactant foams (0.5 wt% Stepanform and nitrogen)) analyzed by a sketch of a series of straight pressure contour lines for model fit. (See Figure 3.8 for original data)

Once these average slopes in both regimes are estimated and applied, the pressure contours can be re-visited in order to find updated best-fit straight line equations again as shown in Fig. 4.5 (Note that in each regime, the lines have the same slopes as a result, but with different y intercepts). At each value of pressure drop, extensions of the two corresponding straight contour lines (one for low-quality regime and the other for high-quality regime) end up with an intersection point at that particular pressure drop. A collection of the six intersection points from 4 to 14 psi pressure drops, as shown in Fig. 4.6, can be plotted all together, and the best-fit straight line is then no other than the f_g^* line. Note that this f_g^* line constructed in Fig. 4.6 successfully reproduces the f_g^* line schematically drawn in Fig. 4.3, showing the same slope. (The f_g^* line in Fig. 4.6 has a slope of about 27 which is equivalent to 96% foam quality.

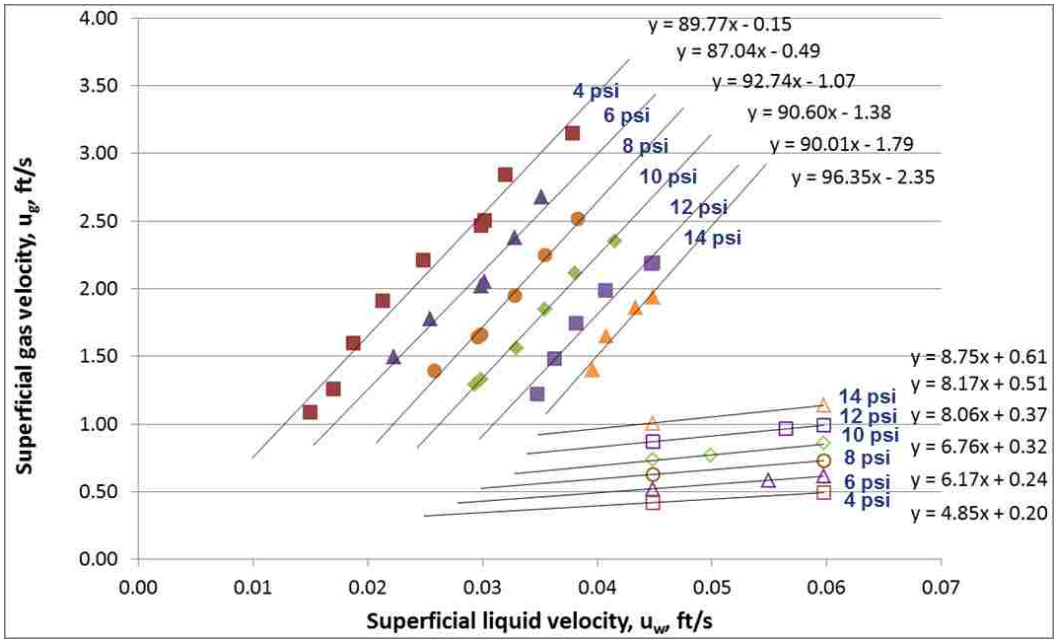

Figure 4.4: Construction of the best-fit straight lines for each set of pressure contours. (See Figure 3.8 for original data)

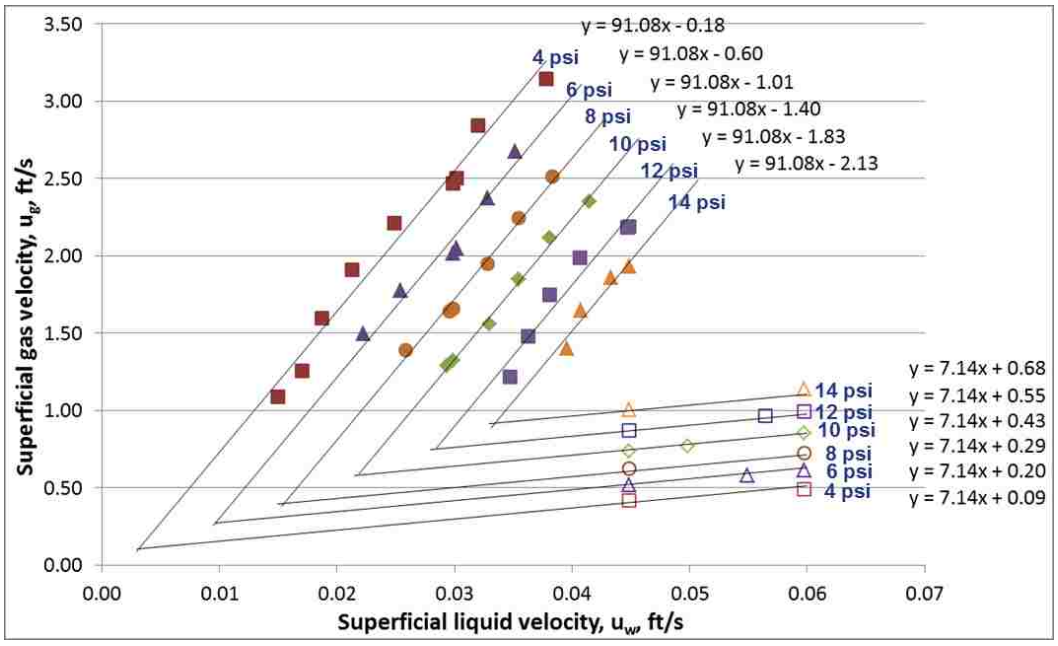

Figure 4.5: Unified pressure contours by using representative slopes from both regimes. (See Figure 3.8 for original data)

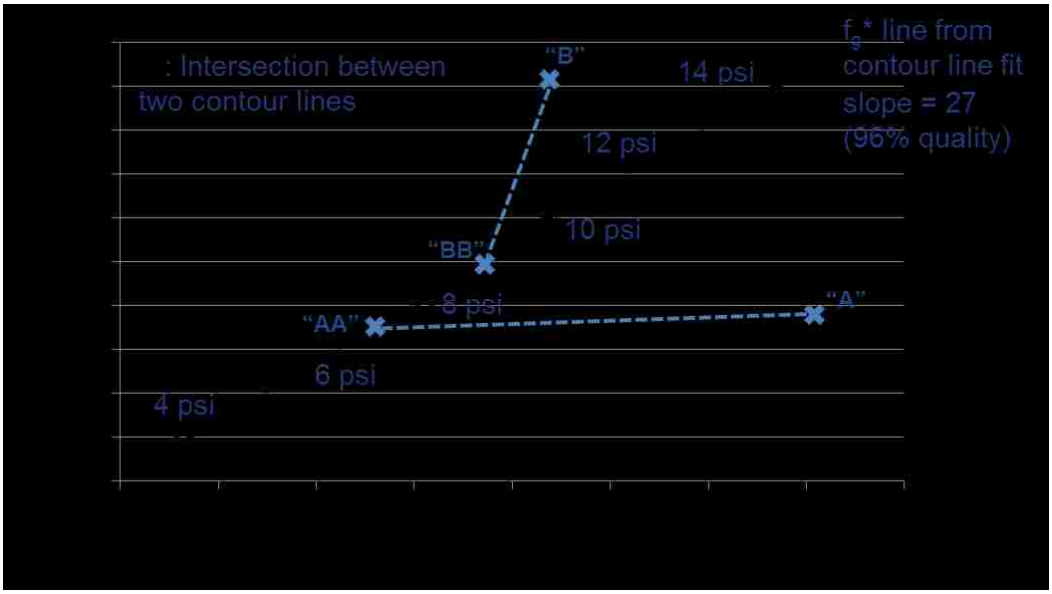

Figure 4.6: Construction of f_g* line from the model fit to pressure contours (Fig 4.5). (See Figure 3.8 for original data)

Next step is to establish foam rheology model along the f_g* line. Fig. 4.7 shows the relationship between shear rate and shear stress for those six data points in Fig. 4.6, with a model fit by using power-law model (Fig. 4.7(a)) and Bingham-plastic model (Fig. 4.7(b)). When the power-law model is applied, the flow consistency index (K) is 0.0706 $lb.s^n/ft^2$ and the flow behavior index (n) is 0.5876, with the square of correlation coefficient (R^2) of 0.9881 (cf. Eq. 4.10). On the other hand, the use of Bingham-plastic model gives the plastic viscosity of 0.0062 $lb.s/ft^2$ and the yield stress of 0.3704 lb/ft^2 with R^2 of 0.9981 (cf. Eq. 4-11). Although both models are shown to be equally satisfactory, the power-law model is selected for further analysis in this study because of the relatively high shear rate used in field applications (Gardiner et al., 1999). The selection of different rheology model such as Bingham-plastic or Hershel-Bulkley model, however, can also be applied in the same manner.

Once foam rheology model is determined for the points sitting on the f_g* line, foam rheology off the f_g* line can be modeled. This requires the rheology along the f_g* line (i.e., $y = 0.0706x^{0.5876}$ in Fig. 4.7(a)) and the slopes of contour lines in two flow regimes (i.e., 7.14 and 91.08 for the low-quality and

high-quality regimes, respectively, in Fig. 4.5). For example, suppose there is an arbitrary foam flow condition showing gas and liquid velocities represented by the point "A" in Fig. 4.6, which happens to be in the low-quality regime. Then, by using the representative slope of the low-quality regime (i.e., 7.14) calculated above, the point "A" can be traced back to the point "AA" *on the f_g* line*. Similarly, an arbitrary point in the high-quality regime, point "B", can also be traced back to the point "BB" *on the f_g* line* by using the representative slope of the high-quality regime (i.e., 91.08). The pressure values at point "A" and point "B" can then be determined by point "AA" and point "BB", using foam rheology model *along the f_g* line* as obtained from Fig. 4.7(a).

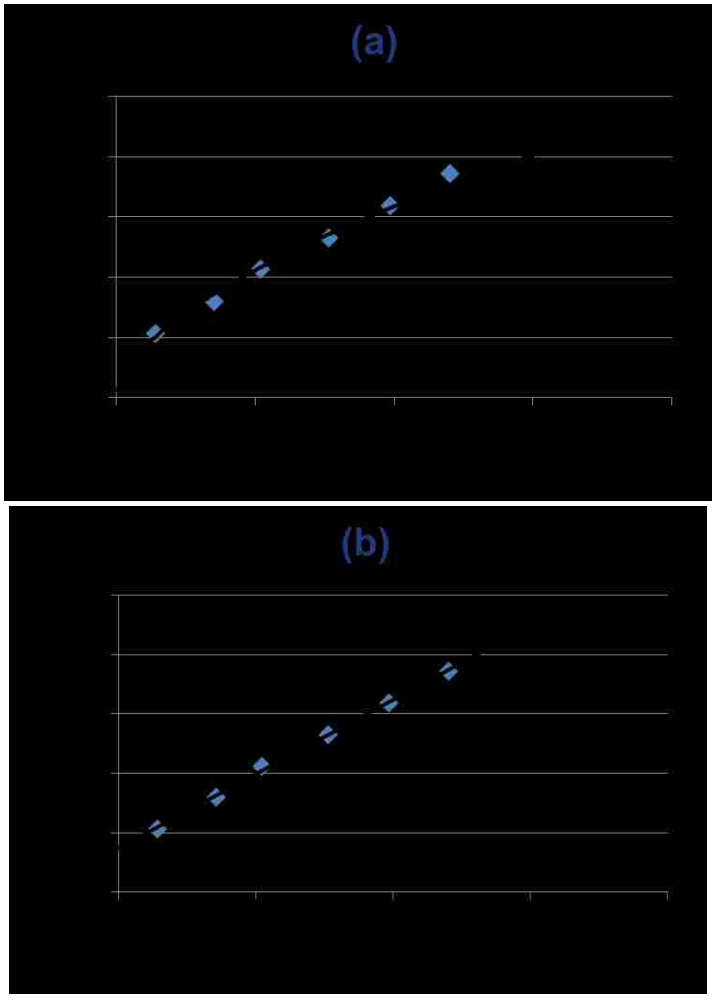

Figure 4.7: Foam rheology along the f_g* line by using (a) power-law model and (b) Bingham-plastic model.

4.2.3 Rebuilding Two Flow Regime Map and its Implications

Fig. 4.8 shows how this modeling concept can be applied in order to construct pressure contours. First, from the f_g* line as shown in Fig. 4.6, select six data points sitting on the line, for example, u_w = 0.005, 0.010, 0.015, 0.020, 0.025, and 0.030 ft/s, and read the corresponding values of u_g, roughly, 0.14, 0.27, 0.4, 0.54, 0.67 and 0.81 ft/s. Second, by using each set of (u_w, u_g), calculate the wall shear rate ($\dot{\gamma}_w$) (Eq. 4-9) and the corresponding wall shear stress (τ_w) (Eq. 4-10) with obtained values of K and n from Fig. 4.7(a). The resulting sets of (($\dot{\gamma}_w$) [1/sec], τ_w [lbf/ft^2]) are (35.32, 0.57), (70.65, 0.86), (105.97, 1.09), (141.29, 1.29), (176.62, 1.48) and (211.94, 1.64). Third, convert the shear stress (τ_w) into the steady-state pressure drop (Eq. 4-8) and mark the resulting values of 4.32, 6.49, 8.23, 9.75, 11.115 and 12.37 psi as a function of (u_w, u_g), as shown in Fig. 4.8. Finally, by drawing a family of straight lines with the same slope in each regime as observed in the experiments (cf. Fig. 4.5), the entire pressure contours showing two-flow regimes are constructed. As expected, Fig. 4.8 resulting from this modeling effort is similar to the original contour plot of Fig. 4.3 with R^2=0.86.

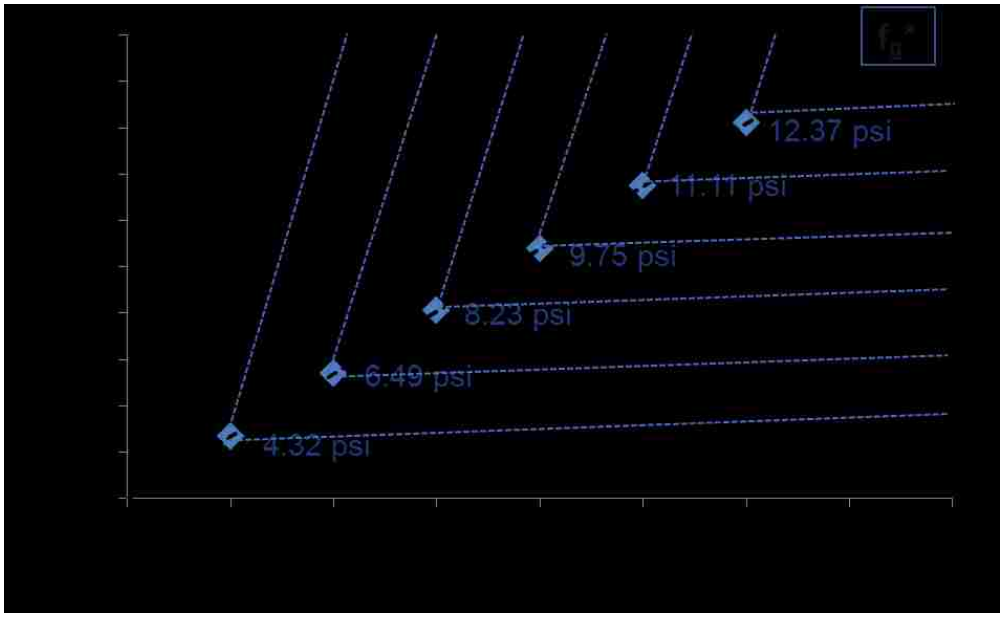

Figure 4.8: Model reconstruction of data points along the f_g* line and corresponding pressure contours. (See Figure 3.8 for original data)

Once the model is ready as shown by Fig. 4.8, the steady-state pressure values can be re-calculated exactly at the same (u_w, u_g) points applied in the original lab experiments. An example is shown in Fig. 4.9(a) with the pressure values in the rectangular boxes. If the same experiments were carried out at even smaller u_g intervals, a new contour plot similar to Fig. 4.9(b) could be created with more steady-state pressure values. Notice that the contour lines in Fig. 4.9(b) are more similar to those in Fig. 4.8 because of the increasing number of data points, compared with Fig. 4.9(a), as expected.

In addition to modeling two distinct foam flow regimes, it is interesting to investigate what kinds of flow mechanisms present almost horizontal pressure contours in the low-quality regime and inclined pressure contours in the high-quality regime. For this discussion, it should be reminded that in this modeling study (i) the low-quality regime only consists of plug-flow pattern and the high-quality regime only consists of slug-flow pattern, because segregated-flow pattern and mist-flow pattern are not likely to be observed within the velocity range of interest; (ii) if plug-flow pattern is formed, there are no noticeable changes in foam texture. Any change in liquid flowing fraction leads to the change in the thickness of water film at the wall (i.e., wetter foams with thicker water film at the wall, and drier foam with thinner water film at the wall); and (iii) if slug-flow pattern is formed, it repeats free-gas segment and foam-slug segment, and the property of foam-slug segment is identical to the property of foams at the f_g* on the same pressure contour. As described earlier, it is believed that these simplifying assumptions are reasonable evidenced by numerous previous studies (Calvert and Nezhati, 1986; Kraynick, 1988; Kroezen et al., 1988; Princen, 1989; Enzendorfer et al., 1995; Bekkour, 1999; Rojas et al., 2001; Briceno and Joseph, 2003; Tisne et al., 2003; Bogdanovic et al., 2009; Gajbhiye and Kam, 2011; Edrisi et al., 2012).

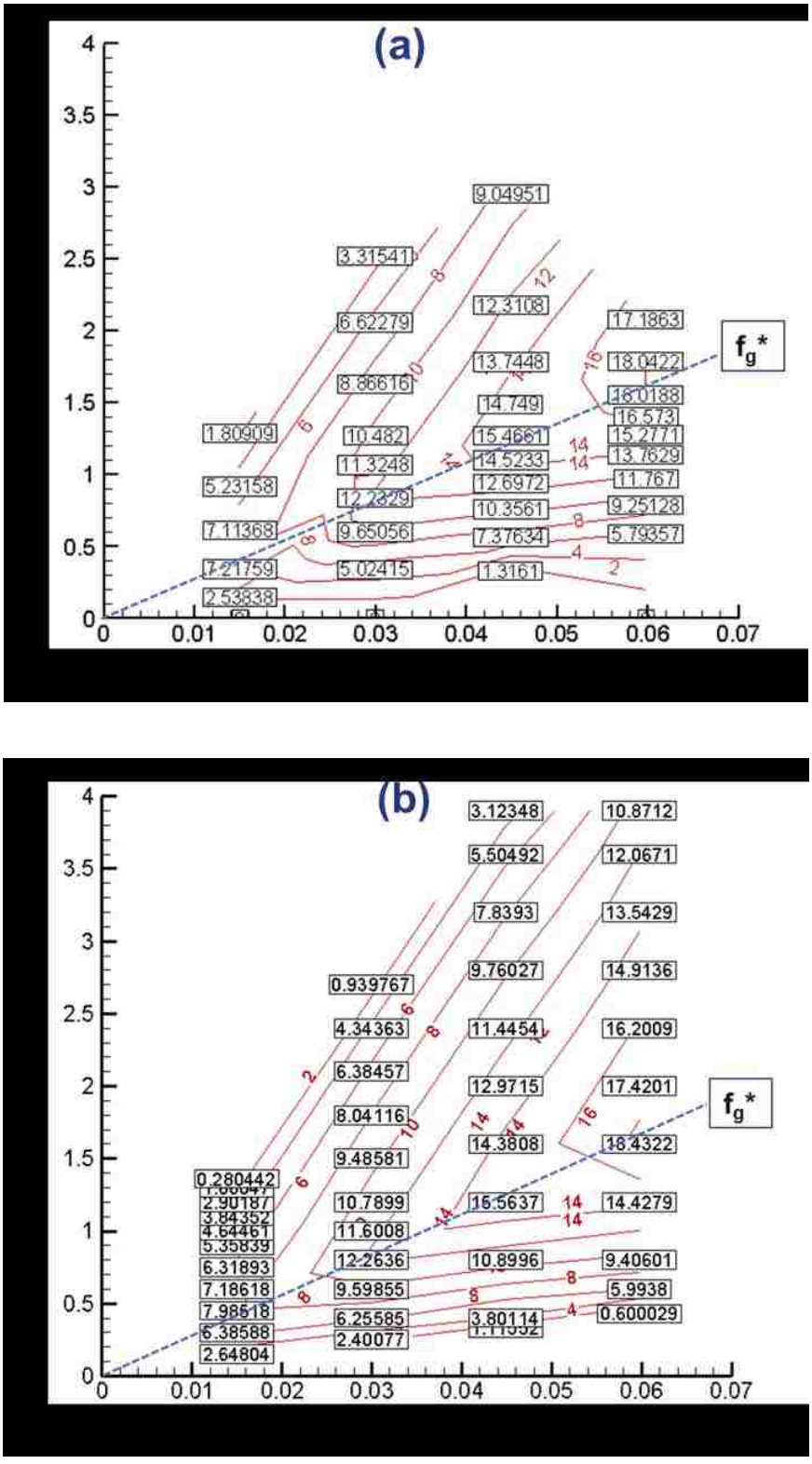

Figure 4.9: Reconstruction of two-flow-regime pressure-drop contours by using the model at a small (a) and a large (b) number of sample data points. (See Figure 3.8 for original data)

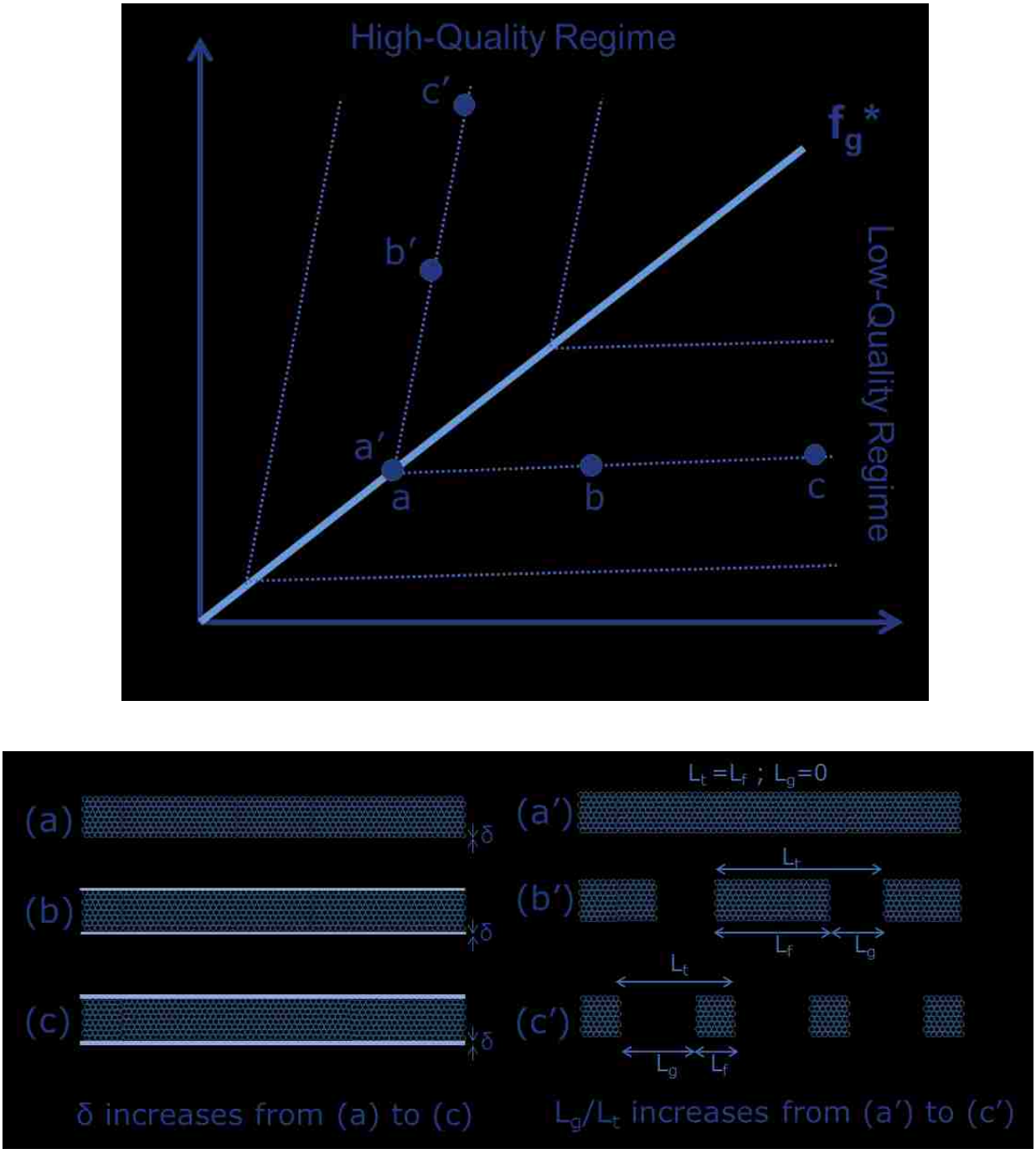

Figure 4.10: A schematic of the change in foam flow mechanisms along the same contour line penetrating both regimes.

Fig. 4.10 schematically shows a summary of what changes are expected along the same pressure contour, following (a), (b) and (c) in the low-quality regime, or (a'), (b'), and (c') in the high-quality

regime. The two points (a) and (a') are identical if the intersection takes place on the f_g* line. Suppose one walks along the same pressure contour from one end to the other by decreasing water flowing fraction (or, increasing f_g), let's say, from (c) to (c') passing through (b), (a), (a'), and (b'), then the following changes would be observed: (i) at first, the system would encounter the reduction in water film thickness at the wall within the low-quality regime (moving from (c) to (a)); (ii) if the water film at the wall could not be thinner any longer without maintaining the same foam texture, the system steps into the high-quality regime ((a) to (a')). This point, reflected by f_g*, is a point at which the formation of free-gas segment (or, large gas pocket) is first observed; and (iii) further reduction in water flowing fraction makes the relative size of free-gas segment grow ((a') to (c')), without making any significant changes in the texture of foam slug.

The conversion from (a) to (a') across the f_g* line means that the liquid layer on the pipe wall allowing slip boundary condition is at its minimum thickness and, as a result, the slip velocity on the f_g* line is minimal. If the slip velocity (u_s) can be assumed to be zero, then the total velocity (u_t) becomes equal to the bulk foam velocity (u_f) along the f_g* line as shown in Eq. 4-3. This poses two significant implications. First, for any data point in the low-quality regime, the slip velocity (u_s) can be directly calculated from the distance between the point of interest and f_g* *along the same pressure contour*. This in turn makes it possible to determine the slip coefficient (β_c) and the thickness of liquid slip layer (δ) by using Eqs. 4-4 and 4-5. An example calculation for the slip velocity (u_s) and the slip coefficient (β_c) is shown in Figs. 4.11(a) and 4.11(b), respectively. As expected, as foam becomes drier (i.e., (c) to (a) in Fig. 4.10), both slip velocity and slip coefficient decrease due to the reduction in water film thickness. Second, for any data point in the high-quality regime, it is possible to calculate the fraction of free-gas segment (i.e., L_g/L_t) (or foam-slug segment, equivalently, because $L_f/L_t = 1 - L_g/L_t$) using the distance between the point of interest and f_g* *along the same pressure contour* as shown in Eq. 4-7. An example calculation in Fig. 4.12 shows that as the point of interest moves off the f_g* line further (i.e., (a') to (c')), the relative size of free-gas segment increases sharply (or, the relative size of foam-slug segment

decreases sharply, equivalently). These behaviors in both flow regimes are qualitatively consistent with previous studies (Enzendorfer et al., 1995; Gardiner et al., 1999; Bogdanovic et al., 2009; Gajbhiye and Kam, 2011; Edrisi et al., 2012).

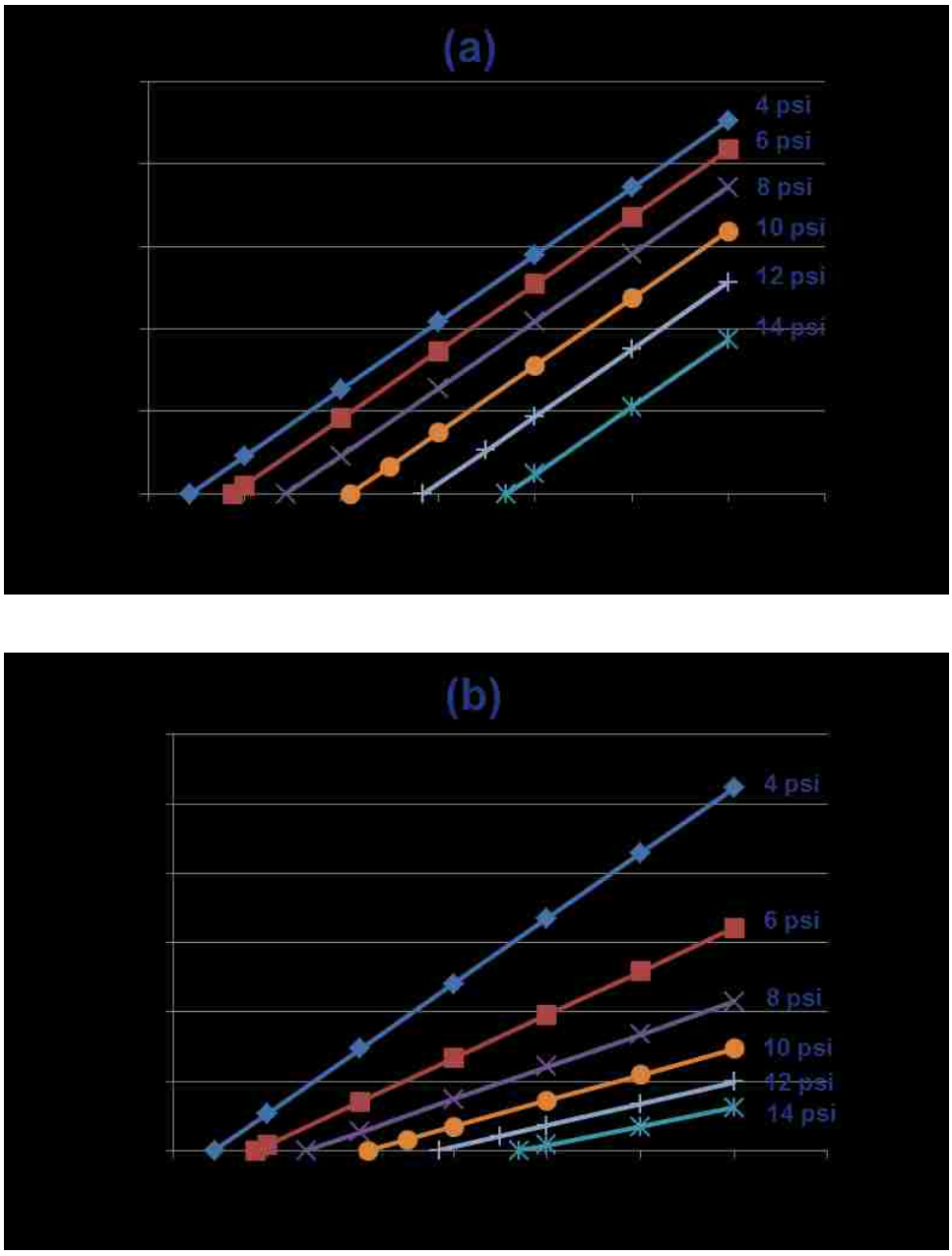

Figure 4.11: Calculated wall slip effect along the same pressure contour lines for foams in the low-quality regime: (a) slip velocity (u_s) and (b) slip coefficient (β_c).

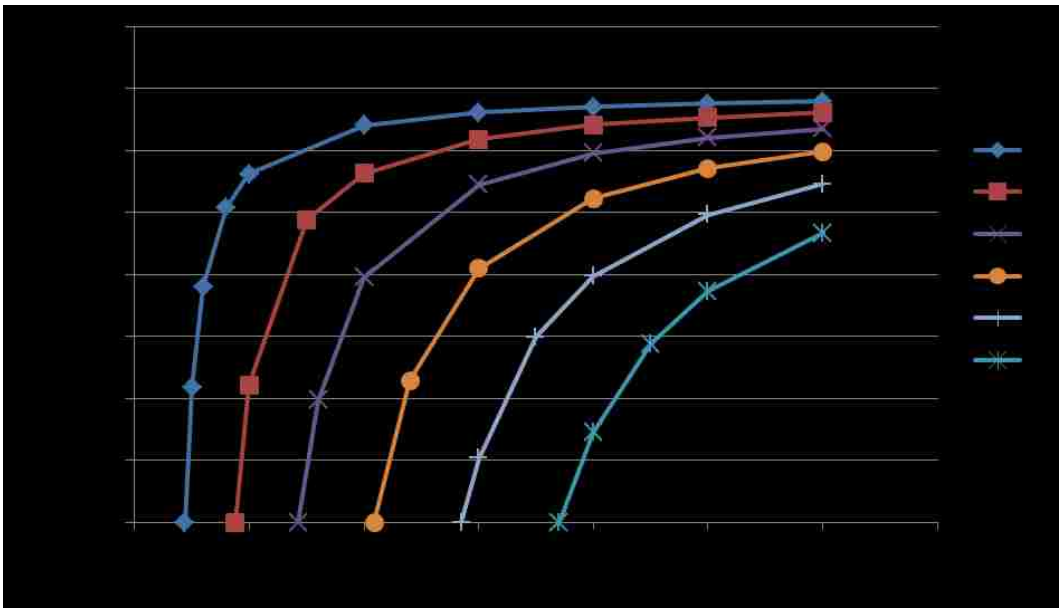

Figure 4.12: Calculated relative size of free-gas segment (L_g/L_t) along the same pressure contour lines for foams in the high-quality regime.

The calculated results in Figs. 4.11 and 4.12 may not be accurate quantitatively. Nevertheless, accounting for the fact that film thickness (δ), slip velocity (u_s), slip coefficient (β_c), and relative sizes of foam-slug and free-gas segments (L_f/L_t and L_g/L_t) are extremely difficult to measure in laboratory foam flow experiments, if not impossible, this modeling method is believed to provide a convenient way of estimating those physical parameters once the pressure contours showing two flow regimes are available.

To recapitulate, the new foam modeling technique presented in this study requires the following steps:

1. Conduct flow experiments to establish a pressure contour plot (cf. Fig. 3.8). The plot needs to have both high-quality and low-quality regimes with a reasonable number of pressure contour lines showing shear-thinning or shear-thickening rheology.

2. Draw a boundary line (f_g*) which separates high-quality regime from low-quality regime. Then draw a family of parallel straight lines in each regime to fit pressure contours obtained from experiments (cf. Fig. 4.3).

3. Read a representative slope in each regime (called m_1 and m_2), and reconstruct individual pressure contour lines by using the determined slopes. Note that the y intercepts of those reconstructed lines are decided such that the straight line fit gives minimum errors (cf. Fig. 4.5).

4. Make sure that the intersection points between pairs of iso-pressure contours (one in the high-quality regime and the other in the low-quality regime) are aligned on a straight line with the slope close to f_g* estimated in step 2 (cf. Fig. 4.6). If it is not the case, step 2 and step 3 should be repeated until this condition becomes satisfied.

5. For those points aligned along the boundary line (f_g*), construct a rheogram (shear stress vs. shear rate) by using pressure and total velocity. If power-law model is used as shown in this study, read the power-law exponent (n) and the consistency index (K) (cf. Fig. 4.7). This completes building a foam model with four model parameters.

6. For demonstration purpose, one may reconstruct data points along the boundary line (f_g*) and create straight pressure contour lines in both regimes (cf. Fig. 4.8). Pressure contours can also be re-plotted just like the way it has been done with experimental data, if necessary (cf. Fig. 4.9).

Once foam parameters are determined and the pressure contours are constructed with f_g* line and a family of straight lines in each regime (cf. Fig. 4.8), a steady-state pressure at any particular gas and liquid velocities within the domain can be decided by following the representative slope and finding the intersection with the f_g* line (cf. Fig. 4.6).

CHAPTER 5: USE OF NEW FOAM MODELING TECHNIQUE IN DRILLING HYDRAULICS

In this chapter, the two foam-flow regimes modeling technique is applied into foam drilling hydraulics calculations and the results are compared with conventional method. The goal of this section is to demonstrate how this new modeling technique can improve the design of foam drilling processes more reliably, by using quantitative analysis.

5.1 Methods

As a reference, this study uses Chen et al.'s study (2009), which thoroughly investigates foam drilling hydraulics with foam rheology modeled by empirical equations based on fine-textured foams showing only low-quality regime (more details following in the next section). Considering vertical, inclined, and horizontal well trajectories, Chen et al. (2009) uses power- law model as follows:

$$\tau_w = K\,\dot{\gamma}_w^n \tag{5-1}$$

where τ_w and $\dot{\gamma}_w$ are the wall shear stress and wall shear rate. The consistency index (K) and the power-law exponent (n) are defined as

$$K = \mu_w\left(e^{af_g^2+bf_g+c}\right) \quad \text{and} \tag{5-2}$$

$$n = -0.45f_g + 0.7633 \quad , \tag{5-3}$$

where, f_g is foam quality and μ_w is viscosity of liquid solution. Three empirical parameters (a, b, and, c) are functions of liquid viscosity (μ_w) such as

$$a = (-0.533\mu_w^2 + 3.6735\mu_w - 13.546) \quad , \tag{5-4}$$

$$b = (0.8926{\mu_w}^2 - 6.5877\mu_w + 29.966) \quad \text{, and} \tag{5-5}$$

$$c = (-0.3435{\mu_w}^2 + 2.5273\mu_w - 14.218) \quad . \tag{5-6}$$

Note that foam quality, which is means gas fraction, is defined as follows:

$$f_g = \frac{Q_g}{Q_t} = \frac{Q_g}{Q_w + Q_g} = \frac{u_g}{u_t} = \frac{u_g}{u_w + u_g} \tag{5-7}$$

For a measured pressure drop ΔP (psi) over the length of L (ft) in a pipe with inner diameter of d_{pin} (inch) during the injection rate of u_t (ft/sec), τ_w (lb_f/ft^2) and $\dot{\gamma}_w$ (1/sec) in Eq (5-1) are expressed by

$$\tau_w = 3\, d_{pin}\, \frac{\Delta P}{L} \quad \text{and} \tag{5-8}$$

$$\dot{\gamma}_w = 96\, \frac{u_t}{d_{pin}} \quad . \tag{5-9}$$

For the annulus with inner diameter of d_{ann} (inch) and a pipe with outside diameter of d_{pout} (inch), Eq (5-8) and Eq (5-9) can be modified as

$$\tau_w = 3\, (d_{ann} - d_{pout})\, \frac{\Delta P}{L} \quad \text{and} \tag{5-10}$$

$$\dot{\gamma}_w = 144\, \frac{u_t}{(\, d_{ann} - d_{pout})} \quad . \tag{5-11}$$

For foam drilling hydraulics calculations, this study uses a technique called pressure traverse calculation, widely used in petroleum production and drilling engineering. The calculation starts from the node (eg. inlet) where the pressure (P) value is given (or assumed to be given), and then determines the total pressure gradient ($(\frac{\Delta P}{\Delta z})_{tot}$) at given total mass rate of foam mixture (m_t), which consists of gas mass rate (m_g) and liquid mass rate (m_w) (i.e., $m_t = m_g + m_w$), by adding up hydrostatic

pressure gradient ($(\frac{\Delta P}{\Delta z})_{ele}$), acceleration/deceleration pressure gradient ($(\frac{\Delta P}{\Delta z})_{acc}$), and frictional pressure gradient ($(\frac{\Delta P}{\Delta z})_{fri}$), before moving on to the next node. The calculation is continued until it reaches the last node, and if the pressure at the last node is specified as an input (eg., backpressure (P_b) given), the entire calculation should be repeated by assuming a new pressure at the first node to satisfy the P_b given. Because the gas phase in the foam mixture is compressible, this algorithm requires calculations of gas compressibility factor (or, commonly called Z factor) by using Equation of State (EOS). Details about equations and procedures are included in Appendix 1, and further knowledge on the pressure traverse calculation can be found elsewhere (Economides et al., 1994).

Table 5.1: Input data for foam hydraulics calculation

Parameters	Description	Values
μ_w	Liquid Viscosity (cp)	1
ρ_w	Liquid Density (lbm/ft^3)	62.4
M_g	Gas Molecular Weight (lbm/lbmol)	28.9
Q_w	Inlet Liquid Rate (gpm)	40
Q_g	Inlet Gas Rate (scfm)	1200
$\Delta T/\Delta z$	Temperature Gradient (˚F/100ft)	1.5
T_{sur}	Inlet Temperature (˚F)	80
P_b	Outlet Back Pressure (psia)	100
n_{noz}	Number of Nozzles	3
d_{noz}	Diameter of Nozzles (inch)	13/32
TVD	True Vertical Depth (ft)	10000

For foam drilling hydraulics in this study, the following assumptions are made for simplicity.

1. Steady-state and isothermal flow condition in each node
2. No effect of cuttings on pressure losses and density of fluid

3. Fluid temperature same as the wellbore temperature at each node

4. Continued drill pipe string with no tool joints and no pipe rotation

5. Circular wellbore diameter with concentric drill string

6. No lost circulation or formation influx

A schematic of well configuration and input parameters are shown in Fig. 5.1 and Table 5.1 respectively.

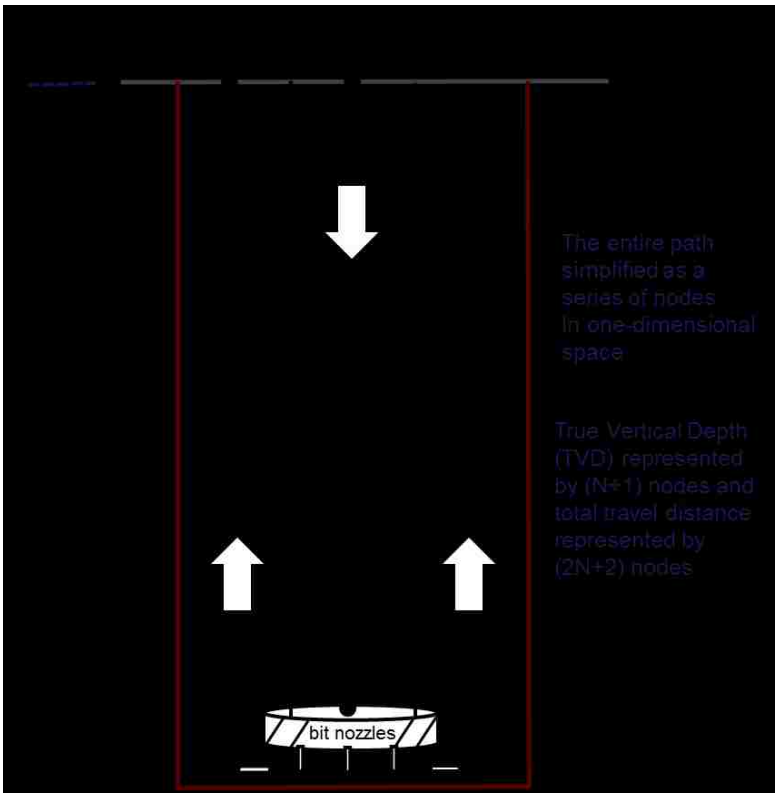

Figure 5.1: A schematic of the well configuration used in this study.

5.2 Results and Discussions

The results of this study are presented in the following three major steps: (i) creating a foam hydraulics simulator (Base Case) and comparing the results with Chen et al.'s study (2009) for model verification (note that existing empirical equations for fine-textured foams exhibits only low-quality

regime); (ii) improving the foam hydraulics simulator with both high-quality and low-quality regimes, assuming that foams inside drill string and outside in the annulus have the same f_g* (f_g* = 85%) (Case 1); and (iii) updating the foam hydraulics simulator with both regimes, assuming that foams inside drill string and outside in the annulus have different f_g* values (f_g* = 85% in the drill pipe and f_g* = 75% in the annulus) (Case 2). Although this study does not account for fluid intrusion from the formation at this stage, the reduction of f_g* in the annulus seems to be more realistic because formation fluids, such as brine and oil, tend to destabilize foams and thus lower f_g* evidently.

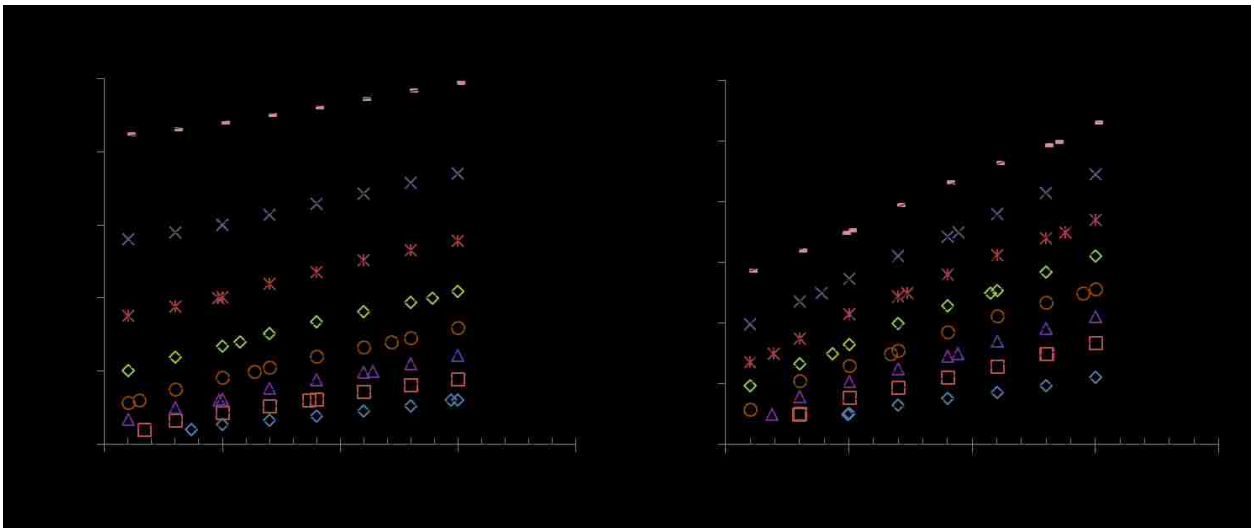

Figure 5.2: Base Case pressure contours in a wide range of gas and liquid velocities by using empirical equations from Chen et al. (2009) showing only low-quality regime: (a) foam inside drill pipe and (b) foam in the annulus.

Base Case calculation requires a construction of two flow regime map. Fig. 5.2 shows foam rheology plotted in a form of pressure contours by using empirical equations given by Chen et al. (2009) for foams inside drill pipe and in the annulus. As expected, the contours show only low-quality regime because the empirical equations deal with fine-textured homogeneous foam mixture. The symbols represent actual values calculated, and each line represents the best-fit straight line for that particular pressure gradient (ranging from 0.01 to 0.08 psi/ft) shown. Fig. 5.3 shows how the Base Case calculation

carried out by this study can be contrasted with Chen et al.'s case of aqueous foams (i.e., the thick line in Fig. 5.3(a)). There is good agreement between the two cases.

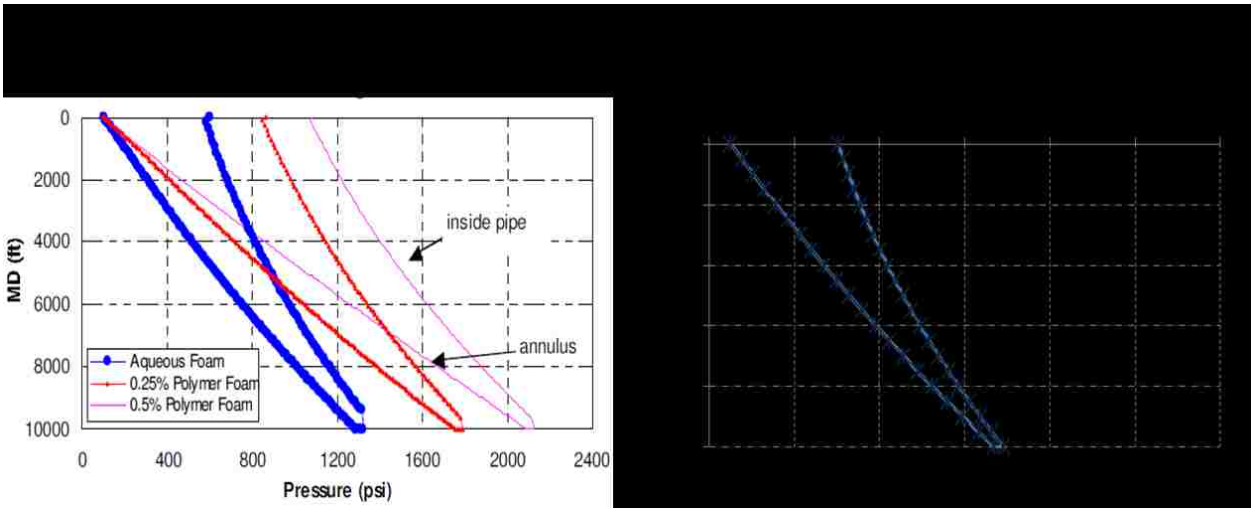

Figure 5.3: Comparison between (a) Chen et al. (2009) and (b) Base case of this study; the aqueous foam case in (a) is reproduced successfully by the hydraulics model developed in this study.

Case 1 calculation requires pressure contours showing both high-quality and low-quality regimes. Because Chen et al. (2009) provides foam-rheology empirical equations only for the low-quality regime, this study borrows foam rheological properties in the high-quality regime from Edrisi et al. (2013) where 0.5 wt % Stepanform surfactant solution was injected with nitrogen. Figs. 5.4(a) and 5.4(b) show the resulting two flow regime maps for foams inside drill pipe and in the annulus, respectively, with f_g* value of 85%. Note that the pressure contours in the low-quality regime in Figs. 5.4(a) and 5.4(b) are identical to those in Fig. 5.5(a) and 5.5(b), respectively. Following the technique presented by Edrisi and Kam (2013), the representative slopes of pressure contours in the high-quality and low-quality regimes are 90.0 (i.e., $m_1 = 90.0$) and 2.74 (i.e., $m_2 = 2.74$) within drill pipe. Similarly, the representative slopes of pressure contours in the high-quality and low-quality regimes are 90.0 (i.e., $m_1 = 90.0$) and 2.24 (i.e., $m_2 = 2.24$) in the annulus.

For the data points along the f_g* line marked by black dots in Figs. 5.4(a) and 5.4(b), the corresponding rheograms are constructed with shear stress (τ_w) and shear rate ($\dot{\gamma}_w$) (cf. Eqs. 5-8 through 5-11), as shown in Figs. 5.5(a) and 5.5(b). From the best-fit equations, the consistency index (K) and the power-law exponent (n) are determined to be 0.0614 and 0.411 inside drill pipe and 0.0724 and 0.366 in the annulus, respectively. Putting Fig. 5.4 and Fig. 5.5 together, the four foam model parameters to capture two flow regimes are decided.

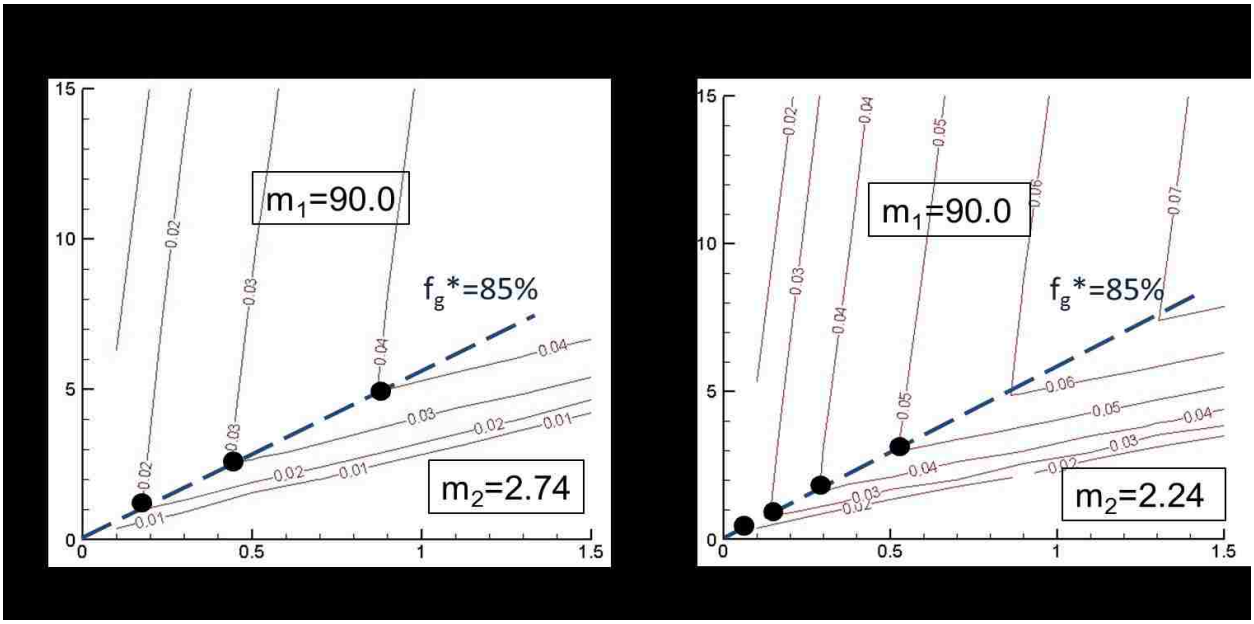

Figure 5.4: Case 1 pressure contours by using Chen et al. (2009) and Edrisi et al. (2013) at f_g^*= 85%; (a) inside drill pipe and (b) inside annulus.

Figs. 5.6(a) and 5.6(b) show the two flow regime map and rheogram for foams in the annulus in Case 2 where the f_g* value of 75 % is used. The representative slopes of pressure contours in the high-quality and low-quality regimes are 90.0 (i.e., m_1 = 90.0) and 1.84 (i.e., m_2 = 1.84) in the annulus. Foam rheology within drill pipe in Case 2 is identical to that in Case 1 as shown in Figs. 5.4(a) and 5.5(a).

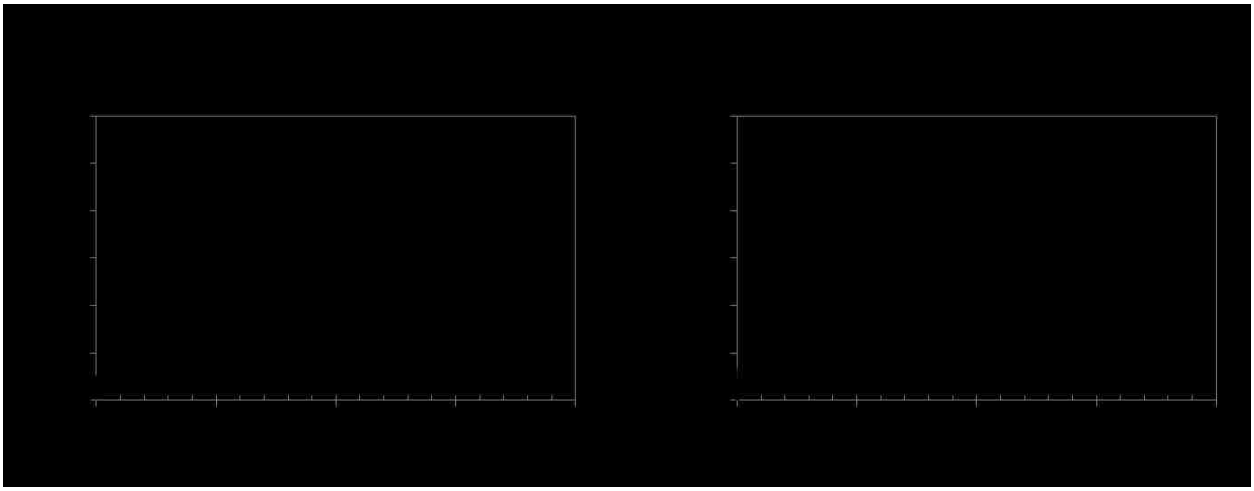

Figure 5.5: Case 1 constructed rheograms (shear stress τ_w vs. shear rate $\dot{\gamma}_w$) for foams along f_g^* line; (a) inside drill pipe and (b) inside annulus.

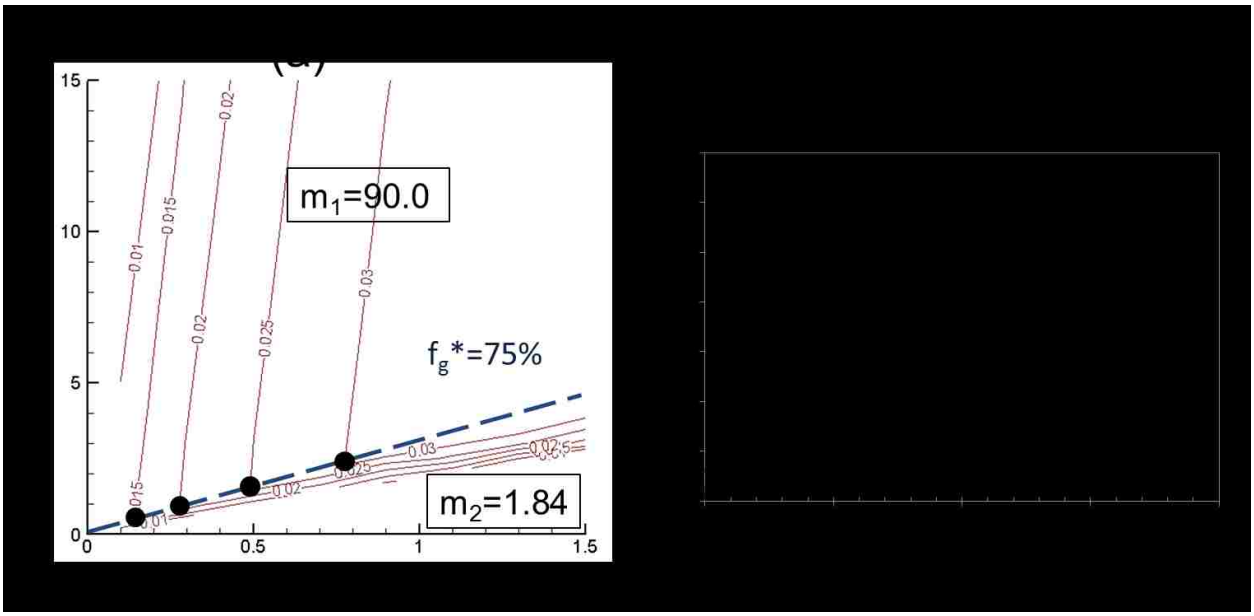

Figure 5.6: Case 2 (a) pressure contour and (b) rheogram in the annulus where f_g^* = 75% (foam rheology within drill pipe is identical to Case 1 as shown in Fig 5.4 (a) and Fig 5.5 (a))

In order to compare Base Case with Case 1 and Case 2, foam drilling calculation with input conditions specified in Table 5.1 are conducted for a well depicted in Fig. 5.1. The case of interest can be briefly summarized as follows: a vertical well with 10,000 ft , back pressure (p_b) of 100 psi, and gas and

liquid rates of 1200 scfm (standard cubic feet per minute) and 40 gpm (gallon per minute) at the inlet. Because there is not any sinks nor any sources present in the discussed cases in this study (No formation influx or lost circulation), foam quality of 97% at P_b can be calculated for these specific input parameters.

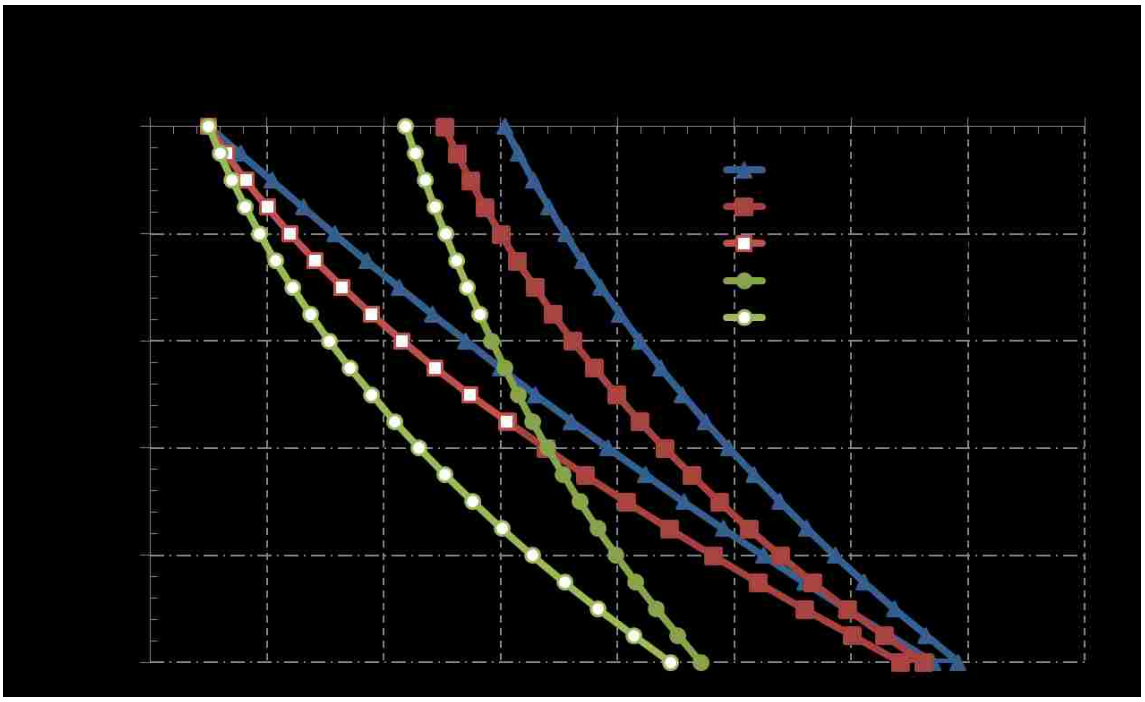

Figure 5.7: Comparison of Base Case, Case 1 and Case 2 in term of pressure along the well. (see Fig. 5.1 and Table 5.1 for more details)

Figs. 5.7 and 5.8 show the comparison in terms of pressure (P) and foam quality (f_g), respectively, as a function of vertical depth (z) (the pressure profile of the Base Case is identical to that in Fig. 5.3(b)). In all three cases, the pressure at the last node are the same as pre-specified back pressure (P_b = 100 psi, as expected. Note that for both Case 1 and Case 2, open marks represent foams in the high-quality regime while filled marks represent foams in the low-quality regime (Because Base Case deals with foams in the low-quality regime only, the results consist of all filled marks).

The calculations show the following results: Case 1 with f_g* of 85 % inside drillpipe and in the annulus exhibits only low-quality regime inside drillpipe and both high-quality and low-quality regimes

in the annulus (f_g* around vertical depth (z) = 5500 ft); and Case 2 with f_g* of 85% inside drillpipe and f_g* of 75% in the annulus exhibits both regimes inside drillpipe (f_g* around z = 3500 ft) and only high-quality regime in the annulus. Such a dramatic change is caused by the implementation of two flow regimes (more precisely, implementation of foam rheology in the high-quality regime) which impacts calculation of frictional pressure loss. Comparing the maximum pressure values at the bottomhole (1340 psia, 1285 psia, and 890 psia of Base Case, Case1, and Case 2 respectively), Case 1 and Case 2 have more than 4 % and 34 % deviation from the Base Case. This deviation is also found in terms of calculated inlet pressures, as much as17 % and 28 % for Case 1 and Case 2, respectively, compared with Base Case.

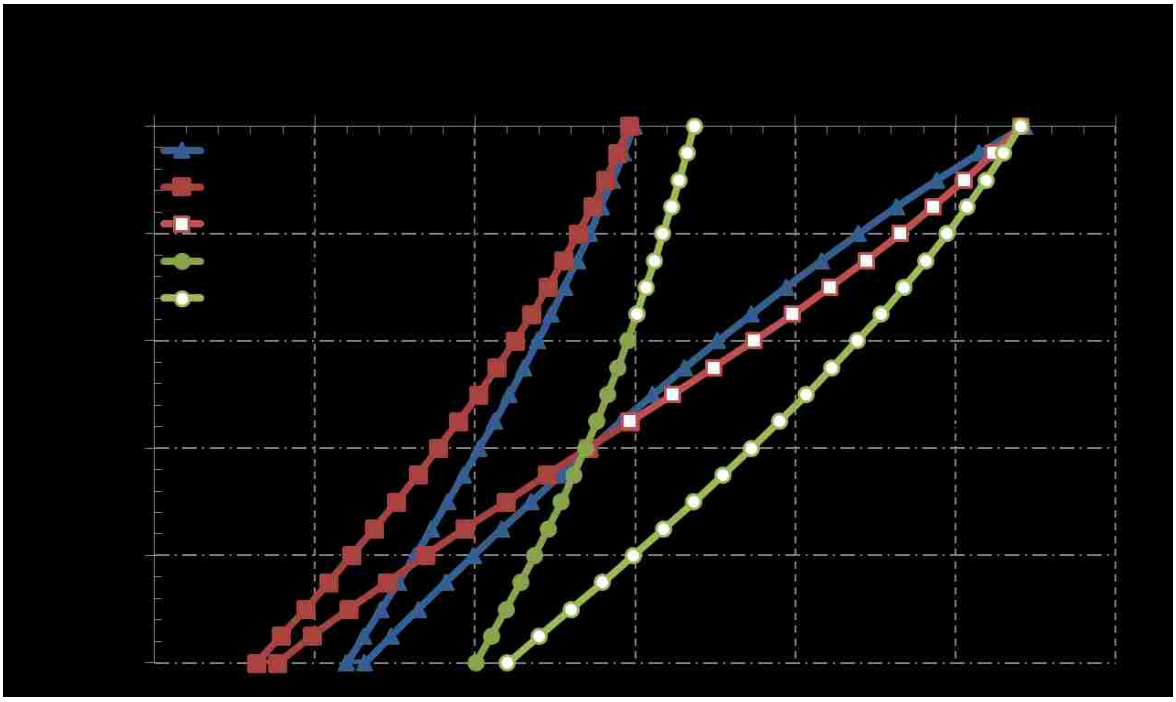

Figure 5.8: Comparison of Base Case, Case 1 and Case 2 in term of foam quality along the well. (see Fig. 5.1 and Table 5.1 for more details)

Similarly, when the foam quality at the bottomhole is compared (77 %, 74 %, and 81 % of Base Case, Case1, and Case 2 respectively), as much as 4 % and 5 % deviations from the Base Case are observed for Case 1 and Case 2 respectively. These results clearly show that, without both regimes accounted for, foam

drilling hydraulics calculations cannot be carried out reliably, and the amount of error associated becomes more significant as f_g* value becomes lower (or, as the high-quality regime becomes more pronounced during the process, equivalently).

Corresponding changes in mud density (i.e., density of foam mixture), total velocity, and total pressure gradient as a function of depth are also plotted in Figs. 5.9 through 5.11, again with open marks for the high-quality regime and filled marks for the low-quality regime. Compared with Base Case, Case 1 and Case 2 have 11% and 19% deviations in terms of density, 11% and 23% deviations in terms of total velocity, and 11% and 16% deviations in terms of total pressure gradient at the bottomhole condition. In all these plots, larger difference is between Base Case and Case 2 due to lower f_g* value of 75% compared to Case 1 (f_g* = 85%). This is consistent with the findings in Figs. 5.7 and 5.8, that is, as the high-quality regime dominates more in the annulus, the accuracy of the traditional drilling hydraulics calculations based on empirical foam rheology correlations becomes reduced further.

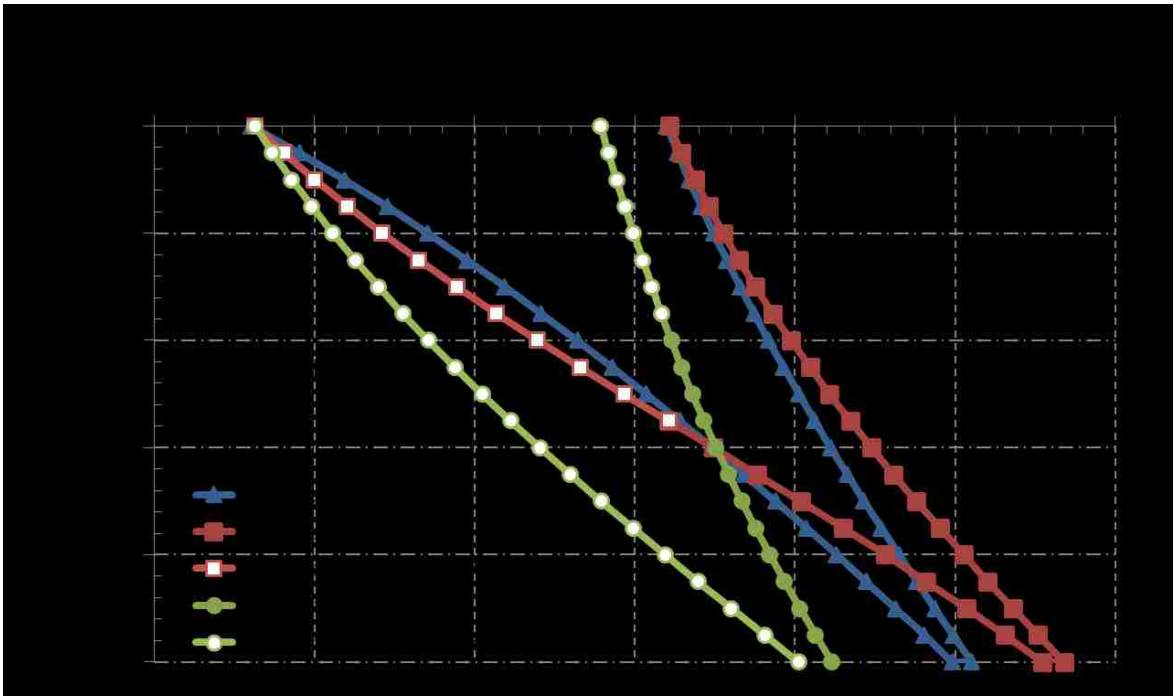

Figure 5.9: Comparison of Base Case, Case 1 and Case 2 in term of density of foam mixture along the well. (see Fig. 5.1 and Table 5.1 for more details)

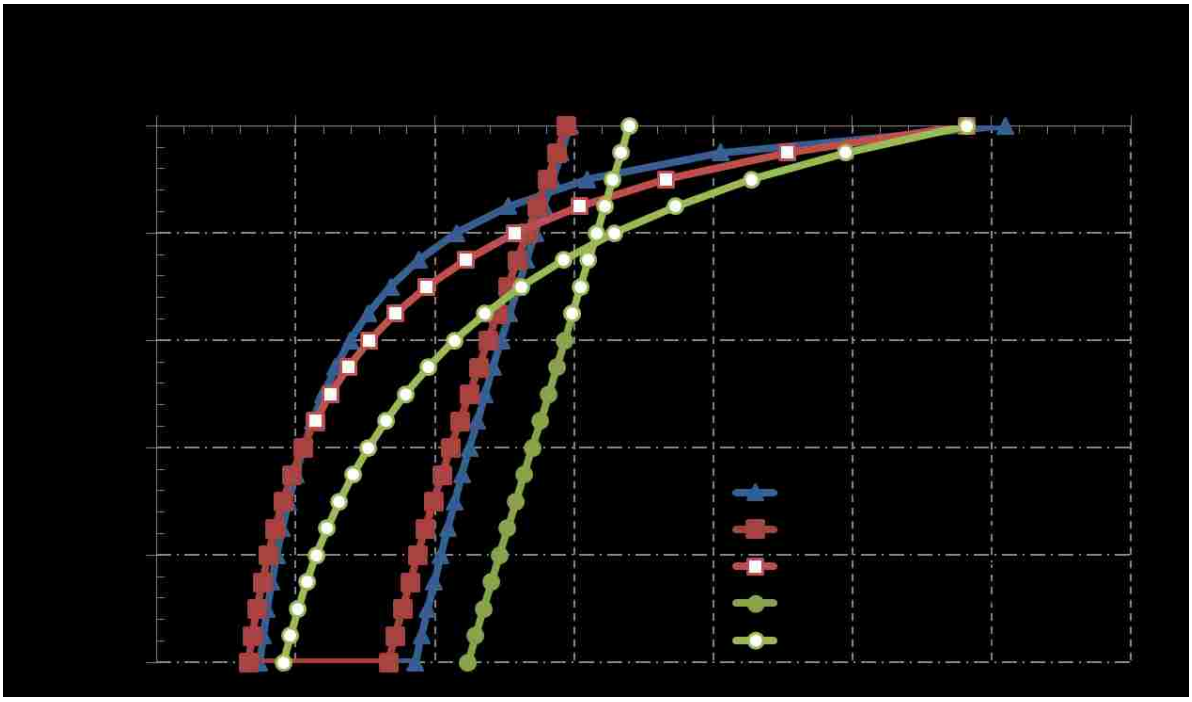

Figure 5.10: Comparison of Base Case, Case 1 and Case 2 in term of foam total velocity along the well. (see Fig. 5.1 and Table 5.1 for more details)

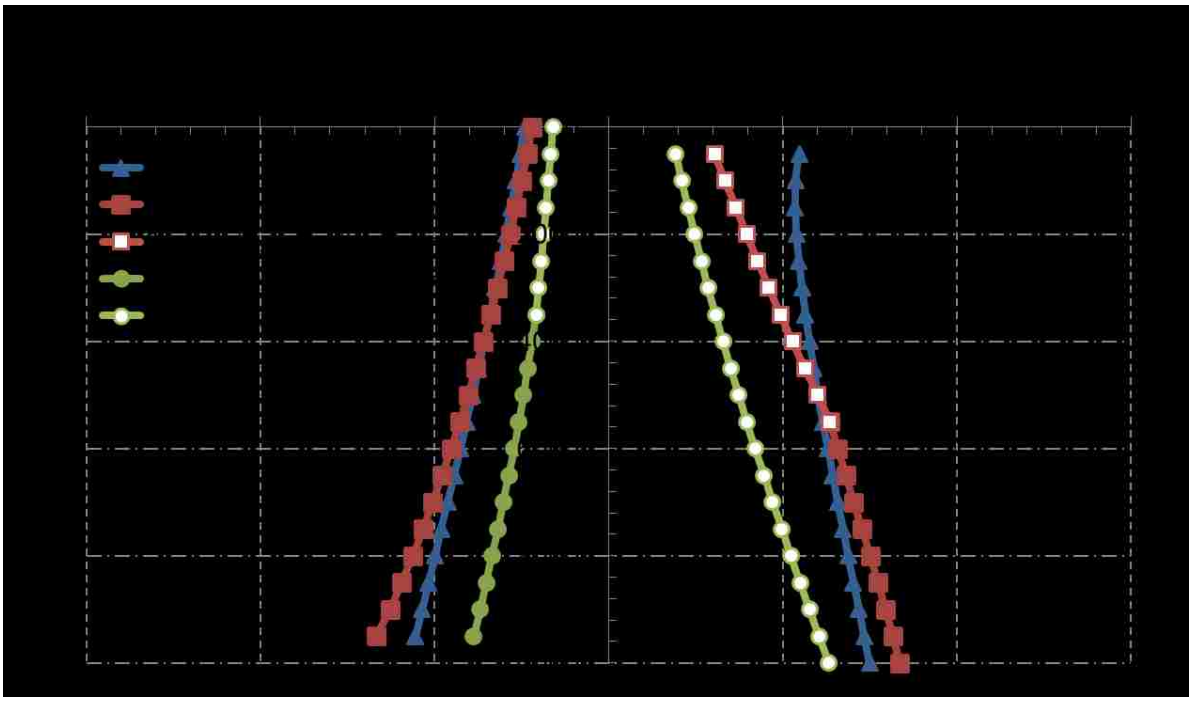

Figure 5.11: Comparison of Base Case, Case 1 and Case 2 in term of total pressure gradient along the well. (see Fig. 5.1 and Table 5.1 for more details)

CHAPTER 6: ADDITIONAL DISCUSSIONS

This chapter provides additional information related to the subjects investigated in earlier chapters. More specifically, included below are the effect of surfactant and polymer on interfacial tension, the use of dimensionless capillary number for two flow regime plot compared to those plots with pressure gradient and foam viscosity, and the extension of the four-parameter foam model into the cases with oil and polymer.

6.1 Surface tension measurement of surfactant polymer solutions

The experimental study in Chapter 3 with surfactant and polymer chemicals needs measurements of interfacial tension as an indirect indicator for foamability and foam stability. This is performed by pendant drop method in which the shape of a droplet is analyzed to estimate surface tension. Figure 6.1 shows pictures of drops taken from the experiments. Each reported value of surface tension and density in Table 1 is from the average of three separate measurements. Fig 6.2 shows how surface tension changes as a function of surfactant concentration in the surfactant solution. The critical micelle concentration (CMC) appears to be around 0.3 wt% beyond which the interfacial tension does not seem to vary significantly.

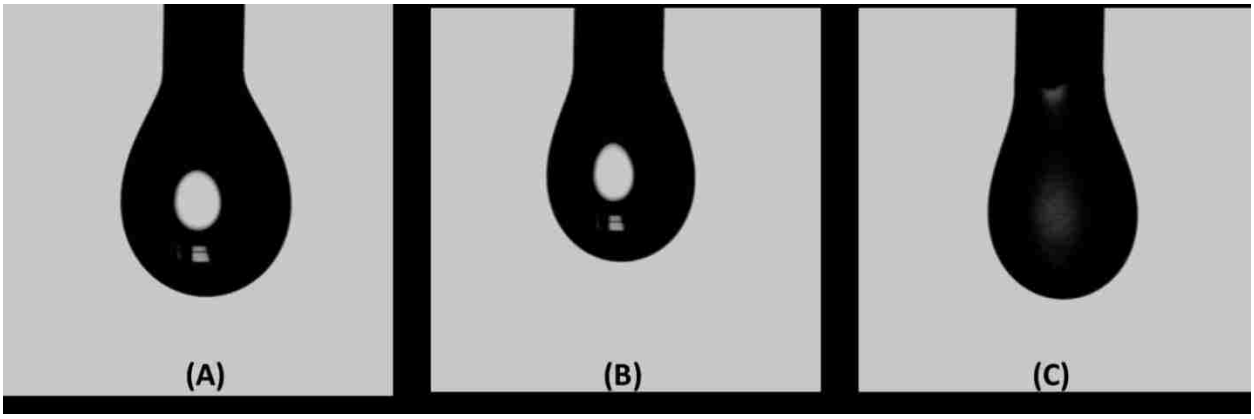

Figure 6.1: Pictures taken from surface tension measurements: (A) deionized water; (B) 0.5 wt% Stepanform surfactant solution; and (C) 0.5 wt% liquid guar CM in 0.5 wt% Stepanform solution.

Table 6.1: Surface tension and density measurements of Stepanform 1050 surfactant solutions

Concentration (wt% of Stepanform 1050)	Density (g/cm3)	Surface Tension (mN/m)
0	**0.9974**	**74.62**
0.1	**0.9975**	**55.99**
0.3	**0.9977**	**39.19**
0.5	**0.9978**	**37.88**
1	**0.9982**	**37.07**

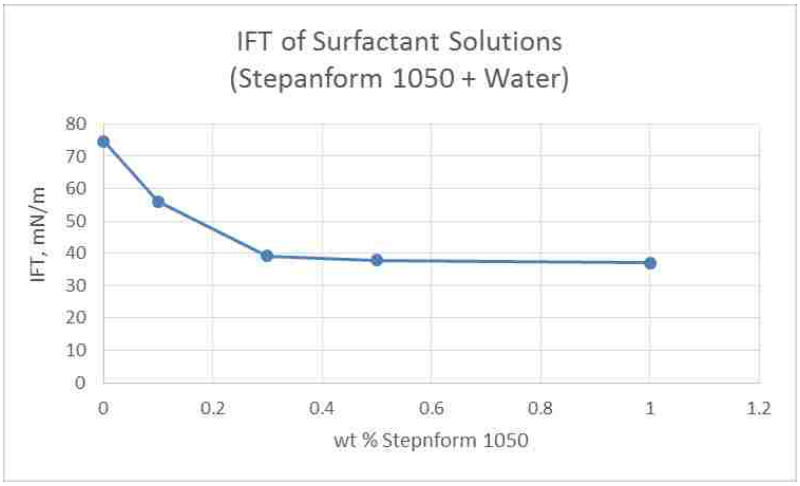

Figure 6.2: Surface tension measurement as a function of surfactant concentration wt% of Stepanform 1050 in deionized water) with no polymer.

Figs. 6.3 and 6.4 show the effect of polymer or surfactant concentration on surface tension measurements, more precisely, the effect of polymer concentration at 0.5 wt% Stepanform surfactant solution (Fig. 6.3) and the effect of surfactant concentration at 0.5 wt% Liquid Guar CM polymer solution (Fig. 6.4). The results show that the polymer concentration does not seem to affect the surface tension of the solution, while surfactant concentration does impact the surface tension significantly just like the case without polymer (Fig. 6.2).

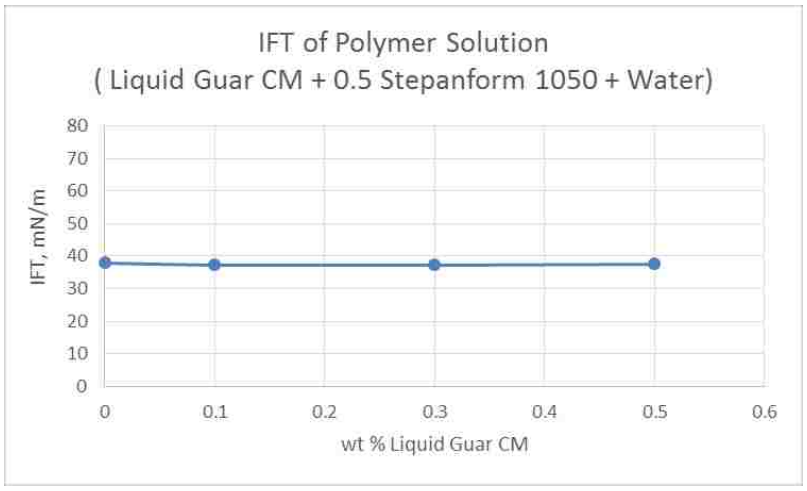

Figure 6.3: Surface tension measurement as a function of polymer concentration (0.5 wt% Stepanform 1050 solution).

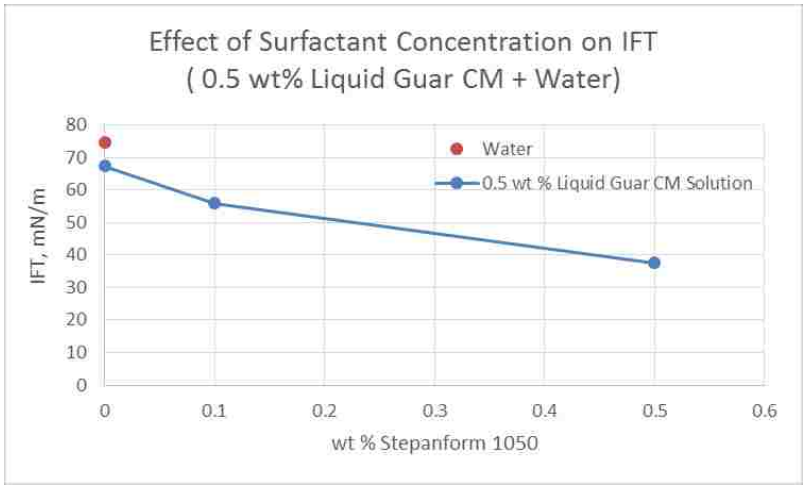

Figure 6.4: Surface tension measurement as a function of surfactant concentration (0.5 wt% Liquid Guar CM solution).

6.2 Use of dimensionless numbers for two flow regime map

Dimensionless capillary number is a concept popular to understand how non-wetting phase is trapped by capillary force in a pore network where wetting phase is introduced. Applying a similar concept of using dimensionless variable may have additional benefits for foam flow in pipes. Dimensionless capillary number (N_{ca}) can be expressed as follows in terms of fluid viscosity (μ), velocity (u), and interfacial tension (σ) (Kraynik, 1988):

$$N_{ca} = \frac{\mu u}{\sigma} \tag{6-1}$$

This implies that the translation from pressure data to dimensionless capillary number requires apparent foam viscosity (μ_{app}), which can be calculated using definitions of wall shear stress (τ_w) and wall shear rate (γ_w) [See Eqs.s (3-3) through (3-5) in Chapter 3 for more information].

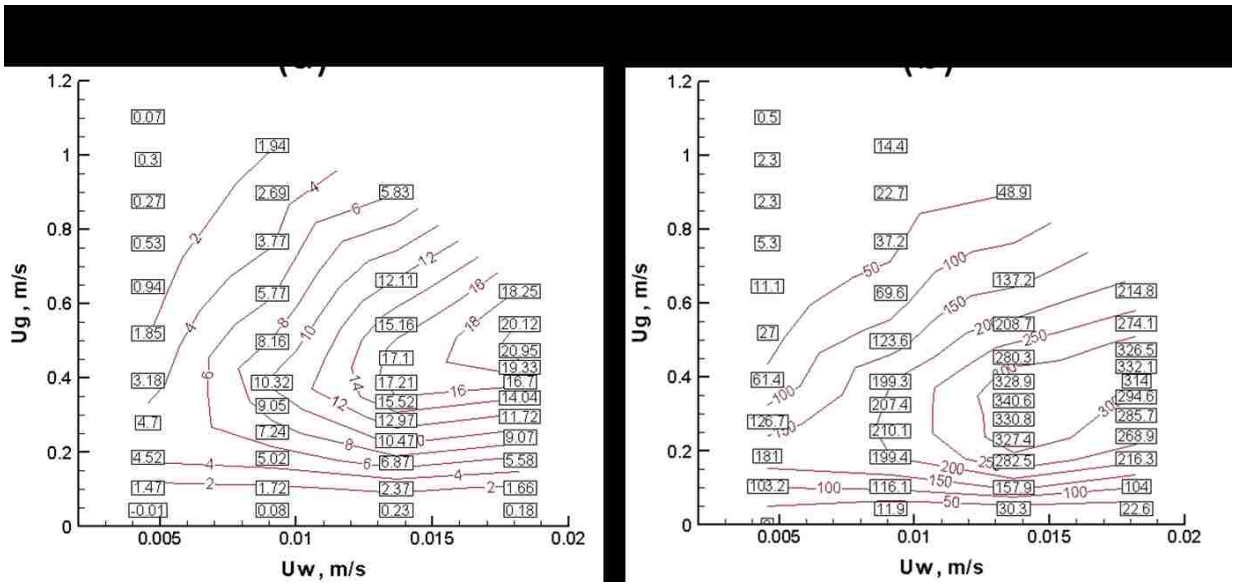

Figure 6.5: Translation of (a) pressure contours (psi) into (b) apparent foam viscosity (centipoise) contours.

Fig. 6.5 show one example showing how to convert pressure contours into foam viscosity contours. The plot is somewhat distorted because of nonlinear relationship between foam viscosity and pressure drop through injecting gas and liquid velocities and resulting bubble size distributions. Note that Fig. 6.5 is no other than Fig. 3.8 in Chapter 3.

Fig. 6.6 shows the translation into dimensionless capillary number by using pressure and foam viscosity contours in Fig. 6.5. As expected, the general trend is very similar to the pressure contours because the definition of dimensionless capillary number has foam viscosity as one of the scaling factors (cf. Eq. (6.1)), even though the magnitude is altered. Using the same approach one can produce contour

plots for dimensionless Reynolds number (Re) and Froude number (Fr) by using equations 6-2 and 6-3 (Darby, 2001) as shown in Fig. 6.7. Figure 6.8 shows the changes in these dimensionless numbers during drilling hydraulics calculations along the example cases discussed in chapter 5.

$$Re = \frac{\rho v D}{\mu} \tag{6-2}$$

$$Fr = \frac{v}{\sqrt{gD}} \tag{6-3}$$

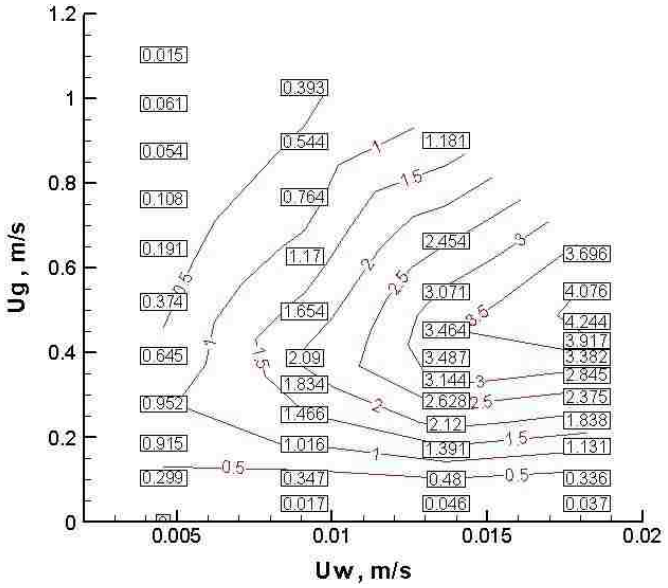

Figure 6.6: Translation into dimensionless capillary number contours.

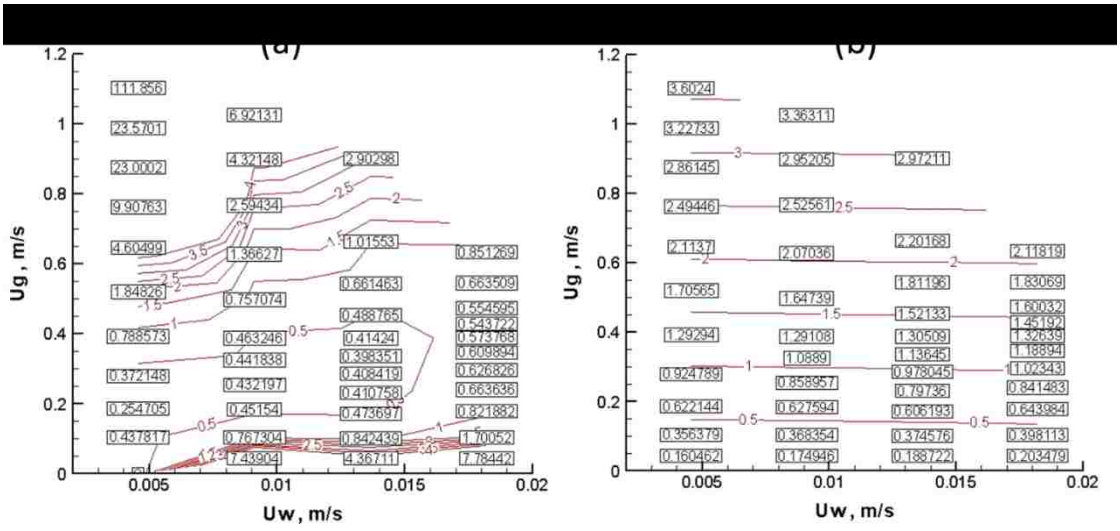

Figure 6.7: Translation of pressure contours into (a) Reynolds number and (b) Froude Number.

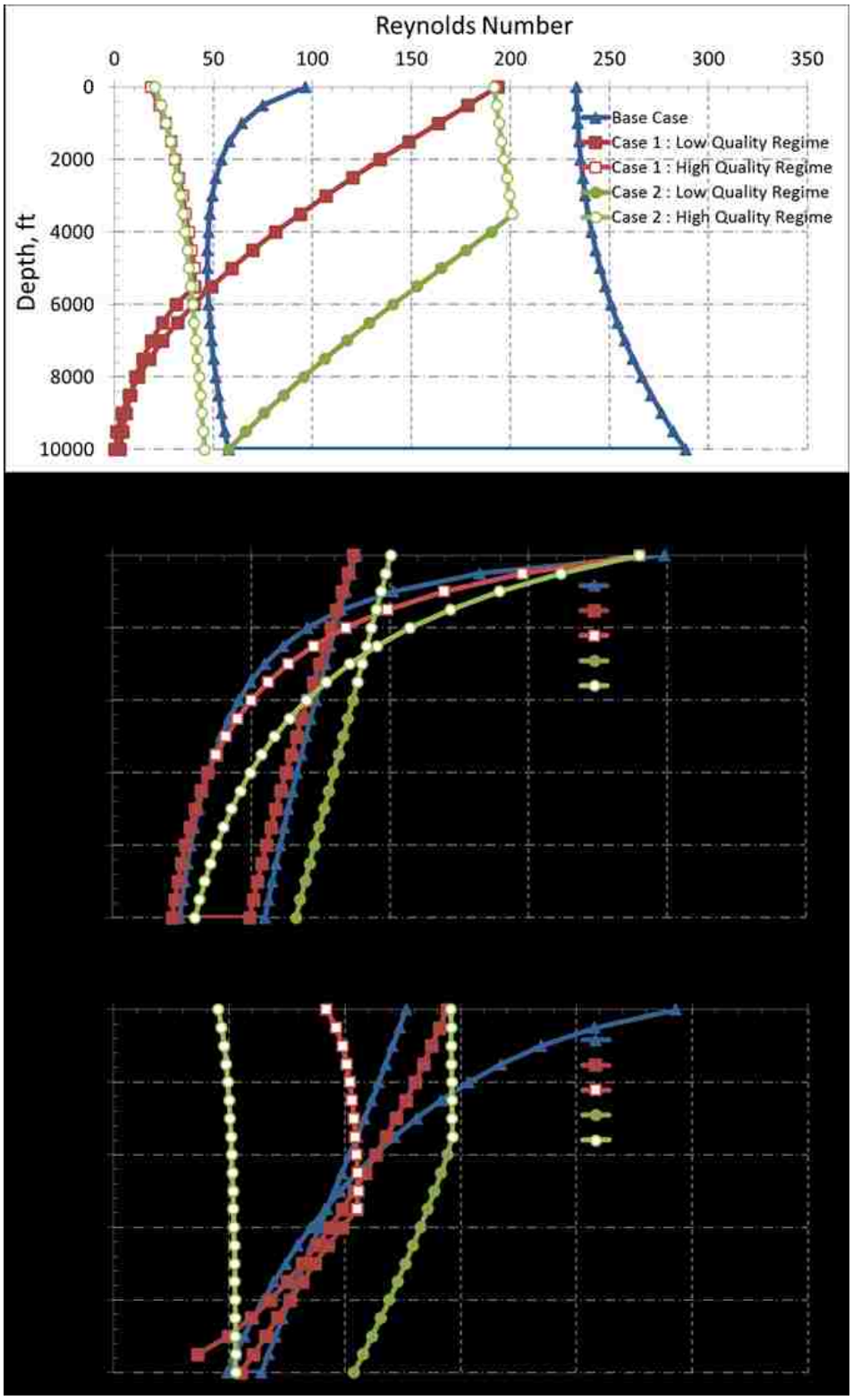

Figure 6.8: Comparison of Base Case, Case 1 and Case 2 in terms of dimensionless numbers along the well. (see Fig. 5.1 and Table 5.1 for more details)

6.3 Extension of two foam-flow regimes model into other cases

The new foam model introduced in this study, demonstrated with experimental data with surfactant foams in 0.38 inch ID (Chapter 4), can ideally be applied to a wide range of experimental conditions. Three examples are shown below.

6.3.1 Surfactant foams with oil

Fig. 6.7 shows pressure contours for surfactant foams and oil (i.e., 0.5 wt% Stepanform 1050 surfactant solution and 0.5 ccm n-Decane; the same as Fig. 3.11). Fig. 6.8 is the reconstructed contours by using a small and a large number of sample data points (Fig. 6.8(a) and Fig. 6.8(b), respectively), both of which are in good agreement with the original plot in Fig. 6.7.

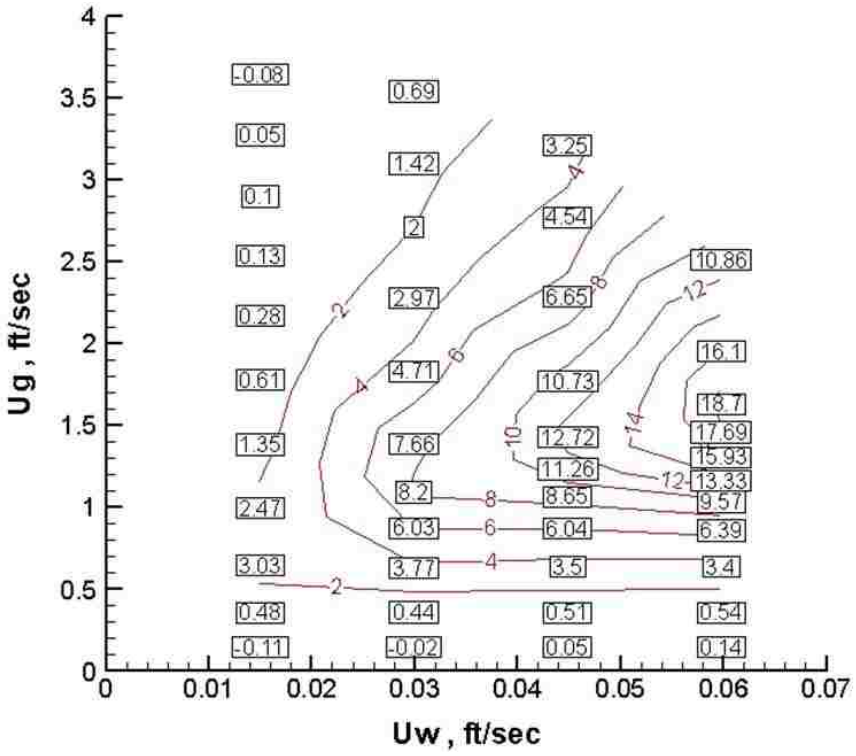

Figure 6.7: Pressure-drop contours for surfactant foams and oil.

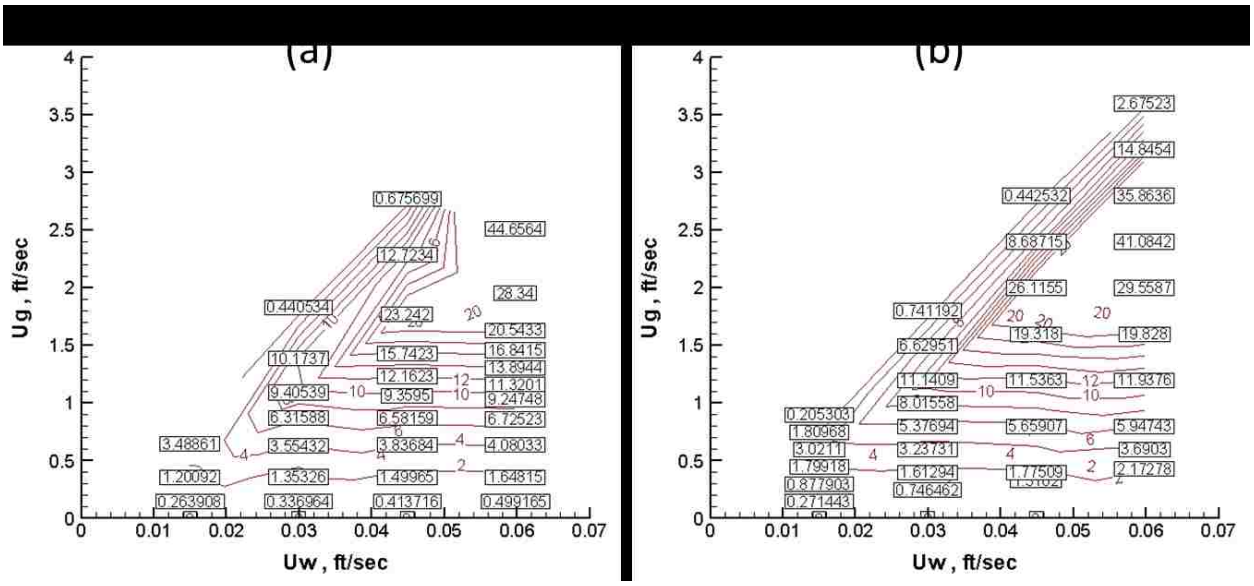

Figure 6.8: Reconstruction of two-flow-regime pressure contours for surfactant foams and oil.

6.3.2 Surfactant foams with polymer

Fig. 6.9 shows pressure contours for surfactant foams with polymer (the same as Fig. 3.16x) followed by the reconstructed contours showing good agreement.

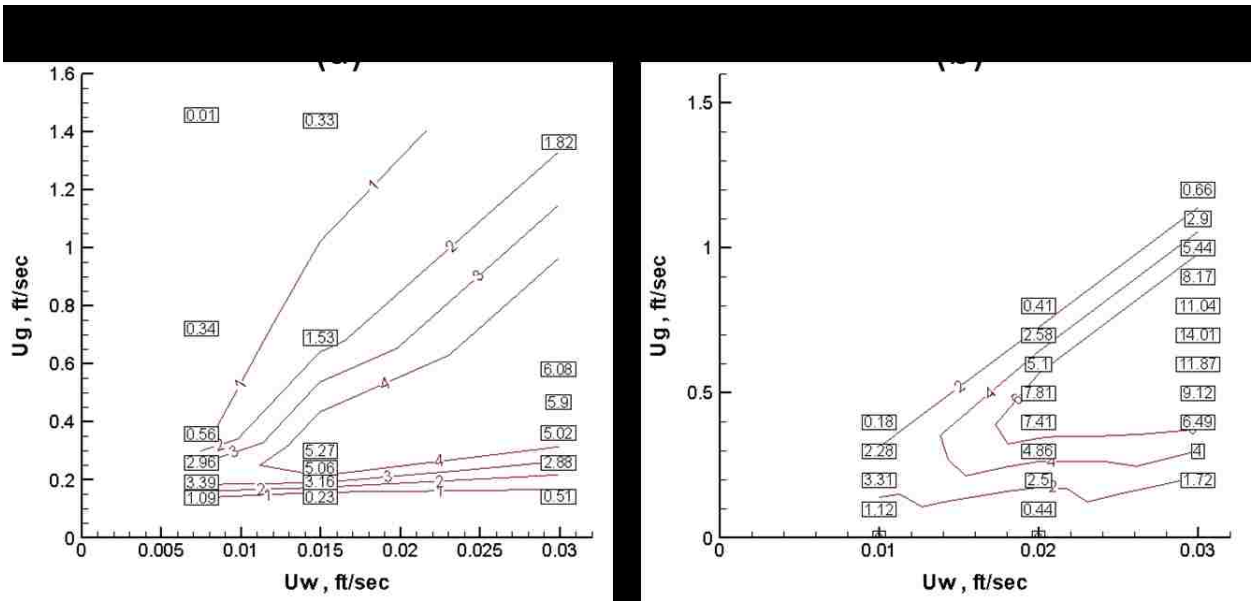

Figure 6.9: Original (a) and reconstructed (b) pressure contours for polymer-added surfactant foams.

6.3.3 Surfactant foams for a larger pipe diameter

Fig. 6.10 shows pressure contours from Bogdanovic et al. (2009) with 1 wt% Cedepal FA-406 in a 12 ft long 1 inch NPS stainless steel pipe. The reconstructed plot is in good agreement with original data.

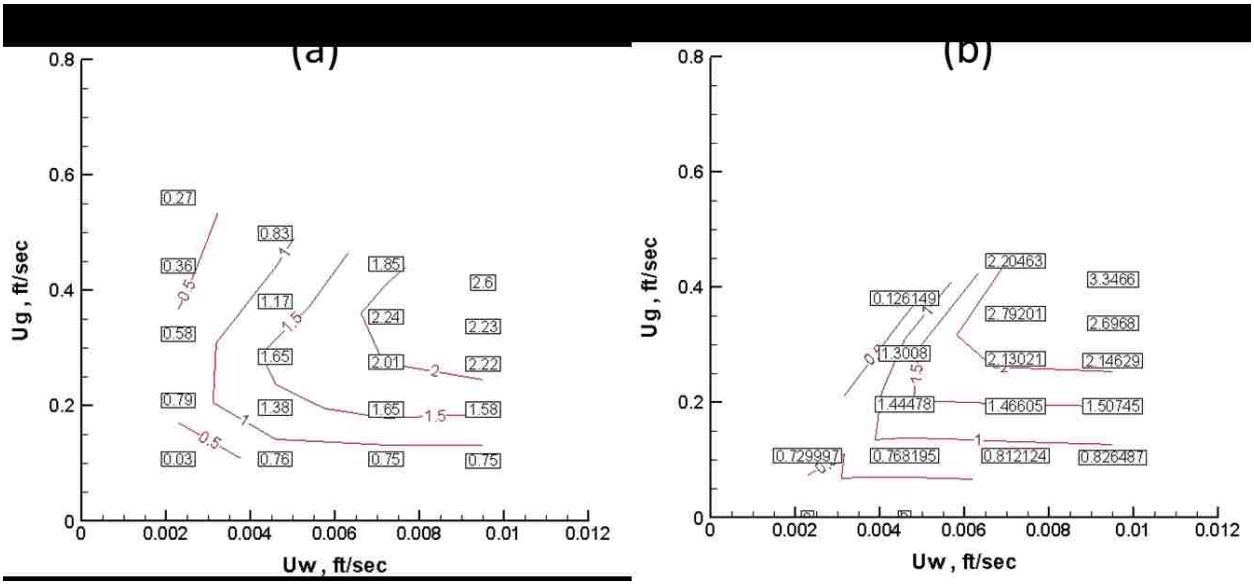

Figure 6.10: Original (a) and reconstructed (b) pressure contours (1 wt% Cedepal FA-406 surfactant solution in 12 ft length 1 inch NPS stainless steel horizental pipe).

CHAPTER 7: CONCLUSIONS AND RECOMMENDATIONS

7.1 Conclusions

This study consists of three major parts: (1) experimental investigation of foam rheology in pipes (Chapter 3); (2) building up of a new foam model consistent with lab-measured experimental data (Chapter 4); and (3) the application of the model in drilling hydraulics modeling and simulation (Chapter 5). The followings show detailed conclusions based on three different components of the study.

7.1.1 Two Foam-Flow Regimes in Presence of Oil and Polymer (Part 1)

A series of foam flow experiments were carried out in horizontal pipes in order to investigate foam flow characteristics by using Stepanform surfactant, Liquid Guar CM polymer, and decane oil. Major conclusions of this study can be summarized as follows:

1. In all three different types of experiments (surfactant foams, surfactant foams with oil flowing together, and polymer-added surfactant foams), the presence of both high-quality and low-quality regimes were observed consistently. This finding was evidenced by two distinct pressure contours (i.e., almost horizontal slope in the low-quality regime and finite slope in the high-quality regime) as well as bubble-size distribution and foam flow patterns.

2. The experiments with polymer-free surfactant foams showed that the low-quality regime consisted of segregated and plug flow patterns, while the high-quality regime consisted of slug and mist flow patterns. The experiments with polymer-added surfactant foams showed that there existed a chaotic transition region between slug and plug flow patterns in which the pressure response and flow pattern did not converge. This chaotic transition region with dramatic changes in foam flow characteristics seemed to be because of viscosity increase with polymers, which resulted from not only reduced bubble creation even at high shear stress, but also slow water transport through foam films reducing bubble coalescence. Irrespective of the presence of polymers, though, a single foam model capturing both high-quality and

low-quality regimes was believed to be used consistently.

3. The presence of oil impacted the stability of surfactant foams negatively. This led to a reduction in steady-state pressure drop as well as easier transition from plug flow to slug flow patterns. The effect of oil on polymer-added surfactant foams was expected to be material specific. This implied that even a small quantity of oil intruding from the formation during underbalanced foam drilling might have a non-negligible effect on foam drilling hydraulics.

4. Preparation of polymer solutions at high shear rate should be performed carefully in order to obtain polymer solutions with reproducible viscosity and with long-term stability. It is because the rheology of polymer solutions was very sensitive to the way how they were prepared.

7.1.2 Modeling Foam Flow in Pipes Using Two Foam-Flow Regimes Concept (Part 2)

This study has established a new foam modeling technique in order to fit experimental data exhibiting two foam-flow regimes. Because of a wider range of gas and liquid velocities it covers, this improved foam modeling technique potentially can help optimize many foam-associated field applications, such as tight-gas and shale-gas fracturing, foam drilling, cutting transport, and liquid unloading. The major outcomes of this study can be summarized as follows:

1. This new improved foam modeling technique is comprehensive so that it can cover foam rheological behaviors in a wide range of gas velocity (u_g) and liquid velocity (u_w), encompassing both slug-flow pattern in the high-quality regime and plug-flow pattern in the low-quality regime. The model successfully reproduces two distinct pressure contours – almost horizontal pressure contours in the low-quality regime and inclined pressure contours in the high-quality regime.

2. If the (u_g, u_w) flowing condition falls on the boundary between the high-quality and low-quality regimes (or, on the f_g* line equivalently), the corresponding pressure drop can be calculated directly from the foam rheology model. If the flowing condition is off the f_g* line and resides either in the high-quality or low-quality regime, the corresponding pressure drop can be calculated from both (i) foam

rheology model along the f_g* line and (ii) slopes representing foam characteristics in each regime.

3. For foams in the low-quality regime showing plug-flow pattern with a homogenous fine-textured mixture, the model shows that the level of wall slip (represented by slip velocity and slip coefficient) is a key to understand foam rheology. This new model and previous studies agree well in that the wall slip increases, as foam becomes wetter and thus water film thickness at the wall increases.

4. For foams in the high-quality regime showing slug-flow pattern with repeating free-gas and foam-slug segments, the relative size of these two segments is a key to understand foam rheology. The model shows that the relative size of free-gas segment increases rapidly as foam becomes drier and moves off from the f_g* line, which is consistent with observations from previous visualization studies.

7.1.3 Use of New Foam Modeling Technique in Drilling Hydraulics (Part 3)

For the first time, this study incorporates the new concept of "two foam-flow regimes" into drilling hydraulics calculations, dealing with both high-quality and low-quality regimes separated by a threshold foam quality (f_g*). Three different cases investigated are as follows: Base Case with only low-quality regime based on existing empirical foam rheology correlations, Case 1 with both high-quality and low-quality regimes with f_g* = 85 %, and Case 2 with both regimes with f_g* = 85 % within drillpipe and f_g* = 75 % in the annuls. The results show that a reliable design and evaluation of foam drilling process cannot be achieved without taking both regimes into consideration.

More precisely, for the example of a vertical well with total depth of 10,000 ft, back pressure of 100 psia, and outlet foam quality of 97% selected in this study, Case 1 and Case 2 show 4 % and 34 % deviations in terms of pressure, 11 % and 19 % deviations in terms of foam density, and 11 % and 23 % deviations in terms of foam velocity at the bottomhole conditions and 17 % and 28 % deviations in terms of inlet pressure.

7.2 Recommendations and Future Directions

Following suggestions can be made as the future directions based on the experiences gained by this study.

1. This study used a limited number of surfactant and polymer formulations: two surfactants (Stepanform 1050 and Cedepal FA-406) (both anionic surfactants) at the concentration ranging from 0.1 to 0.5 wt% and only one polymer solution (Liguid Guar CM) at one concentration of 0.5 wt % mixed with surfactant solutions. In addition, there is also one type of oil (n-Decane) applied at one oil injection rate (0.5 ccm). Because the two foam-flow regimes concept modeled in this study has not been verified beyond the ranges of chemicals, concentrations and flow rates, further laboratory experiments are required in these conditions to collect more experimental evidence. How the theory and modeling technique deviate in presence of solids is also of great interest in cutting transport during drilling and in proppant delivery during fracturing.

2. Although the boundary between the low-quality and high-quality regimes (f_g*) is approximated by a straight line in pressure contour plots in this study, the exact trend may not be the case (showing a slightly concave trend). In addition, the pressure contours in the high-quality regime, modeled by a family of straight lines, seem to be curved downward somewhat. Although the model proposed in this study uses only four foam model parameters to capture the linear f_g* line and linear pressure contours in both regimes, one may sacrifice the "simplicity" of the model to capture more detailed responses observed in the experiments. More experimental data to investigate these behaviors should be collected in parallel with updating the model with model parameters more than four. Furthermore, this study uses power-law model for foam rheology. The choice of Bingham plastic model may make more sense for some applications dealing with laminar flow conditions.

3. The insight on how to make this model "predictive" seems an interesting topic to visit. This issue is related to the practical use of the model, i.e., how to take advantage of the model to go from one case to another by minimizing the number of experiments to be conducted. Using the framework

established in this study, one requires enough experimental data to determine four model parameters together with f_g*. The minimal level would be the number of data points to draw two pressure contours so that one can extract foam rheology (n and K in this study), two slopes (m_1 and m_2), and the boundary between the regimes (f_g*). For foam applications in which the transient behavior is important, developing a "predictive" model using mechanistic approaches and interpreting the results with dimensionless numbers may play a key role in the optimal design, which remains as a future research topic. Upscaling the model for a bigger system, especially where the pipe radius is larger, would be an interesting future research topic.

4. This study presented how to extract model parameters consistent with two foam-flow regimes concept, but the model parameter values may vary significantly, depending on actual applications of interest. A wide range of flow conditions in these applications may include, but not limited to, different chemical additives (viscosity modifiers, lubricants, corrosion inhibitors, etc.), shear rates, conduit shapes and sizes (slits, pipes, annulus, etc.), conduit materials, presence of solid particles and , if so, types and sizes of solids, and so on.

5. The model in its current form only concerns the rheological properties of foam itself, not accounting for additional mechanisms associated with various foam field applications. For example, foam-assisted liquid unloading process requires an understanding of foam rheology as well as foam's ability to displace liquid on top of foams in a deep vertical well. Another example is hole cleaning process in a long horizontal well where foam rheology is commingled with foam's capability of delivering rock cuttings. Such application-specific characteristics obviously impose additional research challenges on the top of rheological properties of foams in pipe as shown in this study.

6. The example of using foams in drilling process as shown in this study may not be complicated enough at this stage to be applied in actual foam drilling hydraulics calculations, because it does not account for interactions between foams and drilling muds/rock cuttings, foam rheology in narrow annular spaces, interaction between foams and formation fluids, and so on. Extension of foam

drilling into Managed Pressure Drilling and Dual-Gradient Drilling in the future can be an important step for deepwater drilling technique.

REFERENCES

Aadnoy, B., Cooper, I., Miska, S., et al. 2009. Advanced Drilling and Well Technology. *Society of Petroleum Engineering.*

Abbott, W. A. and Vaughn, H. F. 1976. Foam Frac Completions for Tight Gas Formations. *Petroleum. Engineering* (April): 38-50.

Aleklett, K. 2013. U.S. rig count for oil and gas and future economic growth. Retrieved from http://aleklett.files.wordpress.com/2013/01/usa_riggcount_2012.jpg

Aubert, J. H.; Kraynik, A. M.; and Rand, P. B. 1986. Aqueous Foams. *Scientific American* **254** (5): 58-66.

Baker, D. 1954. Simultaneous Flow of Oil and Gas. *Oil and Gas J* **53** : 183-195.

Baker Hughes Inc. 2012. North America Rotary Rig Count Archive. Retrieved from http://phx.corporate-ir.net/phoenix.zhtml?c=79687&p=irol-reportsother

Beggs, D.H. and Brill, J.P. 1973. A Study of Two-Phase Flow in Inclined Pipes. *Journal of Petroleum Technology* **25** (5): 607-617. SPE 4007-PA.

Bekkour, K. 1999. Evaluation of slip effects in the capillary flow of foams. *Applied Rheology* **9** : 10–16.

Bennion, D. B., Lunan, B. Saponja, J. 1996. Underbalanced Drilling And Completion Operations to Minimize Formation Damage-Reservoir Screening Criteria For Optimum Application. *Journal of Canadian Petroleum Technology* **37** (9). DOI : 10.2118/98-09-03.

Beyer, A.H., Millhone, R.S., and Foote, R.W. 1972. Flow Behavior of Foam as a Well Circulating Fluid. Paper SPE 3986. Presented at Fall Meeting of the Society of Petroleum Engineers of AIME, San Antonio, Texas, 8-11 October.

Bietz, R. F., Bennion, D. B. and Thomas, F.B. 1993. Optimizing drilling fluids in horizontal wells – laboratory advancements. Presented at the fifth international conference on horizontal well technology, Amsterdam, Netherlands, July 14-16, 1993.

Bikerman, J. 1973. *Foams.* Applied Physics and Engineering. Vol. 10. Springer-Verlag, Berlin.

Blauer, R.E. and Kohlhaas, C.A. 1974. Formation Fracturing with Foam. Paper SPE 5003 presented at Fall Meeting of the Society of Petroleum Engineers of AIME, Houston, Texas, 6-9 October.

Blauer, R. E., Mitchell B. J., and Kolhaas, C. A. 1974. Determination of Laminar, Turbulent, and Transitional Foam-flow Friction Losses in Pipes. Paper SPE 4885 presented at 44th SPE annual California regional meeting, San Francisco, California, 4-5 April.

Bogdanovic, M., Gajbhiye, R. N., and Kam, S. I., 2009. Experimental study of foam flow in pipes: Two Distinct flow regimes. *Colloids and Surfaces A: Physicochemical and Engineering Aspect* **344** (1): 56-71.

Bonilla, L.F. and Shah, S.N. 2000. Experimental Investigation on the Rheology of Foams. Paper SPE 59752 presented at 2000 SPE/CERI Gas Technology Symposium, Calgary, Alberta, Canada, 3-5 April.

Bourgoyne Jr., A.T., Millheim, K.K., Chenevert, M.E. and Young Jr., F.S. 1986. *Applied Drilling Engineering.* Vol. 2. Society of Petroleum Engineers. ISBN:978-1-55563-001-0

Briceno, M.I. and Joseph, D.D. 2003. Self-lubricated transport of aqueous foams in horizontal conduits. International Journal of Multiphase Flow **29**: 1817-1831.

Calvert, J. R. and Nezhati, K., 1986. A Rheological Model for a Liquid-Gas Foam. *International Journal of Heat and Fluid Flow* **7** (3): 164-168.

Capo, J., Yu, M., Miska, S.Z., et al. 2006. Cuttings Transport with Aqueous Foam at Intermediate Inclined Wells. *SPE Drilling & Completion* **21** (2): 99-107. SPE-89534-PA.

Chen, Z., Duan, M., Miska, S.Z., Yu, M., Ahmed, R.M., and Hallman, J. 2009. Hydraulic Predictions for Polymer-Thickened Foam Flow in Horizontal and Directional Wells. *SPE Drill & Compl* **24** (1): 40-49. DOI: 10.2118/105583-PA.

Chen, Z., Ahmed, R.M., Miska, S.Z., Takach, N.E., Yu, M., Pickell, M.B. and Hallman, J. 2007. Experimental Study on Cuttings Transport with Foam under Simulated Horizontal Downhole Conditions. *SPE Drilling & Completion* **22** (4): 304-312. DOI: 10.2118/99201-PA.

Chen, Y., Pope, T.L., and Lee, J.C. 2005. Novel CO2-Emulsified Viscoelastic Surfactant Fracturing Fluid System. Paper SPE 94603 presented at SPE European Formation Damage Conference, Sheveningen, The Netherlands, 25-27 May.

Curtis, J.B. 2002. Fractured shale - gas systems. *AAPG Bulletin* **86** (11): 1921-1938.

Darby, R., 2001. *Chemical Engineering Fluid Mechanics*. Second Editions, Revised and Expanded. Marcel Dekker Inc., New York, NY. ISBN: 0-8247-0444-4.

David, A., and Marsden, S.S. Jr. 1969. The Rheology of Foam. Paper SPE 2544 presented at SPE Annual Meeting, Denver, 28 September - 1 October.

Dranchuk, P.M., and Abou-Kassem, J.H. 1975. Calculation of z-factors for natural gases using equations of state. *Journal of. Canadian Petroleum Technology* **14** (3), 34-36.

Edrisi, A.R., Gajbhiye, R.N., and Kam, S.I. 2012. Experimental Study of Polymer-free and Polymer-added Foams for Underbalanced Drilling: Are Two Foam-Flow Regimes Still There? Paper SPE162712 presented at the SPE Canadian Unconventional Resources Conference, Calgary, Canada, 30 October – 1 November.

Edrisi, A.R. and Kam, S.I. 2012. A New Foam Rheology Model for Shale-Gas Foam Fracturing Applications. Paper SPE162709 presented at the SPE Canadian Unconventional Resources Conference, Calgary, Canada, 30 October – 1 November.

Enzendorfer, C., Harris, R.A., Valko, P., et al. 1995. Pipe viscometry of foams. *Journal of Rheology* **39** : 345–358.

Falk, K. and McDonald, C. 1995. An Overview of Underbalanced Drilling Applications in Canada. Paper SPE 30129 presented at the SPE European Formation Damage Conference held in The Hague, The Netherlands, 15-16 May.

Gajbhiye, R.N. 2011. Characterization of Foam Flow in Pipes Using Two- Flow Regime Concept. PhD dissertation, Louisiana State University, Baton Rouge, LA (August 2011).

Gajbhiye, R. N. and Kam, S. I. 2011. Characterization of Foam Flow in Horizontal Pipes by Using Two-Flow Regime Concept. *Chemical Engineering Science* **66** (8): 1536-1549.

Gajbhiye, R. N. and Kam, S. I. 2012. The Effect of Inclination Angles on Foam Rheology in Pipes. *J Pet. Sci. Eng.* **86–87**: 246–256.

Gardiner B. S., Dlugogorski, B. Z., and Jameson, G. J. 1999. Prediction of Pressure Losses in Pipe Flow of Aqueous Foams. *Industrial & Engineering Chemistry Reseaarch* **38** : 1099-1106.

Gauglitz, P.A., Friedmann, F., Kam, S.I., Rossen, W.R. 2002. Foam Generation in Homogeneous Porous Media.*Chemical Engineering Science* **57:**4037-4052.

Gupta, D.V.S., Leshchyshyn, T.T., *and* Hlidek, B.T. 2005. Surfactant Gel Foam/Emulsion: History and Field Application in Western Canadian Sedimentary Basin. Paper SPE 97211 presented at SPE Annual Technical Conference and Exhibition, Dallas, Texas, 9-12 October.

Guo, B., Sun, K. and Ghalambor, A. 2003. A Closed Form Hydraulics Equation for Predicting Bottom-Hole Pressure in UBD with Foam. Paper SPE 81640-MS presented at the IADC/SPE Underbalanced Technology Conference and Exhibition, Houston, Texas, 25-26 March. DOI: 10.2118/81640-MS.

Hall, D.L. and Roberts, R.D. 1984. Offshore Drilling with Preformed Stable Foam. Paper SPE 12794 presented at the SPE California Regional Meeting, Long Beach, California, 11-12 April. DOI: 10.2118/12794-MS.

Harris, P.C. and Heath, S.J. 1996. Rheology of crosslinked foams. *SPE Production and Facilities* **11** (2): 113–116. SPE-28512-PA.

Hill, D. G. and Nelson, C. R. 2000. Gas productive fractured shales—an overview and update: *GasTIPS* **6** (2): 4–13.

Hutchins, R. D. and Miller, M. J. 2005. A Circulating Foam Loop for Evaluating Foam at Conditions of Use. *SPE Production and Facilitie* : 286-294.

Jain, A.K. 1976. Accurate explicit equation for friction factor. *Journal of the Hydraulics Division* **102** (5): 674-677.

Kam, S.I. 2008. Improved mechanistic foam simulation with foam catastrophe theory. *Colloids and Surfaces A: Physicochemical and Engineering Aspects* **318** (1): 62–77.

Kam, S.I., Gauglitz, P.A., and Rossen, W.R. 2002. The yield stress of foamy sands. *Colloids and Surfaces A: Physicochemical and Engineering Aspects* **202** (1): 53–62.

Kam, S.I., Frenier, W.W., Davies, S.N., Rossen W.R. 2007. Experimental Study of High-Temperature Foam for Acid Diversion. *Journal of Petroleum Science and Engineering* **58**: 138-160.

Kam, S.I., Rossen, W.R. 2003. A Model for Foam Generation in Homogeneous Media. *SPE Journal* **8** (4): 417-425.

Khade, S.D. and Shah, S.N. 2004. New Rheological Correlation for Guar Foam Fluids. *SPE Production and Facilities* **19** (2): 77–85. SPE-88032-PA.

Kim, A. K. and Dlugogorski, B. Z. 1997. Multipurpose Overhead Compressed-Air Foam System and Its Fire Suppression Performance. *Journal of Fire Protection Engineering* **8** (3): 133-150.

Kraynik, A.M. 1988. Foam flows. *Annual Review of Fluid Mechanics* **20** : 325–357.

Kroezen, A.B.J., Groot, W.J., and Schipper, C.A.C. 1988. The flow properties of foam. *Journal of the Society of Dyers and Colourists* **108** : 393–400.

Lage, A.C.V.M., Nakagawa, E.Y., de Souza, A.A. and Santos, M.M. 1996. Recent Case Histories of Foam Drilling in Brazil. SPE 36098-MS presented at the SPE Latin America/Caribbean Petroleum Engineering Conference, Port-of-Spain, Trinidad, 23-26 April. DOI: 10.2118/36098-MS.

Li, Y., Bjorndalen, N. and Kuru, E. 2007. Numerical Modelling of Cuttings Transport in Horizontal Wells Using Conventional Drilling Fluids. *Journal of Canadian Petroleum Technology* **46** (7). DOI: 10.2118/07-07-TN.

Liu, C., Zhang, N., Guo, B. and Ghalambor, A. 2010. An Investigation of Heavy-Foam Properties for Offshore Drilling. Paper SPE 132464 presented at the SPE Annual Technical Conference and Exhibition, Florence, Italy, 19–22 September. DOI: 10.2118/132464-MS.

Lyons, W. C., Guo, B., Graham, R. L. and Hawley, G. D. 2009. *Air and Gas Drilling Manual: Applications for Oil and Gas Recovery Wells and geothermal fluids recovery wells.* 3rd edition. Gulf Professional Publishing. ISBN: 9780123708953.

Manlowe, D.J. and Radke, C.J. 1990. A Pore-Level Investigation of Foam/Oil Interactions in Porous Media. *SPE Reservoir Engineering* **5** (4): 495-502. SPE-18069-PA.

Mannhardt, K., Novosad, J. J., and Schramm, L. L. 2000. Comparative Evaluation of Foam Stability to Oil. *SPE Reservoir Evaluation & Engineering* **3** (1): 23-34. SPE-60686-PA.

Martins, A.L., Lourenco, A.M.F., and Silva, Jr. V. 2001. Foam Rheology Characterization as a Tool for Predicting Pressure While Drilling Wells in UBD Conditions. Paper SPE/IADC 67691 presented at SPE/IADC Drilling Conference, Amsterdam, 27 February - 1 March.

Martins, A.L., Lourenço, A.M.F. and de Sa, C.H.M. 2000. Foam Properties Requirements for Proper Hole Cleaning While Drilling Horizontal Wells in Underbalanced Conditions. Paper SPE 64382-MS presented at the SPE Asia Pacific Oil and Gas Conference and Exhibition, Brisbane, Australia, 16-18 October. DOI: 10.2118/64382-MS.

Mooney, M. 1931. Explicit formulas for slip and fluidity. *Journal of Rheology* **2** : 210–222.

Muqeem, M.A., Jarrett, C.M. and Abdul, H.J. 2008. Underbalanced Drilling of Oil Wells in Saudi Arabia: Case History and Lessons Learned. Paper SPE114258-MS presented at the SPE/IADC Managed Pressure Drilling and Underbalanced Operations Conference and Exhibition, Abu Dhabi, UAE, 28-29 January. DOI: 10.2118/114258-MS.

Neill, G.H., Dobbs, J.B., Pruitt, G.T., et al. 1964. Field and Laboratory Results of Carbon Dioxide and Nitrogen in Well Stimulation. *Journal of Petroleum Technology* **16** (3): 244-248.

Newell, R. 2011. Shale Gas and the Outlook for U.S. Natural Gas Markets and Global Gas Resources. Presentation to the Organization for Economic Cooperation and Development (OECD), June 21. http://www.eia.gov/pressroom/presentations/newell_06212011.pdf.

Nikolov A. D., Wassan, D. T., Huang, D. W., et al. 1985. The Effect of Oil on Foam Stability: Mechanisms and Implications for Oil Displacement by Foam in Porous Media. Paper SPE 15443 presented at the 61st Annual Technical conference and exhibition of the society of petroleum engineers, New Orleans, Louisiana, 5-8 October.

Novosad, J.J., Mannhardt, K., and Rendall, A. 1989. The Interaction between Foam and Crude Oils. Paper SPE 89-40-29 presented at the Annual Technical Meeting of the Petroleum Society of CIM, Banff, Alberta, Canada, 28–31 May.

Ozbayoglu, M. E., Kuru, E., Miska, S., et al. 2000. A Comparative Study of Hydraulic Models for Foam Driling. Paper SPE 65489 presented at the SPE/PS CIM International Conference on Horizontal Well Technology held in Calgary, Alberta, Canada, 6-8 November.

Ozbayoglu, E.M., Miska, S.Z., Reed, T. and Takach, N. 2003. Cuttings Transport with Foam in Horizontal & Highly-Inclined Wellbores. Paper SPE 79856-MS presented at the SPE/IADC Drilling Conference, Amsterdam, Netherlands, 19-21 February. DOI: 10.2118/79856-MS.

Paknejad, A., Schubert, J.J. and Amani, M. 2007. Foam Drilling Simulator. Paper SPE 105338-MS presented at the SPE Middle East Oil and Gas Show and Conference, Kingdom of Bahrain, 11-14 March. DOI: 10.2118/105338-MS.

Patton, J.T., Holbrook, S.T., and Hsu, W. 1983. Rheology of mobility-control foams. *Society of Petroleum Engineers Journal* **23** (3): 456–460. SPE-9809-PA.

Penny, G.S., Conway, M.W., and Schraufnagel, R.A. 1993. The Evaluation of Proppant Transport and Cleanup of Foamed Fluids Used in Hydraulic Fracturing of Shallow, Water-Sensitive Reservoirs. Peper SPE 26923 presented at the 1993 Eastern Regional Meeting, Pittsburgh, Pennsylvania, 2-4 November.

Princen, H.M. 1983. Rheology of foams and highly concentrated emulsions I. Elastic properties and yield stress of a cylindrical model system. *Journal of Colloid* and *Interface Science* **91** (1): 160-175.

Princen, H.M. 1989. Rheology of foams and highly concentrated emulsions: IV. An experimental study of the shear viscosity and yield stress of concentrated emulsions. *Journal of Colloid and Interface Science* **128** (1): 176-189.

Raza, S.H. and Marsden, S.S. 1967. The streaming potential and the rheology of foam. *SPE Journal* **7** (4): 359–368. SPE 1748-PA.

Reidenbach, V. G., Harris, P. C., Lee, Y. N., et al. 1986. Rheological Study of Foam Fracturing Fluids Using Nitrogen and Carbon Dioxide. *SPE Production Engineering* **1** (1): 31-41. SPE 12026-PA.

Rojas, Y., Kakadjian, S., Aponte, A., et al. 2001. Stability and rheological behavior of aqueous foams for underbalanced drilling. Paper SPE 64999 presented at the SPE International Symposium on Oilfield Chemistry, Houston, 13–16 February.

Shadravan, A., Khodadadian, M., Roohi, A. and Amani, M. 2009. Underbalanced Drilling in Depleted Formation Achieves Great Success: Case Study. Paper SPE 119211-MS presented at the EUROPEC/EAGE Conference and Exhibition, Amsterdam, The Netherlands, 8-11 June. DOI: 10.2118/119211-MS.

Shah, S. N., Shanker, N. H. and Ogugbue, C. C. 2010. Future Challenges of Drilling Fluids and Their Rheological Measurements. AADE-10-DF-HO-41 presented at the 2010 AADE Fluids Conference and Exhibition, Houston, Texas, April 6-7, 2010.

Saintpere, S., Herzhaft, B., Toure, A. and Jollet, S. 1999. Rheological Properties of aqueous Foam for Underbalanced Drilling. Paper SPE 56633 presented at SPE Annual Technical Conference and Exhibition, Houston, 3-6 October. DOI: 10.2118/56633-MS.

Saintpere, S., Marcillat, Y., Bruni, F. and Toure, A. 2000. Hole Cleaning Capabilities of Drilling Foams Compared to Conventional Fluids. Paper SPE 63049-MS presented at the SPE Annual Technical Conference and Exhibition, Dallas, Texas, 1-4 October. DOI: 10.2118/63049-MS.

Shale, L.T. 1994. Underbalanced Drilling: Formation Damage Control During High-Angle or Horizontal Drilling. Paper SPE 27351-MS presented at the SPE Formation Damage Control Symposium, Lafayette, Louisiana, 7-10 February. DOI: 10.2118/27351-MS.

Sanghani, V. and Ikoku, C.U. 1983. Rheology of foam and implications in drilling and cleanout operations. *Journal of Energy Resource Technology* **105** : 362–371.

Sani, A.M., Shah, S.N., and Baldwin. L. 2001. Experimental Investigation of Xanthan Foam Rheology. Paper SPE 67263 presented at SPE Production and Operation Symposium, Oklahoma, 24-27 March.

Schramm, L., 2005. *Emulsions, foams, and suspensions: fundamentals and applications*. WILEY-VCH Verlag GmbH & Co. KGaA, Weinheim, Germany. ISBN: 3-527-30743-5.

Taitel, Y. and Dukler, A. E. 1976. A Model for Predicting Flow Regime Transitions in Horizontal and Near Horizontal Gas-Liquid Flow. *AIChE Journal* **22**(1): 47-55.

Tisne, P., Aloui, F., and Doubliez, L. 2003. Analysis of wall shear stress in wet foam flows using the electrochemical method. *International Journal of Multiphase Flow* **29** : 841–854.

U.S. Energy Information Administration. 2011 Annual Energy Outlook with Projects to 2035.

Yao, Y., Xie, G., Nas, S.W., Boutalbi, S. and Du, H. 2011. Which Reservoirs in China Are Best for Underbalanced Drilling? *SPE Drilling & Completion* **26** (4): 550-556. DOI: 10.2118/135796-PA

Zelenev, A.S., Zhou, H., Ellena, L.B., et al. 2010. Microemulsion-Assisted Fluid Recovery and Improved Permeability to Gas in Shale Formations. Paper SPE 127922 presented at the SPE International Symposium and Exhibition on Formation Damager Control, Lafayette, Louisiana, 10-12 February.

APPENDIX 1: FOAM DRILLING HYDRAULICS CALCULATIONS

Following steps and equations are used to calculate foam drilling hydraulics in this study. Notice that wellbore is divided into three sections such as inside drillpipe, across drill bit, and in the annulus.

Inside drill pipe:

1. Read input parameters and the pressure at the first node ($P = P_1 = P_{in}$)

2. Calculate gas compressibility (Z) using Dranchuk and Abou-Kassem EOS equation (1975).

$$Z = 1 + c_1\rho_r + c_2\rho_r^2 + c_3\rho_r^5 + c_4 \quad \text{(A1)}$$

$$\rho_r = 0.27\,\frac{P_r}{Z\,T_r} \quad \text{(A2)}$$

$$c_1 = A_1 + \frac{A_2}{T_r} + \frac{A_3}{T_r^3} + \frac{A_4}{T_r^4} + \frac{A_5}{T_r^5} \quad \text{(A3)}$$

$$c_2 = A_6 + \frac{A_7}{T_r} + \frac{A_8}{T_r^2} \quad \text{(A4)}$$

$$c_3 = A_9\left(\frac{A_7}{T_r} + \frac{A_8}{T_r^2}\right) \quad \text{(A5)}$$

$$c_4 = A_{10}(1 + A_{11}\,\rho_r^2)\left(\frac{\rho_r^2}{T_r^3}\right) Exp(-A_{11}\,\rho_r^2) \quad \text{(A6)}$$

$A_1 = 0.3265$; $A_2 = -1.07$; $A_3 = -0.5339$; $A_4 = 0.01569$; $A_5 = -0.05165$; $A_6 = 0.5475$; $A_7 = -0.7361$;

$A_8 = 0.1844$; $A_9 = 0.1056$; $A_{10} = 0.6134$; $A_{11} = 0.721$

$$P_r = \frac{P}{P_{pc}} \quad \text{(A7)}$$

$$T_r = \frac{T+460}{T_{pc}} \quad \text{(A8)}$$

$$P_{pc} = 756.8 - 131\,SG - 3.6\,SG^2 \quad \text{(A9)}$$

$$T_{pc} = 69.2 + 349.5\,SG - 74\,SG^2 \quad \text{(A10)}$$

3. Calculate gas rate (Q_g) and gas density (ρ_g) using inputs including gas specific gravity (SG).

$$Q_g = \frac{P_{sc}\,Q_{gsc}\,Z\,(T+460)}{P\,Z_{sc}\,(T_{sc}+460)} \quad \text{(A11)}$$

$$\rho_g = \frac{28.97\,SG\,P}{10.732\,Z\,(T+460)} \quad \text{(A12)}$$

4. Calculate gas mass rate (m_g), liquid mass rate (m_w), and total mass rate (m_t).

$$m_g = Q_g\,\rho_g \quad \text{(A13)}$$

$$m_w = Q_w\,\rho_w \quad \text{(A14)}$$

$$m_t = m_g + m_w \quad \text{(A15)}$$

5. Calculate foam density (ρ_f).

$$\rho_f = \frac{m_t}{Q_g+Q_w} \quad \text{(A16)}$$

6. Calculate foam quality (f_g).

$$f_g = \frac{Q_g}{Q_t} = \frac{Q_g}{Q_g+Q_w} \quad \text{(A17)}$$

7. Calculate hydrostatic pressure gradient ($(\frac{\Delta p}{\Delta z})_{ele}$) over the segment length of Δz with the inclination angle, θ.

$$(\frac{\Delta p}{\Delta z})_{ele} = 0.052\, \rho_f \cos(\frac{\pi\theta}{180}) \quad \text{(A18)}$$

8. Calculate total flow rate (Q_t) and total velocity (u_t) when the inner diameter of drillpipe is d_{pin}.

$$Q_t = \frac{m_t}{\rho_f} \quad \text{(A19)}$$

$$u_t = \frac{Q_t}{2.448\, d_{pin}^2} \quad \text{(A20)}$$

9. Calculate acceleration pressure gradient ($(\frac{\Delta p}{\Delta z})_{acc}$) over the length segment of Δz if the total velocity changes from u_{t1} to u_{t2}.

$$(\frac{\Delta p}{\Delta z})_{acc} = \frac{0.0008074\, \rho_f\, (u_{t_1}^2 - u_{t_2}^2)}{\Delta z} \quad \text{(A21)}$$

10. Determine consistency index (K) and power-law exponent (n) by using which regime the flow condition falls into. Then calculate Reynolds number, N_{Re} (Bourgoyne Jr. et al, 1986). If N_{Re}<2100 it is Laminar flow, otherwise it is considered as turbulent flow.

$$N_{Re} = \frac{89100\, \rho_f\, u_t^{2-n}}{K} (\frac{0.0416\, d_{pin}}{3+\frac{1}{n}})^n \quad \text{(A22)}$$

11. Calculate frictional pressure gradient ($(\frac{\Delta p}{\Delta z})_{fri}$) over the length segment of Δz

$$\left(\frac{\Delta p}{\Delta z}\right)_{fri} = \frac{K\, u_t^n}{144000\, d_{pin}^{1+n}} (\frac{3+\frac{1}{n}}{0.0416})^n \quad \text{, if laminar flow} \quad \text{(A23)}$$

$$\left(\frac{\Delta p}{\Delta z}\right)_{fri} = \frac{f\, \rho_f\, u_t^2}{25.8\, d_{pin}} \quad \text{, if turbulent} \quad \text{(A24)}$$

Where friction factor (f) can be approximated by following equation (Jain, 1976)

$$\frac{1}{\sqrt{f}} = 1.14 - 2\log(\varepsilon + \frac{21.25}{N_{Re}^{0.9}}) \quad \text{(A25)}$$

12. Calculate total pressure gradient ($(\frac{\Delta p}{\Delta z})_{tot}$) over the length segment (Δz).

$$(\frac{\Delta p}{\Delta z})_{tot} = -(\frac{\Delta p}{\Delta z})_{ele} + (\frac{\Delta p}{\Delta z})_{acc} + (\frac{\Delta p}{\Delta z})_{fri} \quad \text{(A26)}$$

13. Calculate the pressure in the 2nd node.

$$P_2 = P_1 + (\frac{\Delta p}{\Delta z})_{tot} \times \Delta z \quad \text{(A27)}$$

14. Repeat steps 1 through 13 for the next node until the calculation reaches drill bit ((N+1)th node).

At drill bit:

1. Calculate pressure drop at the drill bit (ΔP_{bit}) using total nozzle cross-sectional area (A_t)

$$\Delta P_{bit} = \frac{8.311\times10^{-5}\rho_f\, Q_t^2}{0.95\, A_t^2} \quad \text{(A28)}$$

2. Calculate the bottomhole pressure ($\text{Pbottom} = P_{N+2}$)

$$P_{bottom} = P_{N+2} = P - \Delta p_{bit} \quad \text{(A29)}$$

In the annulus:

Use $P_{bottom} = P_{N+2}$ as the pressure in the first node in the annulus and repeat the same procedures as described in the drillpipe. Note the use of the following equations in the case of foams in the annulus. Foam velocity (u_t) by using the outer pipe diameter (d_{pout}) and inner casing diameter (d_{ann})

$$u_t = \frac{Q_t}{2.448\,(d_{ann}^2 - d_{pout}^2)} \quad \text{replacing Eq. A20;} \tag{A30}$$

Reynolds Number

$$N_{Re} = \frac{109000\,\rho_f\,u_t^{2-n}}{K}\left(\frac{0.0208\,(d_{ann} - d_{pout})}{2+\frac{1}{n}}\right)^n \quad \text{replacing Eq. A22;} \tag{A31}$$

Friction pressure gradient ($(\frac{\Delta p}{\Delta z})_{fri}$) over the segment length of Δz

$$\left(\frac{\Delta p}{\Delta z}\right)_{fri} = \frac{K\,u_t^n}{144000\,(d_{ann} - d_{pout})^{1+n}}\left(\frac{2+\frac{1}{n}}{0.0208}\right)^n \quad \text{if laminar flow, replacing Eq. A23; and} \tag{A32}$$

$$\left(\frac{\Delta P}{\Delta z}\right)_{fri} = \frac{f\,\rho_f\,u_t^2}{21.1\,(d_{ann} - d_{pout})} \quad \text{if turbulent, replacing Eq. A24.} \tag{A33}$$

Total pressure gradient ($(\frac{\Delta p}{\Delta z})_{tot}$) over the segment length of Δz

$$(\frac{\Delta p}{\Delta z})_{tot} = (\frac{\Delta p}{\Delta z})_{ele} + (\frac{\Delta p}{\Delta z})_{acc} + (\frac{\Delta p}{\Delta z})_{fri} \quad \text{replacing Eq. A26.} \tag{A34}$$

If the calculation is repeated toward the surface, then the pressure at the last node (P_{2N+2}) can be check if it is close to the back pressure (P_b)

$$|P_{2N+2} - P_b| < error \tag{A35}$$

If this condition is not satisfied, then the whole calculation can be carried out again with a new inlet pressure (P_{in}). The entire process can be summarized as shown in Fig. A1.

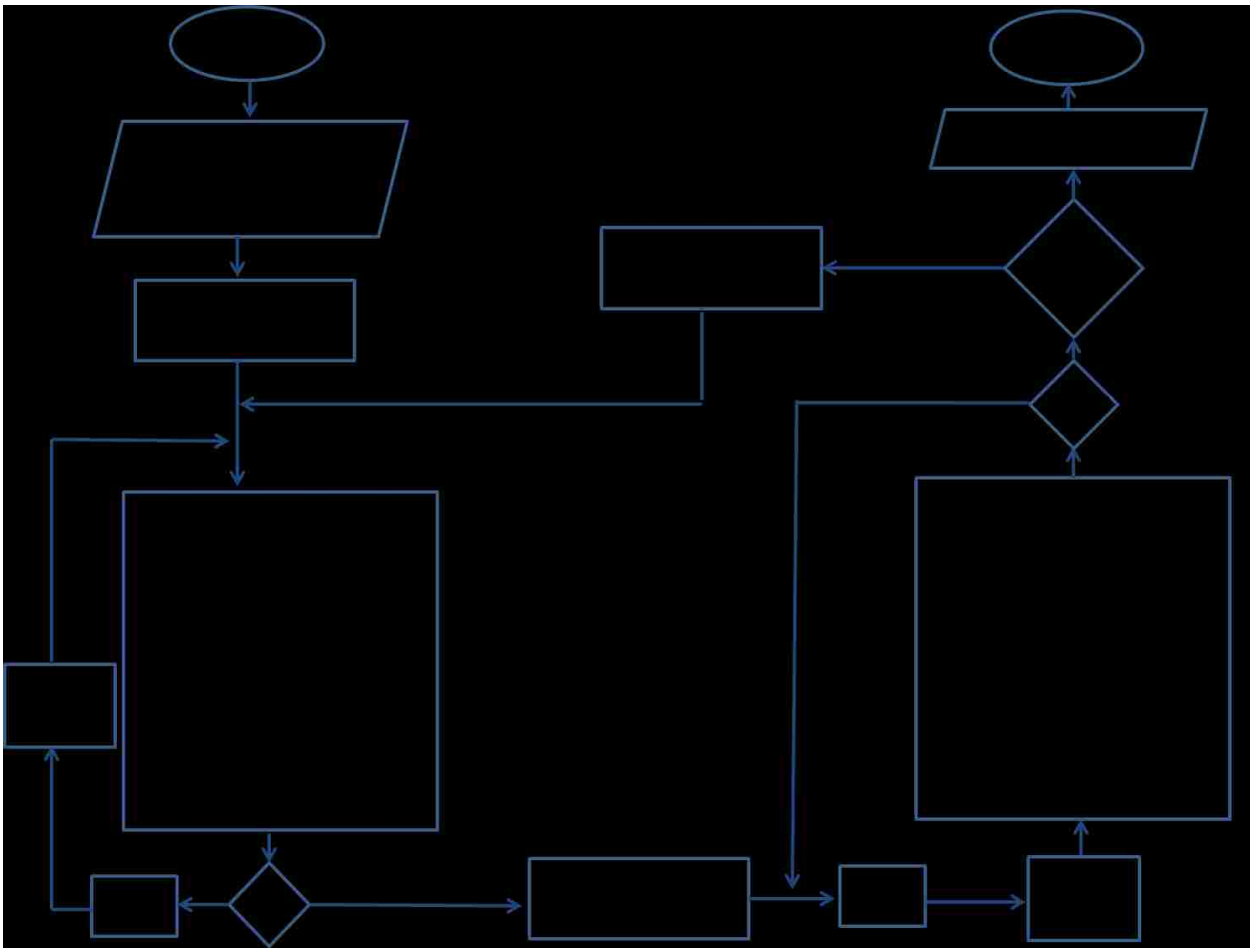

Figure A.1. The algorithm used in this study for foam drilling hydraulics calculation (details on parameters and variables in Appendix 1).

APPENDIX 2: LETTERS OF PERMISSION

SOCIETY OF PETROLEUM ENGINEERS LICENSE TERMS AND CONDITIONS

Nov 20, 2013

This is a License Agreement between Ali reza Edrisi ("You") and Society of Petroleum Engineers ("Society of Petroleum Engineers") provided by Copyright Clearance Center ("CCC"). The license consists of your order details, the terms and conditions provided by Society of Petroleum Engineers, and the payment terms and conditions.

All payments must be made in full to CCC. For payment instructions, please see information listed at the bottom of this form.

License Number	3267751485613
License date	Nov 14, 2013
Licensed content publisher	Society of Petroleum Engineers
Licensed content publication	SPE Proceedings
Licensed content title	A New Foam Rheology Model for Shale-Gas Foam Fracturing Applications
Licensed content author	A. R. Edrisi, S. I. Kam, Louisiana State University
Licensed content date	2012
Type of Use	Thesis/Dissertation
Requestor type	author of the original work
SPE member	yes
SPE member number	3450127
Format	print and electronic
Portion	full article
Will you be translating?	no
Distribution	1
Order reference number	
Title of your thesis / dissertation	Experimental and Modeling Study of Foam Flow in Pipes with Two Foam-Flow Regimes
Expected completion date	Dec 2013
Estimated size (number of pages)	110

Total 0.00 USD

Terms and Conditions

STANDARD TERMS AND CONDITIONS FOR REPRODUCTION OF MATERIAL

1. The Society of Petroleum Engineers, Inc. (“SPE”) holds the copyright for this material. By clicking "accept" in connection with completing this licensing transaction, you agree that the following terms and conditions apply to this transaction (along with the Billing and Payment terms and conditions established by Copyright Clearance Center, Inc. ("CCC"), at the time that you opened your RightsLink account and that are available at any time at).

2. SPE hereby grants to you a non-exclusive license to use this material. Licenses are for one-time use only with a maximum distribution equal to the number that you identified in the licensing process; any form of republication must be completed within six months from the date hereof (although copies prepared before then may be distributed thereafter); and any electronic posting is limited to the period identified in the licensing process.

3. You may not alter or modify the material in any manner (except that you may use, within the scope of the license granted, one or more excerpts from the copyrighted material, provided that the process of excerpting does not alter the meaning of the material or in any way reflect negatively on SPE or any writer of the material or their employer), nor may you translate the material into another language.

4. Total excerpts from the license material may not exceed thirty percent (30%) of the total text. Not more than five (5) excerpts, figures, tables, or images may be used from any given paper. Multiple permission requests may not be used to exceed these limits.

5. SPE reserves all rights not specifically granted in the combination of (i) the license details provided by you and accepted in the course of this licensing transaction, (ii) these terms and conditions and (iii) CCC's Billing and Payment terms and conditions.

6. While you may exercise the rights licensed immediately upon issuance of the license at the end of the licensing process for the transaction, provided that you have disclosed complete and accurate details of your proposed use, no license is finally effective unless and until full payment is received from you (either by SPE or by CCC) as provided in CCC's Billing and Payment terms and conditions. If full payment is not received on a timely basis, then any license preliminarily granted shall be deemed automatically revoked and shall be void as if never granted. Further, in the event that you breach any of these terms and conditions or any of CCC's Billing and Payment terms and conditions, the license is automatically revoked and shall be void as if never granted. Use of materials as described in a revoked license, as well as any use of the materials beyond the scope of an unrevoked license, may constitute copyright infringement and SPE reserves the right to take any and all action to protect its copyright in the materials

7. You must include the appropriate copyright and permission notice and disclaimer in connection with any reproduction of the licensed material.The copyright information is found on the front page of the paper immediately under the title and author. This statement will then be followed with the disclaimer, “Further reproduction prohibited without permission.” Examples:1) Copyright 1990, Society of Petroleum Engineers Inc.Copyright 1990, SPE. Reproduced with permission of SPE. Further reproduction prohibited without permission.2) Copyright 2010, IADC/SPE Drilling Conference and ExhibitionCopyright 2010, IADC/SPE Drilling Conference and Exhibition. Reproduced with permission of SPE. Further reproduction prohibited without permission.3) Copyright 2008, Offshore Technology ConferenceCopyright 2008, Offshore Technology Conference. Reproduced with permission of OTC. Further reproduction prohibited without permission.4) Copyright 2005, International Petroleum Technology ConferenceCopyright 2005, International Petroleum Technology Conference. Reproduced with permission of IPTC. Further reproduction prohibited without permission.If for any reason, the copyright on the paper is missing or unclear, please follow Example 1 above, using SPE as the default copyright holder. SPE administers copyright for OTC, IPTC and other joint

events on behalf of all parties in those events.

8. SPE makes no representations or warranties with respect to the licensed material and adopts on its own behalf the limitations and disclaimers established by CCC on its behalf in its Billing and Payment terms and conditions for this licensing transaction.

9. You hereby indemnify and agree to hold harmless SPE and CCC, and their respective officers, directors, employees and agents, from and against any and all claims arising out of your use of the licensed material other than as specifically authorized pursuant to this license.

10. This license is personal to you, but may be assigned or transferred by you to a business associate (or to your employer) if you give prompt written notice of the assignment or transfer to SPE. No such assignment or transfer shall relieve you of the obligation to pay the designated license fee on a timely basis (although payment by the identified assignee can fulfill your obligation).

11. This license may not be amended except in a writing signed by both parties (or, in the case of SPE, by CCC on SPE's behalf).

12. SPE hereby objects to any terms contained in any purchase order, acknowledgment, check endorsement or other writing prepared by you, which terms are inconsistent with these terms and conditions or CCC's Billing and Payment terms and conditions. These terms and conditions, together with CCC's Billing and Payment terms and conditions (which are incorporated herein), comprise the entire agreement between you and SPE (and CCC) concerning this licensing transaction. In the event of any conflict between your obligations established by these terms and conditions and those established by CCC's Billing and Payment terms and conditions, these terms and conditions shall control.

13. This Agreement shall be governed and interpreted by the laws of the State of Texas, United States of America. Regardless of the place of performance or otherwise, the Agreement, and all schedules, amendments, modifications, alterations, or supplements thereto, will be governed by the laws of the State of Texas, United States of America. If any provisions of the Agreement are unenforceable under applicable law, the remaining provisions shall continue in full force and effect.

Other Terms and Conditions: None

v1.1

If you would like to pay for this license now, please remit this license along with your payment made payable to "COPYRIGHT CLEARANCE CENTER" otherwise you will be invoiced within 48 hours of the license date. Payment should be in the form of a check or money order referencing your account number and this invoice number RLNK501159474.
Once you receive your invoice for this order, you may pay your invoice by credit card. Please follow instructions provided at that time.

Make Payment To:
Copyright Clearance Center
Dept 001
P.O. Box 843006
Boston, MA 02284-3006

For suggestions or comments regarding this order, contact RightsLink Customer Support:customercare@copyright.com or +1-877-622-5543 (toll free in the US) or +1-978-646-2777.

Gratis licenses (referencing $0 in the Total field) are free. Please retain this printable license for your reference. No payment is required.

SOCIETY OF PETROLEUM ENGINEERS LICENSE TERMS AND CONDITIONS

Nov 20, 2013

This is a License Agreement between Ali reza Edrisi ("You") and Society of Petroleum Engineers ("Society of Petroleum Engineers") provided by Copyright Clearance Center ("CCC"). The license consists of your order details, the terms and conditions provided by Society of Petroleum Engineers, and the payment terms and conditions.

All payments must be made in full to CCC. For payment instructions, please see information listed at the bottom of this form.

License Number	3267751150078
License date	Nov 14, 2013
Licensed content publisher	Society of Petroleum Engineers
Licensed content publication	SPE Proceedings
Licensed content title	Experimental Study of Polymer-free and Polymer-added Foams for Underbalanced Drilling: Are Two Foam-Flow Regimes Still There?
Licensed content author	A. R. Edrisi, R. N. Gajbhiye, S. I. Kam, Louisiana State University
Licensed content date	2012
Type of Use	Thesis/Dissertation
Requestor type	author of the original work
SPE member	yes
SPE member number	3450127
Format	print and electronic
Portion	full article
Will you be translating?	no
Distribution	1

Order reference number	
Title of your thesis / dissertation	Experimental and Modeling Study of Foam Flow in Pipes with Two Foam-Flow Regimes
Expected completion date	Dec 2013
Estimated size (number of pages)	110
Total	0.00 USD

Terms and Conditions

STANDARD TERMS AND CONDITIONS FOR REPRODUCTION OF MATERIAL

1. The Society of Petroleum Engineers, Inc. (“SPE”) holds the copyright for this material. By clicking "accept" in connection with completing this licensing transaction, you agree that the following terms and conditions apply to this transaction (along with the Billing and Payment terms and conditions established by Copyright Clearance Center, Inc. ("CCC"), at the time that you opened your RightsLink account and that are available at any time at).

2. SPE hereby grants to you a non-exclusive license to use this material. Licenses are for one-time use only with a maximum distribution equal to the number that you identified in the licensing process; any form of republication must be completed within six months from the date hereof (although copies prepared before then may be distributed thereafter); and any electronic posting is limited to the period identified in the licensing process.

3. You may not alter or modify the material in any manner (except that you may use, within the scope of the license granted, one or more excerpts from the copyrighted material, provided that the process of excerpting does not alter the meaning of the material or in any way reflect negatively on SPE or any writer of the material or their employer), nor may you translate the material into another language.

4. Total excerpts from the license material may not exceed thirty percent (30%) of the total text. Not more than five (5) excerpts, figures, tables, or images may be used from any given paper. Multiple permission requests may not be used to exceed these limits.

5. SPE reserves all rights not specifically granted in the combination of (i) the license details provided by you and accepted in the course of this licensing transaction, (ii) these terms and conditions and (iii) CCC's Billing and Payment terms and conditions.

6. While you may exercise the rights licensed immediately upon issuance of the license at the end of the licensing process for the transaction, provided that you have disclosed complete and accurate details of your proposed use, no license is finally effective unless and until full payment is received from you (either by SPE or by CCC) as provided in CCC's Billing and Payment terms and conditions. If full payment is not received on a timely basis, then any license preliminarily granted shall be deemed automatically revoked and shall be void as if never granted. Further, in the event that you breach any of these terms and conditions or any of CCC's Billing and Payment terms and conditions, the license is automatically revoked and shall be void as if never granted. Use of materials as described in a revoked license, as well as any use of the materials beyond the scope of an unrevoked license, may constitute copyright infringement and SPE reserves the right to take any and all action to protect its copyright in the materials

7. You must include the appropriate copyright and permission notice and disclaimer in connection with any reproduction of the licensed material.The copyright information is found on the front page of the paper immediately under the title and author. This statement will then be followed with the disclaimer, “Further reproduction prohibited without permission.” Examples:1) Copyright 1990, Society of Petroleum Engineers Inc.Copyright 1990, SPE. Reproduced with permission of SPE. Further reproduction prohibited without

permission.2) Copyright 2010, IADC/SPE Drilling Conference and ExhibitionCopyright 2010, IADC/SPE Drilling Conference and Exhibition. Reproduced with permission of SPE. Further reproduction prohibited without permission.3) Copyright 2008, Offshore Technology ConferenceCopyright 2008, Offshore Technology Conference. Reproduced with permission of OTC. Further reproduction prohibited without permission.4) Copyright 2005, International Petroleum Technology ConferenceCopyright 2005, International Petroleum Technology Conference. Reproduced with permission of IPTC. Further reproduction prohibited without permission.If for any reason, the copyright on the paper is missing or unclear, please follow Example 1 above, using SPE as the default copyright holder. SPE administers copyright for OTC, IPTC and other joint events on behalf of all parties in those events.

8. SPE makes no representations or warranties with respect to the licensed material and adopts on its own behalf the limitations and disclaimers established by CCC on its behalf in its Billing and Payment terms and conditions for this licensing transaction.

9. You hereby indemnify and agree to hold harmless SPE and CCC, and their respective officers, directors, employees and agents, from and against any and all claims arising out of your use of the licensed material other than as specifically authorized pursuant to this license.

10. This license is personal to you, but may be assigned or transferred by you to a business associate (or to your employer) if you give prompt written notice of the assignment or transfer to SPE. No such assignment or transfer shall relieve you of the obligation to pay the designated license fee on a timely basis (although payment by the identified assignee can fulfill your obligation).

11. This license may not be amended except in a writing signed by both parties (or, in the case of SPE, by CCC on SPE's behalf).

12. SPE hereby objects to any terms contained in any purchase order, acknowledgment, check endorsement or other writing prepared by you, which terms are inconsistent with these terms and conditions or CCC's Billing and Payment terms and conditions. These terms and conditions, together with CCC's Billing and Payment terms and conditions (which are incorporated herein), comprise the entire agreement between you and SPE (and CCC) concerning this licensing transaction. In the event of any conflict between your obligations established by these terms and conditions and those established by CCC's Billing and Payment terms and conditions, these terms and conditions shall control.

13. This Agreement shall be governed and interpreted by the laws of the State of Texas, United States of America. Regardless of the place of performance or otherwise, the Agreement, and all schedules, amendments, modifications, alterations, or supplements thereto, will be governed by the laws of the State of Texas, United States of America. If any provisions of the Agreement are unenforceable under applicable law, the remaining provisions shall continue in full force and effect.

Other Terms and Conditions: None

v1.1

If you would like to pay for this license now, please remit this license along with your payment made payable to "COPYRIGHT CLEARANCE CENTER" otherwise you will be invoiced within 48 hours of the license date. Payment should be in the form of a check or money order referencing your account number and this invoice number RLNK501159465.
Once you receive your invoice for this order, you may pay your invoice by credit card. Please follow instructions provided at that time.

Make Payment To:

VITA

Ali Reza Edrisi was born and raised in a small town in north of Iran. During his high school educations, he was fascinated by Physics and Mathematics which persuaded him to look for a type of education that best fits his desires in both. Growing up in an oil country, the desire to study petroleum engineering prompted him for an admission to the Petroleum University of Technology, Iran's most prestigious institution of higher learning in the field of petroleum.

He has obtained his Bachelor's degree through 4 years of dedicated academic efforts in petroleum production engineering. His distinguished scholastic aptitudes led him to a master program for petroleum reservoir engineering at University of Tehran, when he had much more practical experiences in addition to the advanced courses that he passed. His outstanding scholastic performance and research achievements granted him a full-time position as a Reservoir Engineer at Petroleum Ministry of Iran where he worked for almost two years.

During his master's study, he found out about his immeasurable appetite for higher education. He joined Louisiana State University to peruse a PhD degree in the field of petroleum engineering in spring 2009. During his PhD study, he has presented and published numerous technical papers in premier oil and gas conferences and journals. He is the first prize winner of student presentation contests at the GOM Deepwater Technical Symposium, New Orleans, LA (2010 and 2011), and the SPE Americas E&P Health, Safety, Security and Environment Conference, Galveston, TX (2013).

His research interest covers rheology of complex fluids in drilling and fracturing, foam drilling and foam fracturing, drilling hydraulics and optimization, multiphase flow behavior in pipes and annulus, pipeline leak behavior and leak detection modeling, and finally reservoir engineering specifically reservoir modeling and simulation.